



UNIVERSITY OF
LIVERPOOL

Therapeutics Development Against
the Apicomplexa Parasites
Plasmodium falciparum and
Toxoplasma gondii

Thesis submitted in accordance with the requirements of the
University of Liverpool for the degree of Doctor in Philosophy

by

Michael J. Capper

September 2015

Abstract

Apicomplexa parasites are the cause of two of the world's most widespread diseases; malaria and toxoplasmosis. Malaria affects two billion people worldwide in some of the poorest regions of the world. Over a million people a year die from malaria, the majority of which are pregnant women or children under the age of 5. *Plasmodium falciparum* is by far the most lethal cause of malaria and is endemic to many regions of sub-Saharan Africa. *Toxoplasma gondii* is the most common parasitic infection of human brain and eyes and is suspected to affect one third of the world's population. Rising drug resistance and the inadequacies of current treatments have spurred a global effort for the development of new therapies targeting these parasites

Cytochrome *bc*₁ (cyt. *bc*₁) is a proven drug target for both treatment and prophylaxis of *P. falciparum* and *T. gondii*. Atovaquone, a potent broad-spectrum anti-parasitic drug, targets the Q_o site, one of two active sites within cytochrome, *b* collapsing the mitochondrial membrane potential and killing the parasites. Single mutations within the Q_o site render atovaquone ineffective and incidences of resistance are rising. Previous work has focussed on overcoming resistance through the design/redesign of compounds targeting the well understood Q_o site. Here we show the binding modes of GSK's next-generation antimalarial 4(1H)-pyridones and a novel 4(1H)-quinolone to the Q_i site of cyt. *bc*₁. These structures reveal the mechanism by which the compounds are able to overcome resistance and point in a new direction for antimalarial drug development. This work reaffirms the importance of structural observation in drug development.

Merozoite surface protein 1–19 (MSP1₁₉) is an important target in vaccine development against malaria. Recent work has shown that cupredoxins bind MSP1₁₉ of *P. falciparum* and result in death for the parasite. Rusticyanin, the most potent of these, has been extensively studied and various mutants have been produced a range of redox potentials and acid stability properties. Here, initial studies of the complex between *P. falciparum* MSP1₁₉ and rusticyanin are carried out and analysed.

Preface

Chapter 1

Malaria and toxoplasmosis

An overview of the diseases, their causative organisms and current treatments.

Chapter 2

Drug development and X-ray crystallography

A brief overview of drug development and the theory behind X-ray crystallography.

Chapter 3

Drug development against cytochrome bc_1

A study of the cytochrome bc_1 bound to several ligands and their relevance to malaria and toxoplasmosis.

Chapter 4

Rusticyanin and MSP1₁₉

Studies on the complex formed between the therapeutic target, MSP1₁₉, and the cupredoxin, rusticyanin.

Chapter 5

General discussion and concluding remarks

Final comments on this work including the future directions this work can take.

Chapter 6

Materials and methods

A description of all the materials and method used in this study.

Acknowledgments

I would like to give my sincerest gratitude and upmost thanks to me entire supervisory team; Dr. Svetlana Antonyuk, Prof. Giancarlo Biagini and Prof. Samar Hasnain. Their guidance and teaching has been the driving force behind me on this project and their support has helped me at all times. I have hugely benefitted from each of their wisdom and expertise. They have each been excellent tutors.

I would also like to thank both Dr. Svetlana Antonyuk and Dr. Richard Strange for their assistance through numerous night shifts at both Diamond Light Source and Synchrotron SOLEIL. Their company, expertise and conversation were much appreciated during the dark nights of beamtime when crystal after crystal would simply refuse to diffract.

Many thanks to Prof. Paul O'Neill who supplied many of the chemicals used in this work and offered guidance in their properties, site of action and ideas for development.

For their help using lipidic cubic phase and the use of their screening robot I am thankful to Prof. Martin Caffrey and Dr. Chia-Ying Huang. The days I spent in Dublin were very informative and their lab was highly accommodating.

I must thank everybody in the MBG, Lab C and Lab D who have shared their equipment, consumables and knowledge with me during the last four years. No matter what time of the day, there was always somebody to have a conversation with and share a drink. Particular thanks to Dr Gareth Wright for his help and ideas throughout my work.

On a personal note I am indebted to by wonderful girlfriend Frances Blow for putting up with me during my writing, the delivery of coffee and lifts home late at night. I must also thank both my Mum and Dad for their constant personal (and financial) support. Their help through my eternal studenthood has been essential and I could not have done this without them; I am very grateful.

Table of Contents

Abstract	iii
Preface	iv
Acknowledgments	v
Table of Contents	vi
List of figures	1
List of tables	4
Glossary of abbreviations	5
Chapter 1 Malaria and Toxoplasmosis	8
1.1 Malaria.....	9
1.1.1 Plasmodium parasites.....	10
1.1.2 The P. falciparum life cycle.....	12
1.1.3 Efforts for the control and elimination of malaria.....	13
1.1.4 Malaria treatment and prevention.....	14
1.1.4.1 Ecological vector control.....	15
1.1.4.2 Insecticides and nets.....	15
1.1.4.3 Vaccination.....	16
1.1.4.4 Drug treatment and prophylaxis.....	16
Quinolines.....	17
Antifolates.....	17
Hydroxynapthoquinones.....	20
Artemisinin Combination Therapies.....	20
1.2 Toxoplasmosis.....	21
1.2.1 Life cycle.....	22
1.2.2 Current treatment.....	24
1.3 Summary.....	25
Chapter 2 Drug discovery and X-ray crystallography	26
2.1 Drug development.....	27
2.1.1 Rational drug design.....	27
2.1.2 Structure based drug design.....	29
2.1.3 NMR assisted drug discovery.....	30
2.1.4 X-ray crystallography assisted drug discovery.....	31
2.2 X-ray crystallography.....	32
2.2.1 A short history of X-ray crystallography.....	32
2.2.2 Protein crystallisation.....	34
2.2.3 Crystallographic theory.....	36
2.2.4 The phase problem.....	37

2.2.4.1 Multiple Isomorphous Replacement	38
2.2.4.2 Using anomalous signal (MAD and SAD)	38
2.2.4.3 Molecular Replacement.....	39
2.2.5 Radiation damage.....	39
2.2.6 Data collection	40
2.2.6.1 Synchrotron Radiation	41
2.2.7 Data reduction	42
2.2.8 Structure solution and refinement	42
Chapter 3 Drug development against cytochrome <i>bc</i>₁.....	44
3.1 Cytochrome <i>bc</i> ₁	45
3.1.1 The electron transport chain.....	47
3.1.2 Modified Q-cycle	48
3.1.3 Role and structure of cytochrome <i>bc</i> ₁ in malaria.....	50
3.1.4 Atovaquone antiprotozoal action.....	50
3.1.5 Drug development targeting cytochrome <i>bc</i> ₁	53
3.1.5.1 4(1H)-Pyridones	53
3.1.5.2 Quinolones.....	54
Tetrahydroquinolones.....	55
2-aryl quinolones.....	56
Quinolone esters	57
3.1.5.3 Acridinediones and acridones.....	57
3.1.6 Binding of novel compounds to cytochrome <i>bc</i> ₁	58
3.2 Results	60
3.2.1 Modified purification of cytochrome <i>bc</i> ₁	60
3.2.2 Crystallisation	63
3.2.3 Cryoprotection and crystal screening	64
3.2.4 Attempted binding of antimalarial compounds.....	65
3.2.5 Binding of 4(1H)-pyridones GW844520 and GSK932121	66
3.2.6 Binding of MJM 170	70
3.2.7 Homology between cytochrome b sequences.....	72
3.3 Discussion	77
3.3.1 4(1H)-pyridones are Q _i site inhibitors.....	77
3.3.2 The 4(1H)-quinolone MJM 170 binds the Q _i site	79
3.3.3 Future drug development targeting the cytochrome <i>bc</i> ₁ Q _i site.....	80
Chapter 4 Therapeutic effects of rusticyanin	84
4.1 Therapeutic effect of cupredoxins against malaria.....	85
4.1.1 Merozoite surface protein 1	85
4.1.1.1 MSP1 ₁₉	87

4.1.2 Cupredoxins.....	88
4.1.2.1 Rusticyanin	89
4.2 Results	91
4.2.1 Rusticyanin expression and purification	91
4.2.2 Rusticyanin crystal structure	92
4.2.3 Expression and purification of MSP1 ₁₉	93
4.2.4 Binding of rusticyanin to MSP1 ₁₉	95
4.2.5 Crystal screening of MSP1 ₁₉ -rusticyanin complex.....	98
4.3 Discussion	98
4.3.1 Structure of rusticyanin.....	98
4.3.2 Purification of complex.....	99
4.3.3 Crystal trials on complex.....	99
Chapter 5 General discussion and summary.....	100
5.1 Cytochrome <i>bc</i> ₁ as a drug target	101
5.2 Further directions for cytochrome <i>bc</i> ₁	101
5.3 Rusticyanin in complex with MSP1 ₁₉	103
5.4 Further directions for rusticyanin and MSP1 ₁₉	104
5.5 Final remarks.....	105
Chapter 6 Materials and Methods	106
6.1 Cytochrome <i>bc</i> ₁	107
6.1.1 Isolation of crude mitochondria	107
6.1.2 Solubilisation of membrane proteins	107
6.1.3 Purification of cytochrome <i>bc</i> ₁	108
6.1.3.1 DEAE-sepharose purification of cytochrome <i>bc</i> ₁	108
6.1.3.2 Hydroxyapatite purification of cytochrome <i>bc</i> ₁	108
6.1.3.3 Size exclusion chromatography of cytochrome <i>bc</i> ₁	108
6.1.3.4 Compound binding prior to crystallisation	109
6.1.3.5 PEG fractionation of cytochrome <i>bc</i> ₁	109
6.1.4 Determining the concentration of cytochrome <i>bc</i> ₁	110
6.1.5 Crystallisation of cytochrome <i>bc</i> ₁	110
6.1.5.1 Initial crystallisation.....	110
6.1.5.2 Micro-seeding.....	111
6.1.5.3 Refined crystallisation.....	111
6.1.5.4 Lipidic cubic phase crystal screening.....	111
6.1.5.5 Crystallisation in Undecyl Maltoside.....	112
6.1.6 Crystal freezing	112
6.1.7 Data collection of cytochrome <i>bc</i> ₁ crystals	113
6.1.7.1 Screening on FRE+ home source.....	113

6.1.7.2 Data collection for cytochrome <i>bc</i> ₁	113
Data collection of cytochrome <i>bc</i> ₁ – pyridones.....	113
Data collection of cytochrome <i>bc</i> ₁ – MJM 170	114
6.1.8 Data reduction and structure refinement.....	114
6.2 Rusticyanin	115
6.2.1 Rusticyanin expression.....	115
6.2.2 Rusticyanin purification	115
6.2.3 Rusticyanin crystallisation and freezing	116
6.2.4 Rusticyanin data collection	117
6.2.5 Rusticyanin data reduction and structure refinement.....	117
6.3 MSP119	117
6.3.1 MSP1 ₁₉ cloning	117
6.3.2 Transformation of <i>P. pastoris</i> and screening.....	118
6.3.3 MSP1 ₁₉ expression	119
6.3.4 MSP1 ₁₉ purification	119
6.4 MSP1 ₁₉ -rusticyanin complex.....	120
6.4.1 Complex purification	120
6.4.2 MSP1 ₁₉ -rusticyanin complex crystal trials.....	120
References.....	121
Supporting publications.....	146
Appendix A.....	147
Appendix B.....	154
Appendix C	155

List of figures

Figure	Page
Figure 1.1 Global maps showing the geographical distribution of malaria and the number of deaths per country	pg. 11
Figure 1.2 The life cycle of <i>P. falciparum</i> .	pg. 12
Figure 1.3 The life cycle of <i>Toxoplasma gondii</i> .	pg. 23
Figure 2.1 The stages of drug development.	pg. 28
Figure 2.2 The crystallisation of proteins.	pg. 35
Figure 2.3 A schematic view to describe Bragg diffraction.	pg. 37
Figure 2.4 Demonstration of different X-ray sources	pg. 40
Figure 3.1 The structure of cytochrome <i>bc</i> ₁ and its role in the electron transport chain (ETC).	pg. 46
Figure 3.2 A schematic view of the modified Q-cycle.	pg. 49
Figure 3.3 The structures of atovaquone and several 4(1H)-pyridones.	pg. 51
Figure 3.4 The chemical structure of endochin and related quinolones.	pg. 55
Figure 3.5 Structures of several further compounds shown to bind cyt. <i>bc</i> ₁ .	pg. 56
Figure 3.6 Alignment between human and bovine cytochrome <i>b</i> amino acid sequences.	pg. 59
Figure 3.7 Chromatographic purification of bovine cytochrome <i>bc</i> ₁	pg. 61
Figure 3.8 A typical result from PEG fractionation.	pg. 62
Figure 3.9 Crystals hits using lipidic cubic phase cyt. <i>bc</i> ₁ .	pg. 64
Figure 3.10 Cytochrome <i>bc</i> ₁ sitting drop crystal hits in complex with 4(1H)-pyridones.	pg. 65

Figure 3.11 Binding of 4(1H)-pyridones to bovine cytochrome <i>bc</i> ₁ .	pg. 67
Figure 3.12 View of the 4(1H)-pyridones overlaid bound in the Q _i site of bovine cytochrome <i>bc</i> ₁ .	pg. 68
Figure 3.13 Several examples of cytochrome <i>bc</i> ₁ crystals grown in complex with MJM 170 at 4 °C.	pg. 70
Figure 3.14 Binding of MJM 170 within the Q _i site.	pg. 71
Figure 3.15 View of MJM 170 bound to cytochrome <i>b</i> .	pg. 72
Figure 3.16 Sequence alignment of mammalian and apicomplexa cytochrome <i>b</i> .	pg. 73
Figure 3.17 Homology models of cytochrome <i>b</i> .	pg. 74
Figure 3.18 Overlaid Q _i sites of bovine, <i>P. falciparum</i> and <i>T. gondii</i> cytochrome <i>b</i> .	pg. 75
Figure 3.19 View of GW844520, GSK932121 and MJM 170 bound in the Q _i site superposed	pg. 76
Figure 3.20 Effects of inhibitors on HEK92 cell viability when grown in different media.	pg. 78
Figure 3.21 Conserved residues between bovine and apicomplexa parasites in the Q _i site shown using the bovine structure.	pg. 80
Figure 3.22 Overlaid homology models of both apicomplexa cytochrome <i>b</i> protein over the bovine cytochrome <i>b</i> structure.	pg. 81
Figure 4.1 Cleavage of the MSP1 polypeptide.	pg. 85
Figure 4.2 MSP1/6/7 complex and subsequent shedding.	pg. 86
Figure 4.3 Solution structure of MSP1 ₁₉ .	pg. 88
Figure 4.4 Structure of the cupredoxin rusticyanin.	pg. 89
Figure 4.5 Purification of rusticyanin.	pg. 91
Figure 4.6 Typical rusticyanin crystals in 3 µl drops.	pg. 92
Figure 4.7 High resolution electron density of rusticyanin.	pg. 94

Figure 4.8 | Purification of *P. falciparum* MSP1₁₉. *pg.* 95

Figure 4.9 | Size-exclusion chromatography demonstrating MSP1₁₉-rusticyanin complex formation. *pg.* 96

Figure 4.10 | SDS-PAGE and western blot analysis of the MSP1₁₉-rusticyanin complex. *pg.* 97

List of tables

Table	Page
Table 1.1 A summary of current antimalarial compounds discussed in this chapter.	<i>pg.</i> 18-19
Table 2.1 Blockbuster drugs developed using structure based drug design.	<i>pg.</i> 30
Table 3.1 Composition of eukaryotic cytochrome <i>bc</i> ₁ , including topology and function of subunits.	<i>pg.</i> 45
Table 3.2 Typical yield of cytochrome <i>bc</i> ₁ throughout the purification process.	<i>pg.</i> 62
Table 3.3 Crystallographic statistics for cytochrome <i>bc</i> ₁ structures in complex with the 4(1H)-pyridones GW844520 and GSK932121.	<i>pg.</i> 66
Table 3.4 Crystallographic statistics for the structure of cytochrome <i>bc</i> ₁ in complex with the novel 4(1H)-quinolone MJM 170.	<i>pg.</i> 70
Table 4.1 Table demonstrating different rusticyanin mutants and their altered biochemical properties.	<i>pg.</i> 90
Table 4.2 Tale of crystallographic statistics for native rusticyanin.	<i>pg.</i> 93

Glossary of abbreviations

Abbreviations	Full name
2Fe-2S	iron-sulphur cluster
3D	three dimensional
ACE	angiotensin-converting enzyme
ACT	artemisinin-based combination therapy
ADMET	absorption, distribution, metabolism, excretion, toxicity
Amp	ampicillin
ATP	adenosine triphosphate
BMGY	buffered-glycerol minimum media
BMMY	buffered-methanol minimum media
CCD	charge-coupled device
CV	column volume
cyt. <i>b</i>	cytochrome <i>b</i>
cyt. <i>bc</i> ₁	cytochrome <i>bc</i> ₁
DM	n-decyl β -D-maltoside
DDM	n-dodecyl β -D-maltoside
DDT	dichloro-diphenyl-trichloroethane
DEAE	diethylaminoethyl
DHFR	dihydrofolate reductase
DHPS	dihydropteroate synthase
DLS	Diamond Light Source
DMSO	dimethyl sulphoxide
DTT	dithiothriitol
EDTA	ethylenediaminetetraacetic acid
EGF	epidermal growth factor
ELQ	endochin-like quinolone
ETC	electron transport chain
Fab	fragment antibody binding
FADH	flavin adenine dinucleotide
FF	fast flow
FTIH	first time in human study

G418	G418 disulphate salt
GMEP	Global Malaria Eradication Program
GPI	glycophosphatidylinositol
HECAMEG	6-O-(N-Heptylcarbamoyl)-methyl- α -D-glucopyranoside
HF	high-fidelity
HG	hexyl β -D-glucopyranoside
HTP	high-throughput
IMM	inner mitochondrial membrane
IMS	inter mitochondrial space
IPTG	isopropyl β -D-1-thiogalactopyranoside
IRS	indoor residual spraying
ITC	isothermal calorimetry
ITN	insecticide treated nets
KPi	phosphate bufer
LB	lysogeny broth
MAP	Malaria Atlas Project
MD	minimal dextrose media
MMV	Medicines for Malaria Venture
MSP	merozoite surface protein
MWCO	molecular weight cut off
NADH	nicotinamide adeninedinucleotide
NaPi	sodium phosphate buffer
NCE	new chemical entity
OD	optical density
PAGE	polyacrylamide gel electrophoresis
PCR	polymerase chain reaction
PDB	Protein Data Bank
PEG	polyethylene glycol
PG	prep grade
PMSF	phenylmethanesulfonyl flouride
PNGaseF	peptide-n-glycoside F
RBC	red blood cell
RMS	root mean square

ROS	reactive oxygen species
SAXS	small-angle X-ray scattering
SBDD	structure based drug design
SDS	sodium dodecylsulphate
SEC	size-exclusion chromatography
SOC	super optimal broth with catabolite repression
SP	sulphopropyl
SUB	subtilisin-like serine protease
UM	undecyl β -D-maltoside
WHO	World Health Organisation
YPD	yeast peptone dextrose media
$\Delta\Psi_m$	membrane potential

Chapter 1 | **Malaria and Toxoplasmosis**

The apicomplexa parasites *Plasmodium spp.* and *Toxoplasmosa gondii* are the pathogens responsible for the diseases malaria and toxoplasmosis respectively. Both of these illnesses can be highly incapacitating and may be lethal. The drugs currently used in the treatment of these diseases have various limitations including high cost, adverse side effects, and are declining in efficacy as result of the emergence of parasite resistance.

1.1 Malaria

Malaria is a catastrophic illness endemic to many of the poorest regions of the world. It is a mosquito-borne disease caused by protozoan apicomplexa parasites of the genus *Plasmodium*. The evidence for cases of malaria and its characteristic fever can be traced back to pre-history and the disease was once found on every continent of the world, excluding Antarctica (Neghina et al. 2010). The first direct evidence of the *Plasmodium spp.* parasite and its role in malaria came in 1880. Charles Louis Alphonse Laveran, who would later win the Nobel Prize in 1907 for his work, described the parasite from microscopy of red blood cells from a patient who had recently died (Laveran 1881). Sir Ronald Ross identified mosquitos as the parasite vector in 1897 when he recognised *Plasmodium* in both the mid gut and salivary glands of mosquitos (Ross 1902). Sir Ronald Ross went on to determine key aspects of the malaria life cycle in birds and was awarded the Nobel Prize in 1902. Since then, despite an increased understanding and the relatively large amount of resources that have been targeted against malaria, the disease continues to affect approximately two billion people worldwide (Snow et al. 2005). There are approximately five million cases a year of which 1.2 million people die. The majority of those who die are children under the age of 5 and pregnant women (World Health Organization 2011). The costly burden of malaria puts strain on national resources and halts development within these countries which further exacerbates the problem (Bremam 2001; Gallup & Sachs 2001).

Malaria symptoms are typically flu-like and include fever, chills, sweating and headaches (Bartoloni & Zammarchi 2012). Symptoms present

after an incubation period within the host that varies in time; typically between 8 and 30 days. The malarial fever is periodic and recurrent. The time between fevers is dependent on the species of *Plasmodium* causing the infection varying from almost daily fevers in *P. falciparum* to months in between fevers for *P. malariae*. Severe malaria is almost exclusively caused by *P. falciparum* (also known as falciparum malaria) due to the unique presentation of sequestration (Dondorp et al. 2004). This occurs as mature forms of the parasite within red blood cells (RBCs) alter the surface properties of the cell causing them to adhere to the endothelium and block blood vessels (Dondorp et al. 2004; Bignami & Marchiafava 1894). This adherence causes damage to various organs which may result in renal failure, respiratory failure, anaemia, jaundice or coma as a result of cerebral malaria (Bartoloni & Zammarchi 2012).

1.1.1 Plasmodium parasites

There are many species of the protozoan *Plasmodium* that infect a variety of animal species including many primates, rodents and birds. Humans are affected by several *Plasmodium* species but two species in particular account for the majority of infections and deaths: *P. falciparum* and *P. vivax* (Carter & Mendis 2002). *P. falciparum* is by far the most lethal of the human infecting species and is highly endemic in sub-Saharan Africa affecting some of the world's most vulnerable people (Figure 1.1) (Snow et al. 2005). *P. vivax* is less lethal but remains highly disabling across much of the globe and is a somewhat neglected malaria (Figure 1.1) (Baird 2007; Gething et al. 2012). This species is not as common in Africa but remains present in South America, India and South East Asia and is capable of surviving at lower temperatures than *P. falciparum*, which extends its range of infection (Gething et al. 2011). *P. vivax* also forms hypnozoites that can remain undetected in the liver for weeks, months or years before reactivation and the subsequent recurrence of fever (Krotoski et al. 1982).

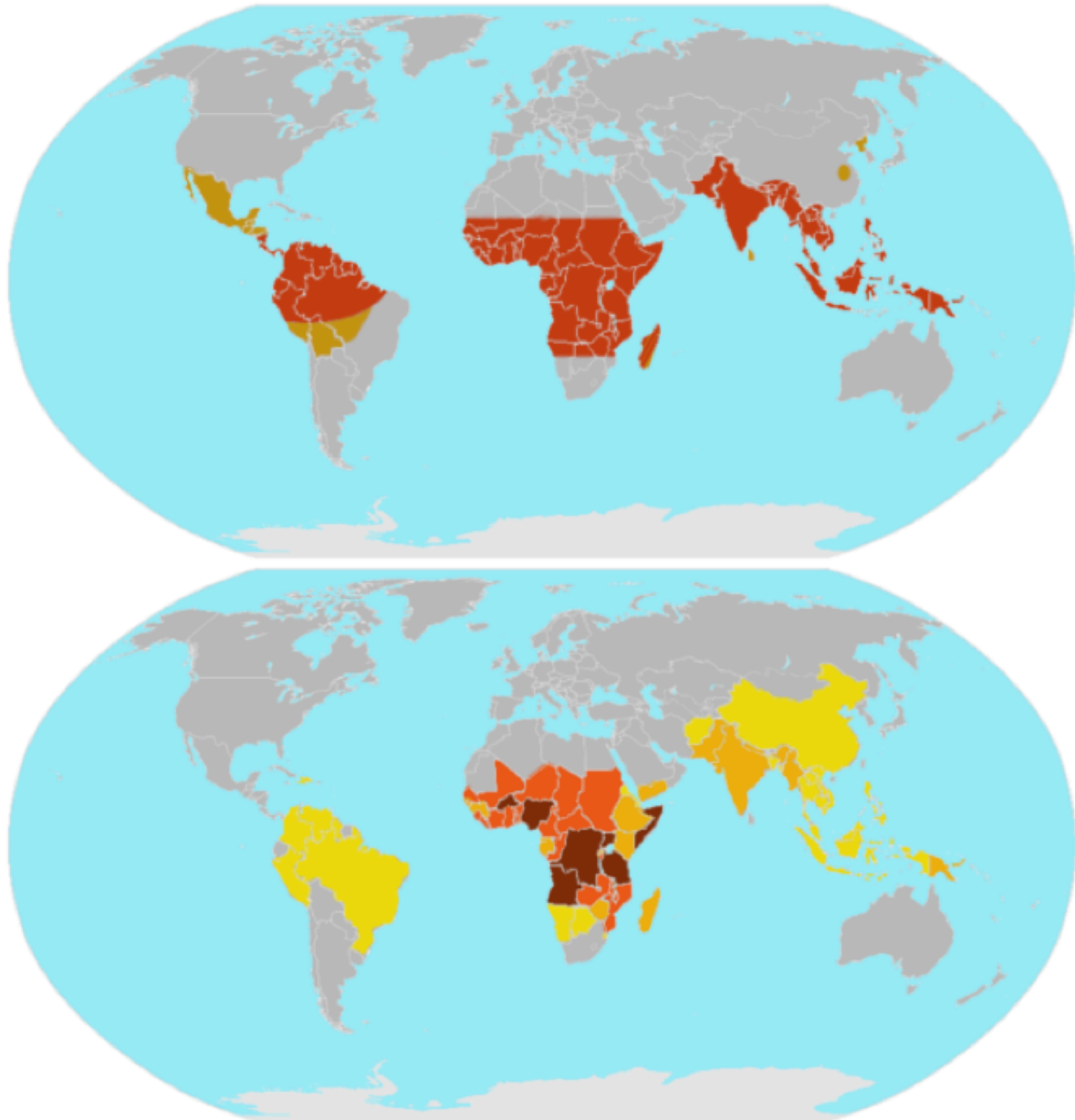


Figure 1.1 | Global maps showing the geographical distribution of malaria and the number of deaths per country. **above** The geographic extend of *P. falciparum* is shown in red and the distribution of *P. vivax* in orange. In countries where both are present, only *P. falciparum* is shown. **below** Countries are coloured by reported indigenous deaths due to malaria (as recorded in the WHO malaria report (World Health Organization 2014)). Yellow indicates between 0 – 50 deaths, orange for 51 – 500 deaths, red shows 501 – 5000 and dark red greater than 5000. The Democratic Republic of Congo makes up greater than 30,000 malaria deaths per year.

1.1.2 The *P. falciparum* life cycle

Like all *Plasmodium* spp., the *P. falciparum* parasite has a complex life cycle that requires both a host and mosquito vector (Figure 1.2). The female *Anopheles gambiae* mosquito is particularly prevalent in the spread of *P. falciparum*; the male does not feed on blood (Fontenille & Simard 2004). Human infection begins when an infected mosquito bites the host. This spreads sporozoites to the host from the mosquito's salivary glands, which quickly accesses the bloodstream and spread to the liver where they infect the hepatocytes in a matter of minutes. Upon entering the hepatocytes the sporozoites differentiate and become trophozoites within a parasitophorous

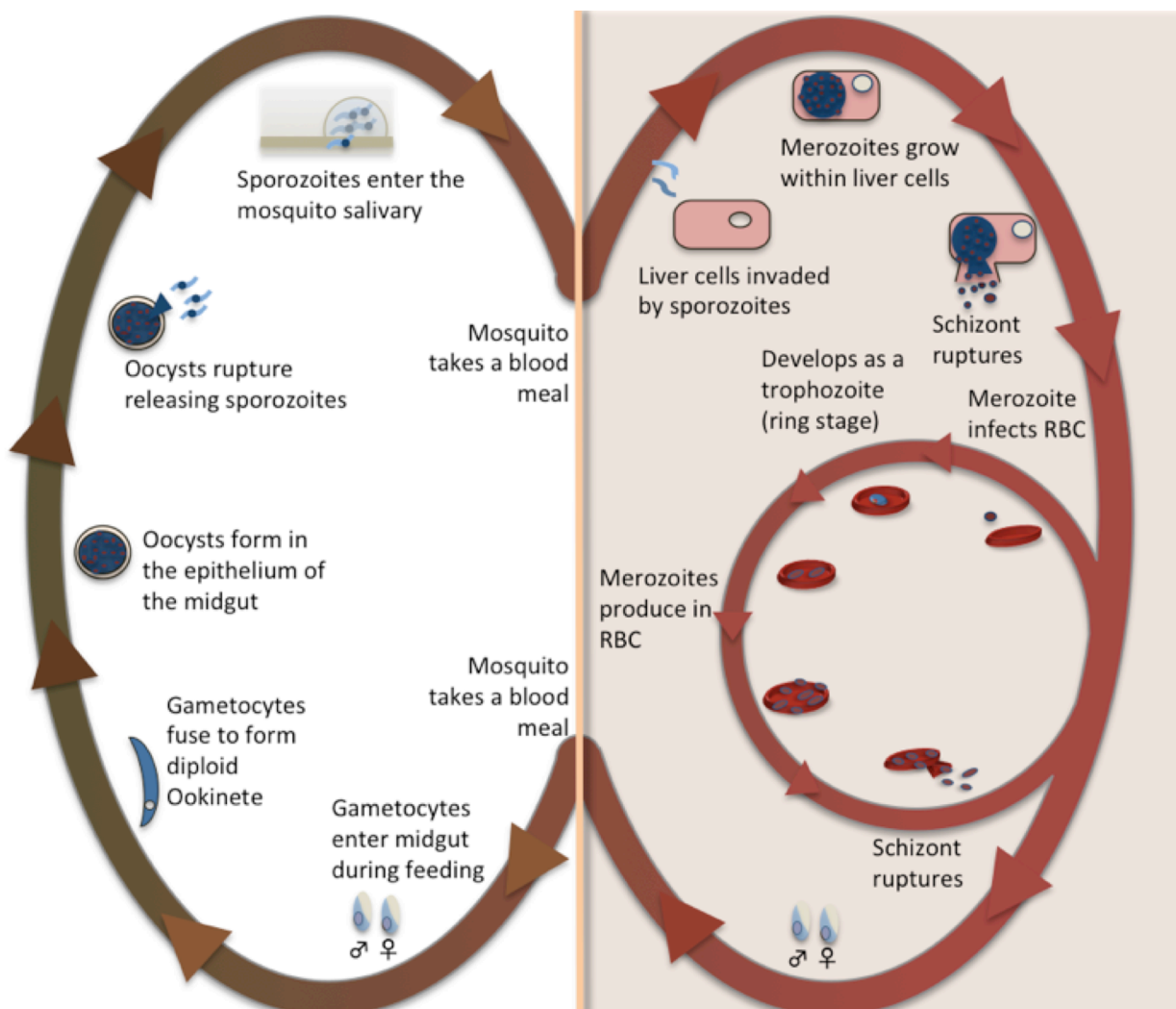


Figure 1.2 | The life cycle of *P. falciparum*. The parasite life cycle takes place across two organisms as indicated by the line dividing the figure and is described in detail in the main body of text.

vacuole where they multiply and eventually become merozoites. The infection remains asymptomatic for around five and a half days yielding tens of thousands of merozoites which then emerge and proceed to invade RBCs before returning to a trophozoite form where it grows into a schizont. The schizonts replicate and produce between 8 – 20 new merozoites every 48 hours. The merozoites rupture the RBCs, exit and quickly attach to and infect more RBCs. This stage of the life cycle is primarily responsible for the pathology of malaria.

Within the RBCs, some of the parasites differentiate into gametocytes through gametocytogenesis. These cells are non-pathogenic and remain in the blood cells until ingestion by a mosquito for further development. Upon ingestion the cells fuse to form a genetically unique zygote that then develops into an ookinete. It is possible for gametocytes from different parental parasites can fuse depending on the frequency of the blood meal. The ookinete exits the midgut and further develops to produce sporozoites in the *Anopheles* salivary gland that await the opportunity for further human infection.

1.1.3 Efforts for the control and elimination of malaria

Control, elimination and eradication of malaria have been the goals of global health organisations and local governments for decades (Greenwood et al. 2008; Mendis et al. 2009; Nájera et al. 2011). Overall, this has resulted in a largely successful reduction of the geographic spread of malaria. The continents of North America and Europe were both identified as malaria free in the second half of 19th century. In 1955, following the development of the insecticide dichloro-diphenyl-trichloroethane (DDT) and the antimalarial drug chloroquine, the World Health Organisation (WHO) began “The Global Malaria Eradication Project (GMEP)” with the opportunistic aim eradicating malaria from the globe (Mayo & Brady 1955). Despite success in eliminating malaria in 79 countries worldwide, the project proved too ambitious and was abandoned in 1969 after fourteen years in favour of malaria control (World

Health Organization 1969). This failure was a result of rising resistance to both chloroquine and DDT, and increased resurgence due to inadequate prevention, monitoring and local health care (Roberts et al. 2000; Nájera et al. 2011). Total eradication no longer seemed a realistic goal and so malaria control became the principal strategy in endemic countries.

Efforts against malaria increased again in early 1990s, as the global burden of malaria reached a peak (Snow et al. 2001). The Roll Back Malaria Partnership began work towards malaria control and elimination in several countries and has resulted in the Global Malaria Action plan. With the development of new tools and resources such as the Malaria Atlas Project (MAP) (Hay & Snow 2006), successes in burden reduction of several countries (Nyarango et al. 2006), and renewed public interest, malaria eradication appears to be possible but only if the lessons of previous attempts have been learnt (Mendis et al. 2009; Lines et al. 2007). There have also been renewed calls for malaria eradication supported by national and international bodies beginning with the Bill and Melinda Gates foundation in 2007 (Bill and Melinda Gates Foundatin 2007).

There are however, several worrying considerations. Global warming is allowing *P. falciparum* to extend its geographic spread and return to areas where malaria had previously no longer been endemic (Siraj et al. 2014; Caminade et al. 2014). Global programs for control and elimination also require strong international and national leadership in the form of representation and economic support (Nahlen & Low-Beer 2007; Njau et al. 2009). Drug resistance has prevented the Global Malaria Eradication Project from reaching its goal after 14 years and has plagued all new insecticides and drugs that have been developed since.

1.1.4 Malaria treatment and prevention

Combatting malaria is a complex problem that will require a multi-vector solution. In the long term, infrastructure in endemic countries needs

to be improved to allow better monitoring, increased hygiene and faster response times (Breman 2001; Carter & Mendis 2002; Rafael et al. 2006; Chareonviriyaphap et al. 2000). In the short term, both control of the vector, *Anopheles*, and the *Plasmodium* parasite is necessary to help reduce the emergence of resistance to any one course of action.

1.1.4.1 Ecological vector control

There are several strategies against *Anopheles* that have been used to limit their numbers and therefore the spread of malaria. Mosquitos have been targeted and displaced from local areas through the removal of still water that acts as breeding grounds or the introduction of fish to eat the larvae before they are able to grow into adult mosquitos (Keiser et al. 2005; Chandra et al. 2008). Genetically modified mosquitos have also been developed and long debated as a way of transmission control through various genetic manipulations (Benedict & Robinson 2003; Marinotti et al. 2013). This has produced a large amount of controversy (Enserink 2010; Alphey et al. 2002).

1.1.4.2 Insecticides and nets

Insecticides have long been used to target the mosquito. DDT was first used for vector control by the US military in World War II and its discoverer Paul Hermann Müller was awarded the Nobel Prize in 1948 (Muller 1946). DDT fell out of favour as an insecticide due to both the emergence of resistance and toxicity issues (Georgopoulos 1954; Roberts et al. 2000). It is however, still used for Indoor Residual Spraying (IRS), a process by which the interior walls of a building are coated with insecticide (Roberts 2007; Roberts et al. 2000). After a blood meal, the mosquito lands on the wall, making contact with the insecticide and dies. This has been shown to greatly reduce vector transmission (Hemingway 2014). Nets can also be used over beds to prevent the infection of sleeping individuals and are particularly useful when combined with insecticides as Insecticide Treated Nets (ITNs) (Phillips-Howard et al. 2003; Alonso et al. 1991). Black market bed nets and

unregulated agricultural use of insecticides have led to the development of resistance to even the latest insecticides (Edi et al. 2012; Elissa et al. 1993). DDT has recently been reintroduced for IRS and research is on going into newer, more long-term insecticides for use with ITNs. Entomopathogenic fungi have recently been suggested as a biopesticide for use with ITNs to infect young mosquitos in the wake of the failing current insecticides (Thomas & Read 2007; Knols et al. 2010).

1.1.4.3 Vaccination

Work on a malaria vaccine has been on going for decades (Crompton et al. 2010). Producing an efficacious vaccine has proven difficult due to the parasite's complex life cycle and large antigenic diversity (Florens et al. 2002; Gardner et al. 2002; Scherf et al. 2008). Several approaches have been used in vaccine development targeting different stages of the life cycle with little success. Recently, the vaccine RTS,S/AS01 (trade name Mosquirix™) has concluded phase III clinical trials and has been approved by the European Medicines Agency (European Medicines Agency 2015). It has substantially reduced cases of malaria in children (RTS 2015) although vaccine efficacy does decrease over time (Agnandji et al. 2014). Vaccines can also prove costly and their deployment requires country-by-country agreement as well as adequate infrastructure (Geels et al. 2011).

1.1.4.4 Drug treatment and prophylaxis

Drug development against *Plasmodium* proves difficult for many of the same reasons as vaccine development. During each stage of its life cycle, the parasite undergoes dramatic proteomic shifts meaning several targets that are present in one stage will not be present in others (Florens et al. 2002). Drug resistance has been seen in *Plasmodium* against all current treatments (Pradines et al. 2006). Resistance can emerge rapidly to monotherapy treatments and so combination therapies have become ubiquitous. This increases the price of treatment but helps combat resistance and was issued as guidance against malaria by WHO in 2006 with regards to Artemisinin

monotherapy (Kremsner & Krishna 2004; World Health Organization 2006). What follows is a brief description of the four principle classes of antimalarial compound. These compounds are summarised in Table 1.1.

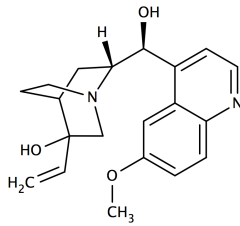
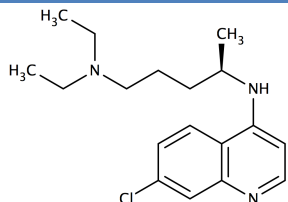
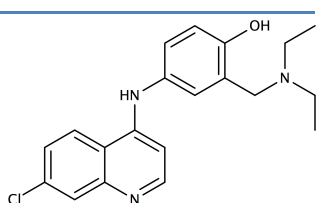
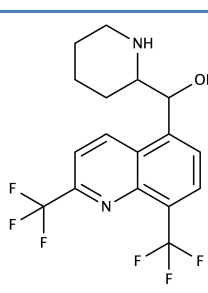
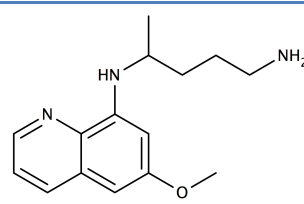
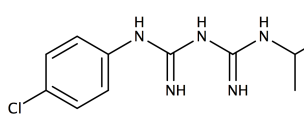
Quinolines

Quinolines are a class of antimalarial medication thought to act through the inhibition of hemozoin biocrystallisation resulting in an increased level of free heme within the RBCs (Warhurst & Hockley 1967; Slater & Cerami 1992). The increase in toxic free heme is lethal to the reproducing merozoites. Chloroquine was developed in the early 20th century as a synthetic substitute for quinine and became the key treatment and prevention of malaria. Due to its low cost and high efficacy, it was used in early attempts at malaria eradication as a monotherapy. Since then, several other quinolones have been developed which are believed to act in a similar manner (Sullivan et al. 1998). These include amodiaquine, mefloquine and primaquine. Resistance to chloroquine took some time to develop but first emerged in South East Asia and is now widespread in *P. falciparum* (Harinasuta et al. 1965; Wongsrichanalai et al. 2002). It is still used as treatment of some cases of *P. vivax* in certain regions of the world, in part due to its low cost (Wellems & Plowe 2001; Laufer et al. 2006). Resistance is also present against all other quinoline derivatives. The rise of *P. falciparum* resistance in Africa resulted in a much higher mortality than elsewhere (Trape et al. 1998). Several of the quinoline compounds produce adverse side-effects in a number of patients which reduces their use (Owens & Ambrose 2005; Kotecka 2015).

Antifolates

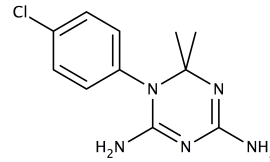
Antifolates including proguanil (Carrington et al. 1951) and cyloguanil, sulfadoxine (Laing 1964) and pyrimethamine (Russel & Hitchings 1951) have been widely used and act to interrupt the folate pathway in *Plasmodium* (Nzila 2006). By inhibiting dihydrofolate reductase (DHFR) or

Table 1.1 | A summary of current antimalarial compounds discussed in this chapter, their mode of action and a description of resistance.

Type of drug	Name	Structure	Mode of Resistance
<p>Quinoline</p> <p>Believed to function through inhibition of heme biocrystallisation leading to build up of toxic heme and parasite death</p>	Quinine		<p>Quinoline resistance is fairly complex. It appears to arise as a result of lower uptake of quinolones into the parasite food vacuole preventing access to the free hemozoin. Multiple mutations to various proteins have been linked to this but the mechanism remains unclear.</p>
	Chloroquine		
	Amodiaquine		
	Mefloquine		
	Primaquine		
<p>Antifolates</p> <p>Inhibitors of enzymes that are key for folate biosynthesis.</p>	Proguanil		<p>Point mutations in DHFR and DHPS are responsible for the failure of these compounds (Cowman et</p>

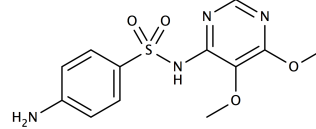
Folate compounds are later required for a range of uses but it is the lack of pyrimidine biosynthesis that is lethal to *Plasmodium spp.*

Cycloguanil

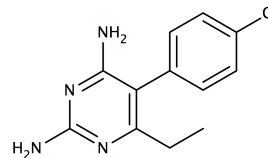


al. 1988; Peterson et al. 1988)

Sulfadoxine



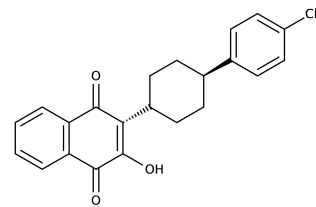
Pyrimethamine



Hydroxynaphthoquinone

Binds and inhibits the Q_o site of cyt. *bc*₁ causing the collapse of mitochondrial membrane potential.

Atovaquone

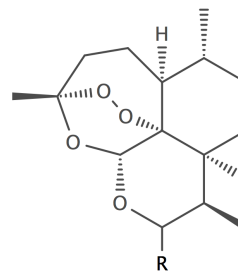
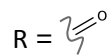


A single point mutation in the Q_o site of cyt. *b* appears to prevent atovaquone binding (Srivastava et al. 1999).

Artemisinin

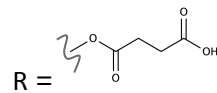
The exact mechanism remains unknown. Endoperoxide bridge found to be the essential moiety and linked with depolarisation of mitochondrial membrane.

Artemisinin

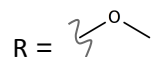


Mutations in the K-14 propeller protein are associated with resistance as molecular marker (Ariey et al. 2014). The mechanism remains unknown.

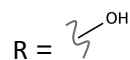
Artesunate



Artemether



Dihydroartemisinin



dihydropteroate synthase (DHPS) downstream pyrimidine and purine biosynthesis are stalled. These drugs are therefore effective across all life stages of the parasite. The antifolates have been shown to be susceptible to resistance as a result of slow elimination (Peterson et al. 1988; Peterson et al. 1990; Nzila et al. 2000; Gregson & Plowe 2005)

Hydroxynaphthoquinones

Atovaquone is the only current hydroxynaphthoquinone licensed for malaria treatment and prophylaxis (Looasreesuwon et al. 1999). The drug was a result of rational drug design by GSK (Gutteridge 1989) and is marketed as Malarone™ when sold in combination with proguanil. It is one of the most popular medications for prophylaxis amongst travellers (Nixon, Moss, et al. 2013). Atovaquone is a ubiquinone analogue that acts on the cytochrome *bc*₁ complex (cyt. *bc*₁) of the parasite mitochondria by inhibiting the Q_o site (Fry & Pudney 1992; Siregar et al. 2015; Birth et al. 2014). Resistance emerges rapidly when used as a monotherapy and a single point mutation within the Q_o site of the cytochrome *b* (cyt. *b*) gene prevents atovaquone action (Korsinczky et al. 2000; Fisher & Meunier 2008). As its mechanism of action is fairly well understood, cyt. *bc*₁ is a strong, validated target for next-generation antimalarials (Barton et al. 2010). Research has continued into the hydroxynaphthoquinones and has resulted in several antimalarial compounds that require further development (Schuck et al. 2013; Kessl, Moskalev, et al. 2007; El Hage et al. 2009).

Artemisinin Combination Therapies

Artemisinin had been used to treat malaria as a herbal tea for millennia and now forms the basis of artemisinin-based combination therapies (ACTs). It was first extracted and identified from the tree *Artemisia annua* in 1972 (Qinghaosu Antimalarial Co-ordinating Research Group 1979) by Chinese scientists and has been proven to be a rapid and potent antimalarial (Klayman 1985). Its synthetic derivatives artesunate, artemether and dihydroartemisinin have also proven highly effective. The

peroxide bridge located within the compound is thought to be the essential moiety. The mode of action is largely unknown, although evidence points to the parasite mitochondria as its site of action, where the generation of reactive oxygen species (ROS) and the collapse of mitochondrial polarisation appear to be important (Wang et al. 2010; Antoine et al. 2013). Artemisinin is a rapid action drug and usually used in combination with a longer acting compound to prevent recurrence. Resistance has been seen in South East Asia and is spreading quickly through an, as of yet, unknown mechanism (Dondorp et al. 2009; Phyo et al. 2012). ACTs currently form the gold standard of treatment in the majority of countries against malaria and if resistance were to arise in *P. falciparum* populations in Africa, the results could be highly damaging (Maude et al. 2010). Multiple methods to avoid resistance have been suggested including the use of triple combinations including artemisinin, which would help combat resistance but make the treatment cost even more prohibitive to many in developing countries (Shanks et al. 2014). Another method recently suggested is the use of whole plant extract which appears to maintain high potency but with reduced rate of resistance (Elfawal et al. 2015).

There are many drugs currently in development against malaria based on existing scaffolds and some with novel modes of action (Held et al. 2015). Those novel compounds are of particular interest as resistance to these is less likely under current selection pressure. A large number of these are supported by the Medicines for Malaria Venture (MMV) and are published along with their current stage of development (Held et al. 2015; Wells et al. 2015; Wells & van Huijsduijnen 2015).

1.2 Toxoplasmosis

Toxoplasmosis is caused by the protozoan *T. gondii* and affects approximately one third of the worlds population (Torgerson & Mastroiacovo 2013; Flegr et al. 2014). It has a near global distribution and is particularly prevalent in tropical regions (Dubey et al. 2012). The majority of

infections remain asymptomatic and go unnoticed as latent toxoplasmosis (Robert-Gangneux & Dardé 2012). In infections of pregnant women it can cause the birth of infants with congenital disease or abortion (Montoya & Remington 2008). The congenital disease can cause both blindness and mental retardation in infants. In immunocompromised patients, such as those suffering from acquired immune deficiency syndrome (AIDS), toxoplasmic encephalitis can occur causing severe brain damage (Luft & Remington 1992; Snider et al. 1983). Latent toxoplasmosis alters the behaviour of infected animals resulting in an increased transmission rate. Rodents that are infected show slower reaction times, reduced cognitive learning and memory and changes in the olfactory system resulting in “fatal attraction” to cat’s urine (Berdoy et al. 2000). Several studies have been carried out in an attempt to determine any mental changes that occur in infected humans (Flegr 2013). These have indicated a link between the presence of *T. gondii* and schizophrenia as well as an increased number of traffic accidents (Flegr et al. 2002; Torrey et al. 2007).

1.2.1 Life cycle

The *T. gondii* life cycle consists of two parts and has been extensively reviewed elsewhere (Dubey 1998; Dubey 2009; Black & Boothroyd 2000). An asexual cycle within a warm blooded mammalian host and a sexual cycle that obligately occurs within a feline (Figure 1.3). Once infected, usually from a rodent meal, the parasites differentiate into infective merozoites before entering the sexual stage and forming zygote-containing cysts. These cysts are called oocysts and develop within the epithelium of the feline intestinal wall. The epithelium ruptures causing the exit of oocysts within the faeces. The oocysts then spread within the environment where they can remain infective for several months. In household cats, oocysts can remain viable as spores in litter trays for up to two weeks and can pose a threat to pet owners, particularly pregnant women (Dubey et al. 2011).

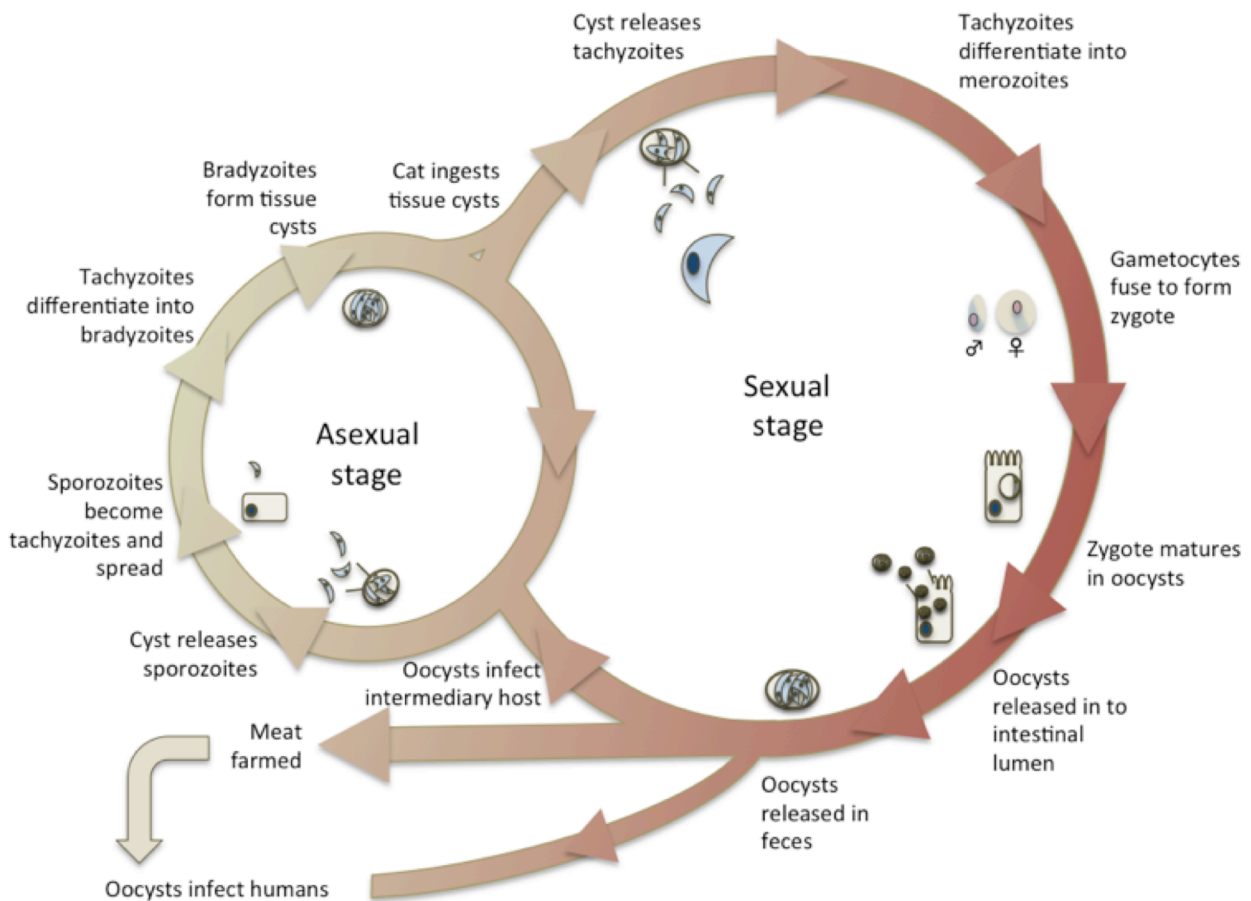


Figure 1.3 | The life cycle of *Toxoplasma gondii*. The sexual stage must taken place in a feline host whilst the asexual stage can take place in almost any warm blooded animal. Humans can be infected directly by oocysts dispersed by cat faeces or as a secondary infection from tissue cysts ingested from animal meat.

Upon infection of an intermediate host, either by ingestion of contaminated food or contact with feline oocysts, cysts rupture. This occurs as a result of the digestive properties of the stomach and releases sporozoites. The sporozoites then embed themselves within the epithelium of the small intestine and differentiate into tachiozoites, the acute, infective form of the parasite. The tachiozoites replicate within a parasitophorous vacuole until rupturing from the host cell and spreading to all organs within the host. Pressure from the host immune system then causes the tachiozoites to differentiate into bradyzoites that grow slowly in clusters within the host tissues as tissue cysts and remain semi dormant. These cysts can form within any organ but are primarily found in striated muscle, eye or brain tissue.

Cysts may remain present in the host for its entire life and result in continuous cycles of rupture and cyst formation.

Human infection occurs either as a result of contact with oocysts from cat faeces or from the consumption of contaminated meat. Non-congenital patients typically show minimal symptoms and rarely suffer. AIDS patients have been historically significant and known to develop toxoplasmosis encephalitis (Luft & Remington 1992; Jones et al. 2002).

1.2.2 Current treatment

The current standard treatment of toxoplasmosis is a synergistic combination of pyrimethamine and sulfadiazine (Montoya & Liesenfeld 2004). Pyrimethamine inhibits the same target as in *P. falciparum*, dihydrofolate reductase (DHFR), whilst, sulfadiazine inhibits dihydropteroate synthase (DHPS). By inhibiting multiple steps of the folate biosynthesis pathway, this combination reduces the availability of folate compounds that are essential for parasite survival. The treatment can also be supplemented with folinic acid to increase efficacy and reduce adverse effects (Van Delden & Hirschel 1996). Due to toxicity, these compounds often cannot be used for an extended period of time in immunocompromised patients (Leport et al. 1988). Resistance can also occur to these compounds and variation in parasite susceptibility is a treatment issue (Meneceur et al. 2008). Recently, Turing Pharmaceuticals acquired U.S. marketing of pyrimethamine tablets and increased the price of a single tablet from \$ 13 to \$ 750 causing a heated debate in the U.S.A (Walters 2015).

Atovaquone is active against tachyzoites at low concentrations and also treats bradyzoites within cysts (Araujo et al. 1992; Ferguson et al. 1994). Atovaquone is also beneficial as it can be used in AIDS patients due to lack of adverse side effects (Kovacs & NIAID-Clinical Center Intramural AIDS Program 1992). Atovaquone acts through a similar mechanism as in *P. falciparum* and has been shown to bind the Q_o site of cyt. *b* within *T. gondii*

cyt. *bc*₁. Unlike in *P. falciparum*, *de novo* pyrimidine biosynthesis is not thought to be the primary mechanism of action and respiration has been seen to be reduced (Pfefferkorn et al. 1993). Drug resistance has been detected through mutations in the Q_o site (Pfefferkorn et al. 1993; McFadden et al. 2000).

1.3 Summary

Both malaria and toxoplasmosis affect some of the world's poorest regions and are the cause for large-scale suffering and death. Despite the huge amount of malaria awareness, it remains one of the largest killers in the world today particularly in the poorer regions of the world where funding does not reach the required level (Mills et al. 2008). Malaria deaths reached a peak in 2004 of 1,817,000 worldwide and 1,613,000 within Africa but have shown a promising decline over recent years (Murray et al. 2012). Though reduced, this is still more deaths worldwide than those caused by traffic accidents (1.24 million deaths each year) (World Health Organization 2013). Global warming and the increasing spread of drug resistance have created a dire need for the development of new compounds that are both easy and cheap to produce whilst remaining effective against drug-resistant malaria. If malaria eradication is to prove a realistic target, an increased range of antimalarial drugs will be an essential tool alongside insecticides, nets and a potential future vaccine as well as improvement in general infrastructure and living conditions. Malaria and toxoplasmosis share a common drug target, cyt. *bc*₁. Inhibition of this target is lethal at all stages of development for both *P. falciparum* and *T. gondii* (Araujo et al. 1992; Fleck et al. 1996). This has made cyt. *bc*₁ a promising target for the development of drugs against these protozoa. Drug development benefits from a clear, strong target and structural information to guide the design pipeline. X-ray crystallography can provide such insights and unambiguously show a drug binding its protein target.

Chapter 2 | **Drug discovery and X-ray crystallography**

The vast majority of drug targets are proteins. By studying the role of a protein in a disease, it can be hypothesised whether a potential drug, or changes to a potential drug, would have a beneficial therapeutic effect. Membrane proteins are estimated to make up 30 % of the human proteome (Krogh et al. 2001) and potentially 60 % of all drug targets (Yildirim et al. 2007; Bakheet & Doig 2009). The membrane bound G-protein coupled receptors (GPCRs) as a class of drug target make up approximately 50 % of drug targets alone (Overington et al. 2006). Drug discovery has historically relied on chance, such as the discovery of penicillin, or the isolation of compounds from natural remedies, for example morphine, without any insight into their molecular action.

2.1 Drug development

The process of taking a lead compound from drug discovery through to a clinically approved pharmaceutical is known as drug development. New chemical entities (NCE) that are produced during this development are first taken through a series of preclinical trials that include characterising the toxicity, pharmacokinetics, metabolism and physiochemical properties of the compound. This information can then be used to direct a first time in human (FTIH) study. After the preclinical work up, the NCE enters the clinical phase. These are increasingly expensive and each stage requires a larger number of people to test both efficacy and toxicity. These trials can take between 6 - 8 years. NCEs can be pulled at any time during trials due to lack of effect or perceived toxicity and surveillance continues throughout the drugs lifetime to assure the absence of long-term toxic effects. The majority of NCEs fail to reach market. The entire process of successfully developing a NCE to a clinical drug has recently been estimated to cost \$2.6 billion (Mullard 2014) as a result of high rate of failure during the expensive clinical trial stage.

2.1.1 Rational drug design

Modern drug discovery has moved away from the serendipitous methods that preceded it and has moved towards rational drug design (Drews 2000). Drug development now begins with the validation of a known molecular target against which a lead compound is identified. This identification usually requires high throughput screening (HTS) *in vitro* or *in silico* using a diverse chemical library. Compounds that appear to prove beneficial, “hits”, can then be optimised through several iterations of modification, testing and analysis into a lead compound (Figure 2.1). The compound is modified through these cycles to improve the efficacy of the hit whilst maintaining several drug-like properties such as “Lipinski’s rule of five” (Lipinski et al. 2001). Lipinski’s rule of five refer to properties that a drug should have if it is to be orally administered. These include a molecular mass of less than 500 Da, less than 5 hydrogen bond donors, less than ten hydrogen bond acceptors and an octanol-water partition coefficient (cLogP) of less than 5.

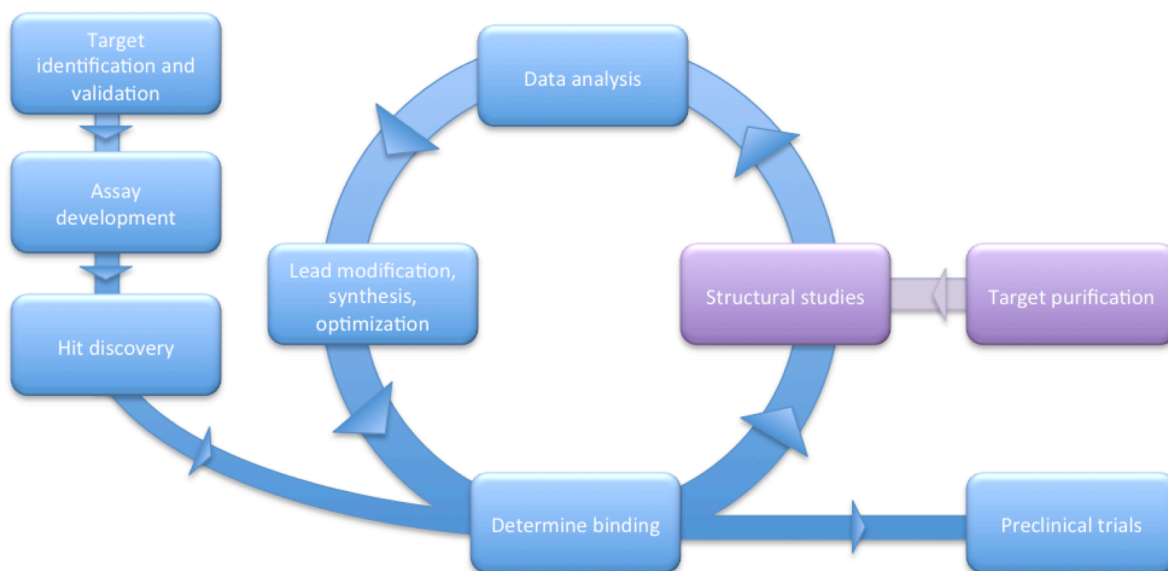


Figure 2.1 | The stages of drug development. After target identification and hit discovery, drug development goes through several rounds of analysis and modification to improve both the efficacy and drug-like properties of the compound. Structure based drug design (SBDD) can assist in this process (boxes in purple) by providing exact information about the binding of compounds and helps to drive rational drug design.

An extension of the rule of five, which defines properties of an effective drug, is Astex's rule of three (Congreve et al. 2003). This attempts to define good lead compounds for initial library screening, which can then be developed into a drug-like compound. These guidelines suggest that the fragment should have a molecular mass of no more than 300 Da, possess no more than three hydrogen bond acceptors, no more than three hydrogen bond donors and that the cLogP should not be greater than 3. Both "Lipinski's rule of five" and the rule of three only serve as guidelines in drug discovery and successful libraries or drugs don't necessarily need to conform to these (Köster et al. 2011; Jhoti et al. 2013).

Compounds can be tailored through this development to assure beneficial absorption, distribution, metabolism, excretion and low toxicity (ADMET) properties in pre-clinical stages. ADMET provides a framework to determine properties of a compound within a that are compatible with a drug-like compound. *In silico* work is now frequently carried out on lead compounds to determine the ADMET properties during development to speed a drugs progress through pre-clinical and clinical trials (van de Waterbeemd & Gifford 2003).

2.1.2 Structure based drug design

Structure based drug design (SBDD) requires a 3D model of the target. Knowledge of a protein's structure allows more input into rational design (Figure 2.1) which can be used to direct the modification of the lead compound. Once the structure is solved, a putative drug-binding site can be identified and then verified with the structure of the protein bound to a hit. The 3D structure of a protein is mostly solved through one of two methods: Nuclear Magnetic Resonance (NMR) or X-ray crystallography. If a structure cannot be solved, it is possible to create a homology model using some 3D homology modelling servers that rely on the structures of previously solved protein structures with significant sequence identity (Hillisch et al. 2004). SBDD has had a huge impact on drug development since its beginning and

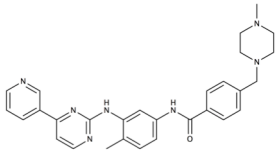
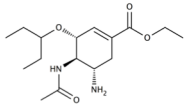
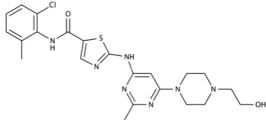
has played a role in bringing multiple pharmaceuticals to market (see Appendix A), including a number of blockbuster drugs (Table 2.1).

Many more compounds are currently being researched using SBDD pipelines, such as those as Contour[®], Vitae (Ishchenko et al. 2012) or the Pyramid[™] platform, Astex (Williams 2011). With the exponential increase in the number of available protein structures, particularly membrane protein structures, SBDD is continuing to grow in its application. This is particularly true with regards to drug discovery against GPCRs as a result of the work done by Heptares Therapeutics (www.heptares.com) to produce stable protein that can be crystallised. Specific research institutes have also been established in order to elucidate human GPCR protein structures (iHuman institute, ShanghaiTech University).

2.1.3 NMR assisted drug discovery

NMR can be used to solve the three dimensional (3D) structure of molecules whilst in solution; a protein crystal is not required. NMR is

Table 2.1 | Blockbuster drugs developed using structure based drug design.

Compound	Structure	Year brought to market	Target disease	Target protein	Reference
Imatinib Glivec™ Novartis		2001	Chronic Myelogenous Leukaemia	BCR-ABL Tyrosine kinase	(Zimmermann et al. 1997)
Oseltamavir Tamiflu™ Roche		1999	Influenza	Viral neuraminidase	(Kim et al. 1998)
Dasatinib Sprycel™ Bristol-Myers Squibb		2006	Chronic Myelogenous Leukaemia	BCR-ABL Tyrosine kinase	(Manley et al. 2005)

dependant on isotope-labelled protein production for the study of macromolecules but proteins over 30 kDa generally prove difficult for NMR. NMR is not highly amenable to the study of membrane proteins, which also precludes it from studying the structures of 60 % of drug targets. NMR is highly suitable for fragment based screening methods as differences in chemical shift can quickly be detected to reveal whether a compound has bound to the protein target and with what affinity (Shuker et al. 1996; Hajduk et al. 1997). NMR also requires less of the molecule to interact with the target to determine a useful hit whereas crystallography can require occupancies as high as 70 % (Jhoti et al. 2013). This can prove useful in HTS before subsequent structure based optimisation using X-ray crystallography.

2.1.4 X-ray crystallography assisted drug discovery

X-ray crystallography allows the study of a protein's 3D structure and can determine the presence of any bound molecules at resolutions that are regularly achieved (Blundell 1996). Unlike NMR there is no upper size limit to the proteins that can be studied. Membrane proteins, though still difficult, can be examined with little or no change to the experimental set up. The first drug brought to market with the assistance of X-ray crystallographic structural information was Captopril, an angiotensin-converting enzyme (ACE) inhibitor primarily used in the treatment of hypertension (Cushman et al. 1977). This was developed using a homologous bovine protein structure as little was known of the ACE proteins at the time. Since then many other compounds have been explored and approved with the assistance of protein crystallography, including multiple HIV drugs in response to the AIDS epidemic (Debouck 1992) and antiviral influenza drugs such as Zanamivir (von Itzstein et al. 1993). The expansion of high throughput-crystallography (Blundell & Patel 2004) has allowed for increased screening of drug-like compounds for little extra cost or time. This makes crystallography useful for screening small chemical fragments as in fragment based drug discovery.

2.2 X-ray crystallography

X-ray crystallography is an incredibly important and versatile tool in the study of protein structure. Of the approximately 112,000 protein structures in the Protein Data Bank (PDB) (Berman et al. 2000), almost 100,000 have been solved using X-ray crystallography compared to 11,000 by NMR, the second largest contributor. It has been stated that “structure is function” and research into a protein’s 3D structure often underpins and gives insight into functional mechanisms. The crystallographic structures provide a useful model for the rational development of drugs through visualisation of the binding environment which can inform further rounds of chemical alteration. As X-ray crystallography has been extensively used in this work, a brief summary of the technique, its development and basic principles are included in this chapter. The extensive details of crystallography have been covered excellently in reviews and textbooks elsewhere (Blundell & Johnson 1976; Rupp 2009; Rhodes 2010).

2.2.1 *A short history of X-ray crystallography*

Crystals have been produced since prehistory but the first recorded protein crystals were produced in 1840 by Friedrich Hünfeld of earthworm haemoglobin. It wasn’t until the discovery of X-rays by W. Röntgen in 1895 (Rontgen 1896) and subsequent work by Max Von Laue and both W. H. Bragg and W. L. Bragg (Bragg 1913; Von Laue 1913) into the nature of X-ray diffraction by crystals, that the idea of structural determination by crystallography became a reality. As a result of this, many inorganic crystal structures were determined. Whilst work into inorganic materials continued, protein crystals began to be produced in earnest; the first enzyme to be crystallised was of urease in 1926 by James B. Sumner. The first diffraction by a “wet” protein crystal was reported in 1934 by John Bernal and Dorothy Hodgkin. In 1958 John Kendrew, with the assistance of Max Perutz, revealed the first protein structure, Sperm Whale Myoglobin (Kendrew et al. 1958).

This began an era of structural biology dominated by X-ray crystallography. David Phillips solved the structure of the first enzyme, lysozyme, in 1965 (Blake et al. 1965). This provided the first structural insight into the functional mechanism of an enzyme. In 1968 the first structure of a human immunoglobulin was solved, which would later have a huge impact on modern pharmaceuticals (Waxdal et al. 1968). Progress continually accelerated and new methods for crystal growth, X-ray generation and data collection were developed. The dawn of recombinant technologies allowed large quantities of proteins to be produced with relative ease and allowed crystallisation to be attempted on new, significantly more complex targets. Dedicated synchrotron light sources were opened to provide users with increasingly bright X-rays. The first such source, the Synchrotron Radiation Source in Daresbury, opened in 1981. In 1985, the first membrane protein structure was solved by Hartmut Michel and colleagues of the photosensitive reaction centre (Deisenhofer et al. 1985). The first structure of a human GPCR was published in 2007 (Rasmussen et al. 2007) with huge implications for the development of drugs owing to their abundance and key role in many diseases.

Progress has continued and the accomplishments of protein crystallography have recently been celebrated during the International Year of Crystallography last year (2014) and the International Year of Light this year (2015). Further improvements to hardware, including third generation synchrotrons (Helliwell & Mitchell 2015; Duke & Johnson 2010), and the development of the X-ray Free Electron Laser (XFEL) (Cohen et al. 2014; McNeil & Thompson 2010; Neutze et al. 2004; Fromme & Spence 2011), which produces X-rays of brightness that has not been achieved before, are propelling the field forward and maintaining its near monopoly in the study of protein structure. These structures, that would have previously been impossible to solve, are being produced using new techniques and more sensitive hardware than ever before to the great benefit of the biophysical sciences and pharmaceutical industry.

2.2.2 Protein crystallisation

The most challenging part of a crystallographic project is often the first: the production of diffracting protein crystals (Chayen & Saridakis 2008; McPherson 1991; McPherson 1985). Protein crystals are required in order to amplify the diffraction signal of the protein of interest. This amplified signal needs to be strong enough to allow detectors to record the diffraction pattern as a series of spots (see section 2.2.3).

Protein crystallisation is a process of precipitation by which protein leaves a solution, first by nucleation and then by crystal growth (Figure 2.2a). Multiple methods have been used and developed in order to produce protein crystals but they all follow the same principle: a slow increase in protein concentration until supersaturation is reached allowing stable nucleation to occur, followed by growth (McPherson 1985). The crystals used in this project were all produced using vapour diffusion in either the sitting or hanging drop procedure (Figure 2.2b, c). The advent of HTP crystal screening robots and crystal viewing hotels has made this process more amenable to even the most difficult targets (Wasserman et al. 2012; Heinemann et al. 2001; O'Reilly et al. 2006; Blundell et al. 2002). Modern laboratories can screen a protein solution against thousands of precipitant conditions using very small amounts of sample (Li et al. 2012; Stock et al. 2005; Zhu et al. 2014).

Membrane protein crystallisation follows the same principles as the crystallisation of a soluble protein. There are however, additional issues. The inherent hydrophobicity of membrane proteins requires the addition of detergent for extraction from a lipid bilayer and further purification (Carpenter et al. 2008; Michel 1983). The detergent micelle that forms around the hydrophobic region of the protein often prevents many protein-protein contacts from forming, which may result in weak diffraction or possibly prevent crystallisation from taking place. There are numerous detergents commercially available that can be screened to improve protein stability (Privé 2007). The lipid cubic phase has been used in crystallisation

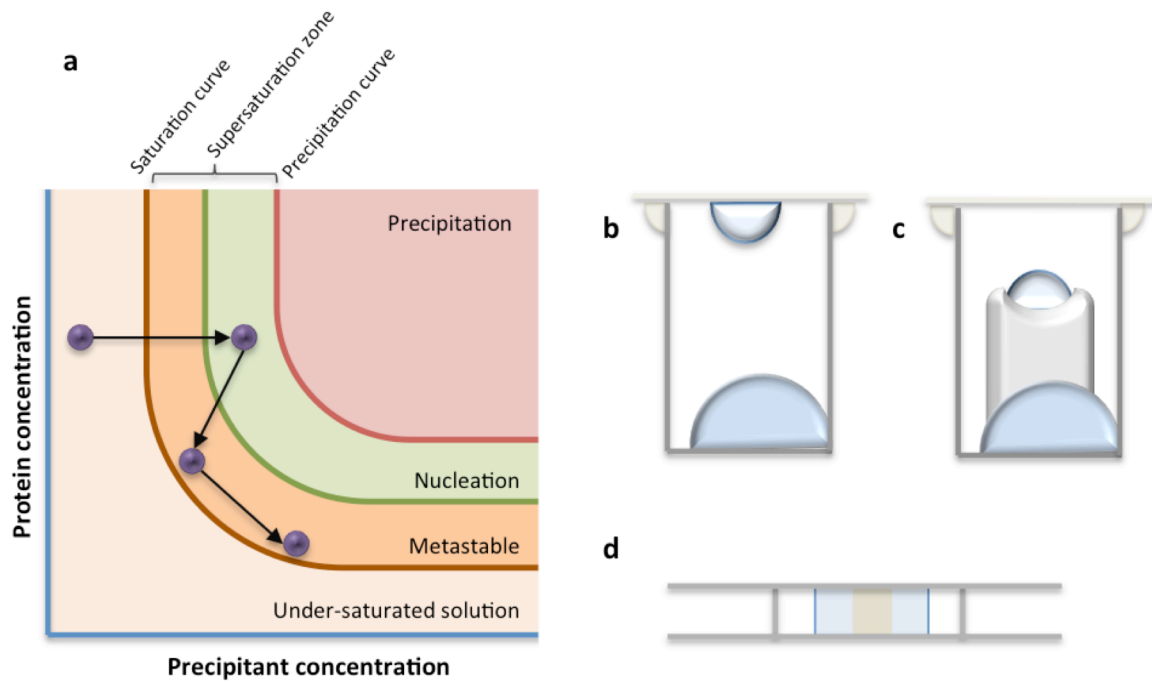


Figure 2.2 | The crystallisation of proteins. **a** A phase diagram depicting crystal nucleation and growth. The aim is to move the conditions into the nucleation zone and then allow crystal growth within the metastable zone. **b** and **c** A schematic diagram of the hanging drop vapour diffusion and sitting drop vapour diffusion techniques for crystal growth. A drop of protein solution is mixed with precipitant solution from the well resulting in a drop of half the precipitant concentration. Vapour then diffuses out of the drop along a concentration gradient slowly increasing the concentration of protein. The wells are sealed with cover slides and grease to create a nearly totally closed environment. **d** An example of lipidic cubic phase (LCP) crystallisation in a sandwich plate. Protein within LCP is covered directly with precipitant solution in batch and sealed under a glass plate to facilitate crystal growth.

in an attempt to overcome some of these limitations and allow crystallisation to take place in a more native-like environment (Figure 2.2d) (Landau & Rosenbursch 1996; Caffrey & Cherezov 2009; Cherezov et al. 2001). This has been used in the successful crystallisation of several novel drug targets (Cherezov et al. 2010). Membrane protein crystals from the same drop are often highly variable in quality and can require more screening than their soluble counterparts before data can successfully be collected and a protein model built.

2.2.3 Crystallographic theory

When placed in an X-ray beam, a crystal will produce a pattern of discrete spots; a diffraction pattern. The incoming X-ray beam is scattered by successive planes within the crystals. If these planes are suitably spaced, constructive interference between the scattered waves takes place producing a diffraction spot. This is dependent on the wavelength of the incoming X-rays (λ), the distance between the planes (d) and the angle of incidence (θ) and is described by Braggs Law (Figure 2.3).

$$n\lambda = 2d \sin \theta$$

Through precession imaging a crystal is rotated within the incoming beam allowing precise degrees of data to be collected and reflections recorded. Each of these reflections is dependent on the scattering direction (\mathbf{S}) and the relative positions of all electrons within the crystal. The scattered wave has amplitude, $|F(\mathbf{S})|$, and phase, $i\Phi(\mathbf{S})$.

$$F(\mathbf{S}) = |F(\mathbf{S})|e^{i\phi(\mathbf{S})}$$

The intensities of each structure factor can be recorded and are directly proportional to the square of the magnitude of each structure factor.

$$I(S) \propto |F(S)|^2$$

The Fourier sum of these structure factors can be used to calculate the electron density $\rho(\mathbf{r})$ at all points of the crystal where \mathbf{r} is a position within the crystal as defined by (x, y, z) .

$$\rho(\mathbf{r}) = \frac{1}{V} \sum F(\mathbf{S}) e^{-2\pi i \mathbf{r} \cdot \mathbf{S}}$$

The phase information however, is lost. This gives rise to the phase problem of crystallography.

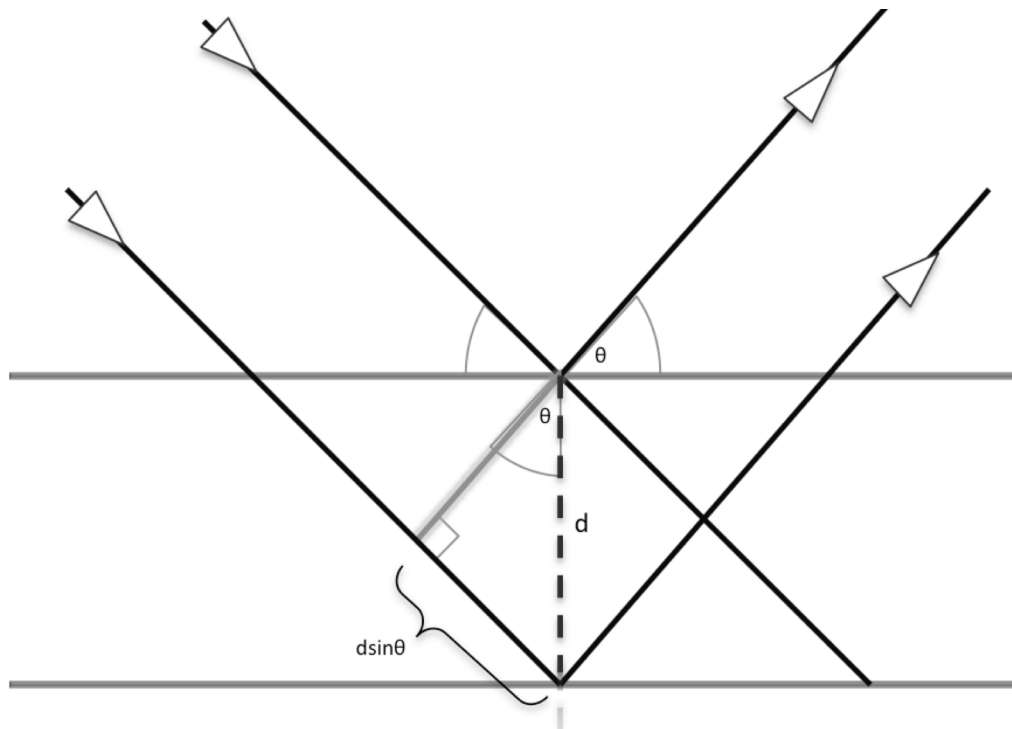


Figure 2.3 | A schematic view to describe Bragg diffraction. To produce constructive interference of the resulting scattered wave, the additional distance travelled by the lower wave, $2d\sin\theta$, must be equal to an integer of λ .

2.2.4 The phase problem

The phase of the structure factor contains vital information required to produce an electron density map. This is effectively demonstrated by Cowtan's example of the Duck and Cat (Taylor 2010; Rupp 2009). In this example the magnitudes of a Fourier transformed duck are combined with the phases from a Fourier transformed cat. The reconstruction of the image using these combined inputs results in the image of a cat. As the phase information is not recorded, it must be determined by other means. Multiple methods have been developed and used to solve the structures of proteins which have been extensively reviewed (Taylor 2003; Hauptman 1991). Though they have largely been used to overcome the phase problem, it can still persist and prevent the elucidation of protein structure.

2.2.4.1 Multiple Isomorphous Replacement

Max Perutz and John Kendrew were the first to show that protein crystals could be modified by the attachment of “heavy” atoms to produce isomorphous heavy atom derivatives. This was first done on haemoglobin and was later used to solve the structure of myoglobin (Green et al. 1954; Kendrew et al. 1958). The resulting diffraction of these derivatives produce diffraction patterns with altered intensity of the resulting reflections. These differences in intensity can then be used to calculate the positions of the heavy atoms within the crystal lattice to generate initial phases and an initial electron density map.

2.2.4.2 Using anomalous signal (MAD and SAD)

Multi-wavelength Anomalous Diffraction (MAD) also relies on heavy atom derivatives. There are many methods that can be used to produce these derivatives of the protein crystals (Garman & James 2003) and by using recombinant technologies it is possible to incorporate selenium atoms directly into the structure of the protein of interest using selenocysteine or selenomethionine. MAD experiments can then be carried out on selenium derivatised protein crystals to solve the phases (Hendrickson et al. 1990). MAD exploits the fact that many heavy atoms have an absorption edges close to wavelengths that are suitable for crystallography. At the absorption edge of an atom, small alterations to the wavelength of the incident light results in large changes in the resultant phase. Datasets are collected from the crystal at wavelengths that will produce the greatest difference in anomalous data. The resulting anomalous signal often very small and so require accurate measurements to produce a result.

Single-wavelength Anomalous Diffraction (SAD) uses the same principle as MAD but only a single dataset is collected at the absorption peak. This was first demonstrated in 1981 (Hendrickson & Teeter 1981). SAD is advantageous as the collection of one dataset is less damaging to crystals than the multiple datasets required by MAD due to less X-ray exposure. Protein crystal structures have previously been solved using the anomalous

signal from sulphur atoms (Dauter et al. 1999). Sulphur-SAD poses difficulties due to the small amount of anomalous signal the sulphur atoms produce. A novel protein crystallography beamline has been developed at Diamond Light Source to try and maximise successful structure determination by this method (Allan et al. 2015).

2.2.4.3 Molecular Replacement

Molecular replacement (MR) has become particularly useful in recent years thanks to the wealth of protein structures present in the PDB (Rossmann 2001). Approximately two thirds of the structures deposited in the PDB have been solved by MR (Vagin & Teplyakov 2010). MR requires an initial homology model that should have a similar overall structure to the crystallised protein; usually a model with greater than 30 % sequence identity is suitable. The model is used to produce a Patterson map which is then rotated and translated against the Patterson map of the crystallographic data to find a suitable solution (Rossmann & Blow 1962). Software is now available that screens libraries of protein fragments against the data to build a model for subsequent molecular replacement (Bibby et al. 2012; Rodriguez et al. 2012).

2.2.5 Radiation damage

Under bombardment from X-rays, protein crystals can become damaged (Garman 2010). This radiation damage can take many forms including reduction of prosthetic groups, reduction of disulphide bonds, loss of resolution, increased mosaicity (a measure of disorder between unit cells within the crystal lattice) and damage to the polypeptide chain. The vast majority of crystallography experiments are now carried out with the crystal maintained under a cryostream at 100 K. This cryocrystallography reduces radiation damage to the sample and allows more data to be collected from a single crystal (Garman 2003). Smaller crystals, metal containing crystals and membrane protein crystals are particularly susceptible to radiation damage.

2.2.6 Data collection

X-rays for protein crystallography data collection tend to be produced in house or at synchrotron facilities. The majority of in house X-rays are produced by bombarding a rotating metal anode with high voltage electrons accelerated through an electric field. One such instrument is the FRE+ by Rigaku currently used in the Barkla X-ray laboratory of biophysics at the University of Liverpool (Figure 2.4a). Rotation is used in order to disperse the heat generated by electrons striking the anode, which allows for brighter X-rays to be produced. The result of this is the emission of characteristic light

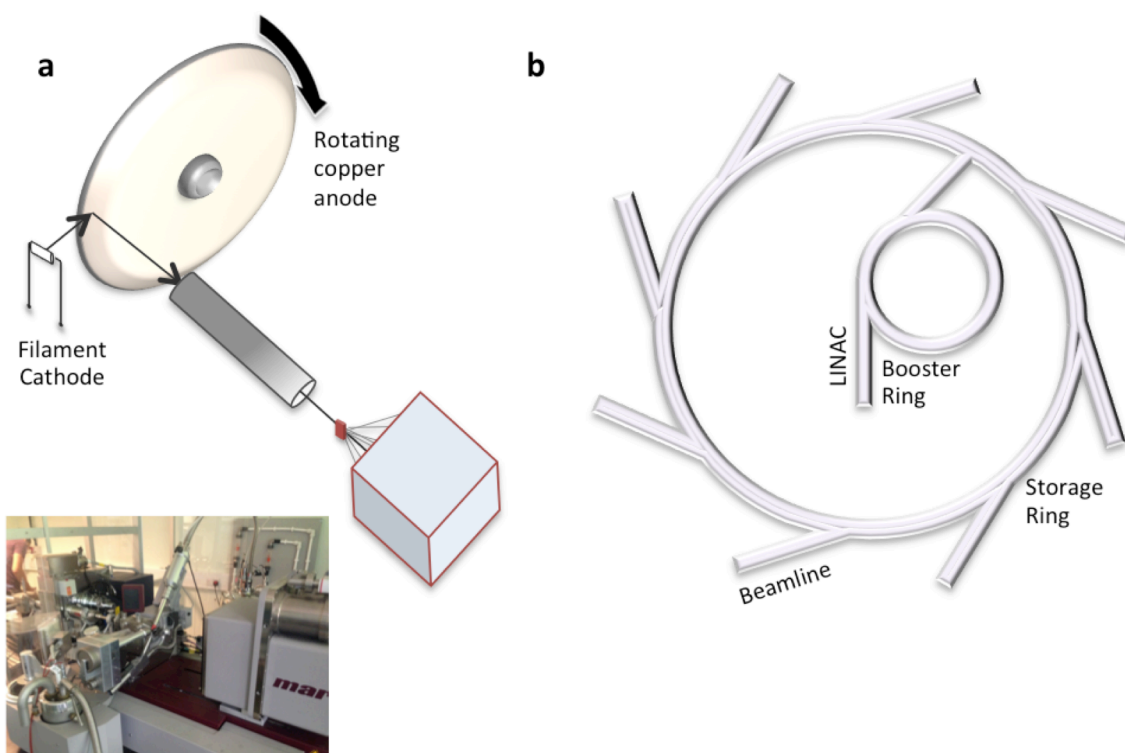


Figure 2.4 | Demonstration of different X-ray sources. **a** Schematic of a rotating copper anode X-ray generator. Electrons are released from a heated filament cathode that strike the rotating copper anode and cause the emission of X-rays. These X-rays can then be focussed and targeted on to a crystal sample and the resulting diffraction pattern is recorded on a detector. *inset* A photograph of the Barkla X-ray laboratory of Biophysics at the University of Liverpool demonstrating this set up. **b** A view of the principle components of a synchrotron light source. Electrons are produced by an electron gun and initially accelerated in the linear accelerator (LINAC). These electrons are then further accelerated in the booster ring to near the speed of light before injection into the storage ring. At each change of direction around the ring, synchrotron radiation is produced and used at a beamline.

dependent on the material used. When struck by electrons, copper emits X-rays at a wavelength 1.54 Å and molybdenum emits X-rays of wavelength 0.71 Å. Both of these wavelengths are suitable for the study of atomic structure. Gallium is also being used to generate X-rays at a wavelength of 1.34 Å by bombarding the liquid metal with electrons (Otendal et al. 2008).

2.2.6.1 Synchrotron Radiation

The broad spectrum of light, ranging from infrared to hard X-rays, emitted by charged particles under radial acceleration is referred to as synchrotron radiation (Figure 2.4b). Synchrotron radiation is used to produce light of multiple, tuneable wavelengths and of high flux for a wide variety of experiments (Bilderback et al. 2005). Initial work carried out with this light were parasitic in nature but dedicated light sources were eventually opened and have continued to be built. The first beamline purposely built for protein crystallography was opened at the storage ring DC1 in Orsay, France in 1978 (Lemonnier et al. 1978) shortly followed by other protein dedicated beamlines such as that at the SRS, Daresbury, UK in 1981 (Helliwell et al. 1982). Modern synchrotrons such as Soleil, Paris, France or Diamond Light Source (DLS), Oxfordshire, UK operate using the same principles as initial synchrotrons but are orders of magnitudes brighter. This increased brightness is a result of the low emittance of the storage ring and the use of high performing insertion devices such as undulators. These devices further accelerate the particles and increase the intensity of the emitted radiation.

This increasing brightness results in an increased signal from diffraction revealing data that may otherwise not been detectable. As a result of this, smaller crystals can now provide usable data despite their smaller diffracting volume. Small crystals can also be used due to the increasingly small beam sizes that are being produced (J. L. Smith et al. 2012). A small beam size is also beneficial as it reduces the radiation damage across the crystal sample (Sanishvili et al. 2011) and removes background from the surrounding solvent and sample support.

The rise of single photon counting pixel array detectors such as the PILATUS (Dectris) has allowed for shorter sample exposures to the beam and methods such as fine angle slicing in order to improve signal to noise ($I/\sigma I$) (Hülse et al. 2006; Mueller et al. 2012). This reduces damage to the sample. therefore both improving data quality and the time required to collect datasets.

2.2.7 Data reduction

Diffraction data are reduced by indexing using software such as HKL2000 (Otwinowski & Minor 1997) or iMosflm (Leslie & Powell 2007). The process of indexing records all reflections according to their Miller indices (hkl), their intensity (I_{hkl}) and the background around the reflection (σI_{hkl}). Multiple intensities of the same reflection are repeatedly collected during data collection. These intensities often vary from one to another. This can be as a result of radiation damage, varying incident beam intensity or differences in absorption due to the thickness of the crystal. For these reasons, the reflections with the same index are scaled to one another to ensure the same intensity throughout the data. Data from multiple collections can be merged together prior to scaling to increase the completeness, redundancy and therefore quality of the final dataset.

2.2.8 Structure solution and refinement

In the work that follows, the phase problem was overcome using the molecular replacement method. The initial calculated phases ($i\Phi_{\text{calc}}(hkl)$) and the observed amplitudes ($|f(\mathbf{S})|_{\text{obs}}$) provide a starting point for refinement, which can then be used to create an initial electron density map.

$$\rho(r) = \int f(S)e^{-i2\pi r \cdot S} d\mathbf{S} = \int |f(S)|_{\text{obs}} e^{i\phi_{\text{calc}}(S)} e^{-i2\pi r \cdot S} d\mathbf{S}$$

After the production of this initial map, rounds of automated refinement followed by manual model building can be carried out to adjust the atomic model to improve the fit to the diffraction data. As the model is

refined, the calculated phases are improved which then allow for more alterations to the model to fit the produced electron density. To ensure that through these iterations of improvement the model comes to better represent the crystallised protein, crystallographic R-factors are employed. By taking the model and calculating the amplitudes of the models structure factors ($|F_{calc}|$) and comparing them to those that were observed ($|F_{obs}|$) we can prevent building an incorrect model.

$$R = \frac{\sum ||F_{obs}| - |F_{calc}||}{\sum |F_{obs}|}$$

To prevent over-fitting the data, a set amount ($\sim 5\%$) of data are left out of model building and labelled R_{free} (Brunger 1992). These data are left unbiased by refinement and can be used to cross-validate with the working set, R_{work} . Only, a small difference between R_{work} and R_{free} is expected for a correct model.

Chapter 3 | Drug development against cytochrome *bc*₁

3.1 Cytochrome *bc*₁

Cytochrome *bc*₁ (cyt. *bc*₁), also known as Complex III or ubiquinol-cytochrome *c* oxidoreductase (E.C. 1.10.2.2), is a homodimeric multi-subunit integral membrane protein found within the inner mitochondrial membrane (IMM) (Figure 3.1a). In eukaryotes, each monomer consists of 10 or 11 subunits depending on the species of origin (Table 3.1). There are three redox active subunits containing prosthetic groups: cytochrome *b* (cyt. *b*), cytochrome *c*₁ (cyt. *c*₁) and the Rieske Iron-Sulphur protein (ISP). Cyt. *b* is the only subunit encoded in mitochondrial DNA and contains two *b*-type hemes at differing redox potentials: a low redox potential heme (heme *b*_L) and a

Table 3.1 | Composition of eukaryotic cytochrome *bc*₁, including topology and function of subunits. Many of the subunits specific functions are unknown but they have shown importance in stability and overall catalysis.

Subunit	Topology	Number of residues	Function
Core complex I	Matrix side	446	
Core complex II	Matrix side	439	
Cytochrome <i>b</i>	8 TM helices	379	Oxidation and reduction of ubiquinol/ubiquinone and electron transfer
Cytochrome <i>c</i>₁	1 TM helix, IMS	241	Electron transfer
Rieske Iron-Sulphur Protein	1 TM helix, IMS	196	Electron transfer
Subunit 6	Matrix	111	
Subunit 7	1 TM helix	82	
Hinge protein (Subunit 8)	IMS	78	Possibly involved in cyt. <i>c</i> binding
Subunit 9	Matrix	78	
Subunit 10	1 TM helix	62	
Subunit 11	1 TM helix	56	

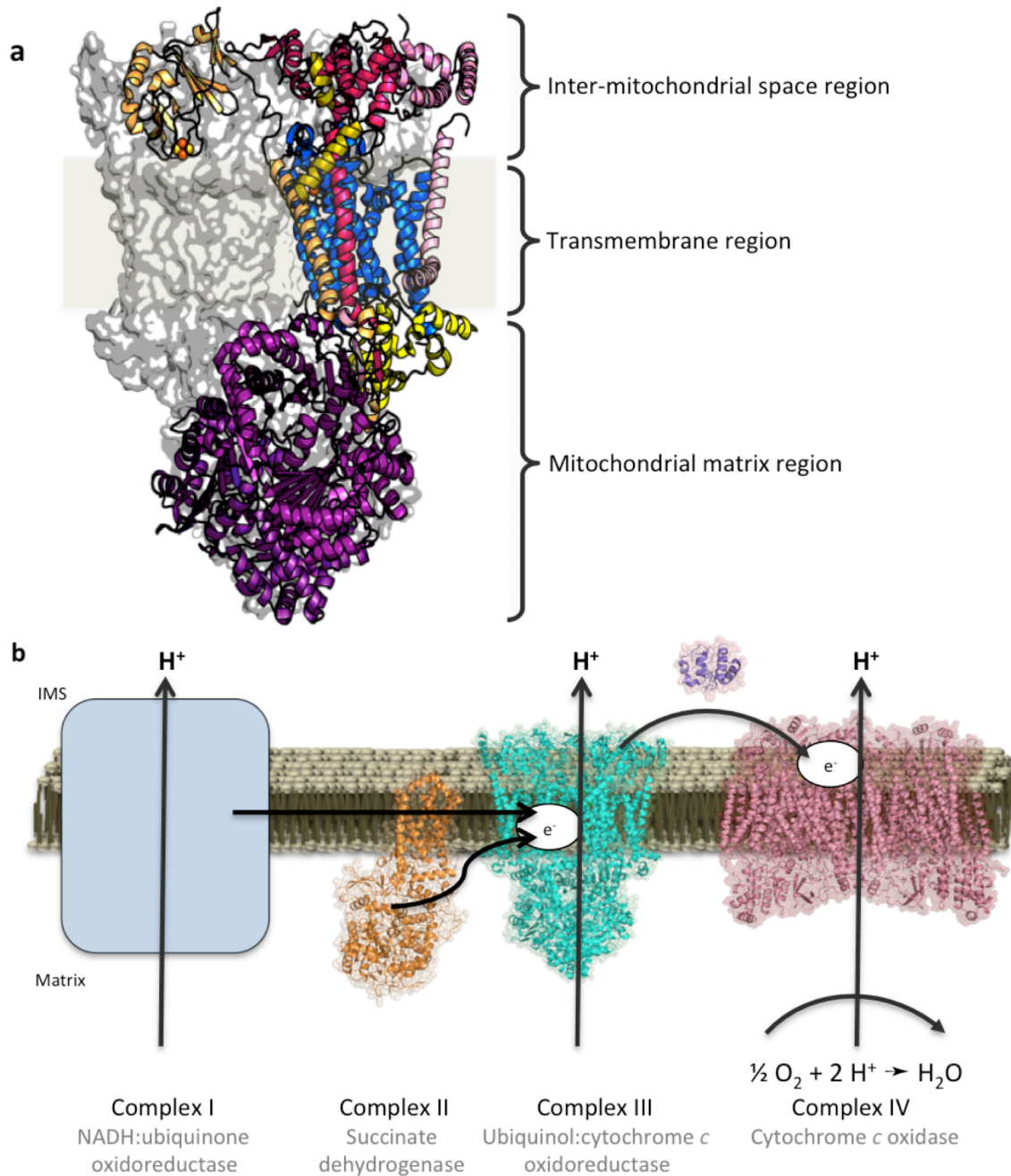


Figure 3.1 | The structure of cytochrome *bc*₁ and its role in the electron transport chain (ETC). **a** A cartoon cutaway view of *cyt. bc*₁. The homodimer is integral across the inner-mitochondrial membrane with the core proteins forming a large soluble portion within the matrix and the soluble domains of cytochrome *c* and the Rieske iron-sulphur protein in the intermembrane space. **b** A schematic view of the ETC. As electrons are passed along the chain, H⁺ are transported into the intermembrane space creating a chemiosmotic membrane potential. Complex I is absent in many organisms including apicomplexa parasites and is replaced with a type II NADH dehydrogenase which does not act to pump H⁺. The PDB models 1nek, 1occ, 1ppj and 2b4z were used to produce representations of complex II, complex IV, complex III and *cyt. c* respectively.

high redox potential heme (heme b_H). Cyt. c_1 contains a single c -type heme and the ISP contains an iron-sulphur cluster (2Fe-2S). The protein is functional as a dimer, as the transmembrane region of the ISP passes across cyt. bc_1 and the head interacts with cyt. b and cyt. c_1 of the adjacent monomer. The flexibility and movement of the soluble region of the ISP appears to be essential for catalysis (Esser et al. 2006; Zhang et al. 1998). The remaining supernumerary subunits appear to play a role in assembly or stability of the complex (P. M. Smith et al. 2012). The production of the full protein requires multiple chaperone proteins for both transport and assembly in the mitochondrial membrane, and has been studied extensively in yeast (P. M. Smith et al. 2012; Zara et al. 2009). The two largest subunits are referred to by the misnomers, core 1 and core 2, and are homologous to the α and β subunits of matrix processing peptidases (Silman et al. 1967; Braun & Schmitz 1995). Core 1 is bound to the membrane and interacts with cyt. b . Core 2 interacts with core 1 in the matrix. Subunit 6, also known as the hinge protein, is highly acidic and has been suggested to assist cytochrome c (cyt. c) binding cyt. c_1 (Kim & King 1983). The remaining small subunits don't appear to have specific functions but are most likely involved in complex stability.

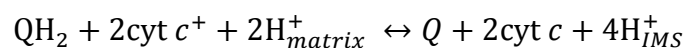
3.1.1 The electron transport chain

Cyt. bc_1 is the third protein in the electron transport chain (ETC) located within the mitochondria (Figure 3.1**b**). The ETC couples redox reactions between several proteins to produce a membrane potential ($\Delta\Psi_m$) across the inner mitochondrial membrane. Two proton donating substrates are required from previous reactions for the ETC, reduced nicotinamide adenine dinucleotide (NADH) and flavin adenine dinucleotide ($FADH_2$), which are produced by glycolysis in the cytosol and the citric acid cycle (Krebs cycle) in the matrix. NADH is used as a substrate by NADH:ubiquinone oxidoreductase (Complex I) transferring H^+ into the intermembrane space (IMS) partially producing the $\Delta\Psi_m$ and reducing ubiquinone to ubiquinol in the process. $FADH_2$ is oxidised by succinate dehydrogenase (Complex II) producing more reduced ubiquinol. Ubiquinol is used as the substrate for cyt.

bc_1 as per the modified Q-cycle (see section 3.1.2) and results in the translocation of more H^+ and the reduction of cyt. c . Complex IV is the terminus of the ETC and oxidises cyt. c to reduce molecular oxygen, producing water, whilst translocating more H^+ across the IMM and into the IMS. The formation of supercomplexes between the ETC complexes have been detected and several have been isolated, studied or visualised using electron microscopy (Althoff et al. 2011; Dudkina et al. 2010; Winge 2012). In several species, including *S. cerevisiae* and *Plasmodium spp.*, complex I is absent and is instead replaced with a non proton translocating Type II NADH:quinone oxidoreductase. The resulting $\Delta\Psi_m$ is essential for multiple cellular processes including oxidative phosphorylation (ATP synthesis) through the ATP-synthase complex.

3.1.2 Modified Q-cycle

The protonmotive Q-cycle was first proposed in 1976 by the biochemist Peter D. Mitchell to describe how cyt. bc_1 both oxidises and reduces ubiquinol and ubiquinone whilst acting as a proton pump (Mitchell 1976). This work contributed to him receiving the Nobel Prize for Chemistry in 1978. It has since been altered and is now known as the “modified protonmotive Q-cycle” (Trumpower 1990; Crofts et al. 2003). The mechanism requires two binding sites located either side of the IMM; the Q_i site located on the matrix side of the IMM and the Q_o site located towards the IMS (Figure 3.2). The equation below describe the overall process:



Two ubiquinol molecules are required for each complete reaction. Upon binding the Q_o site, ubiquinol is oxidised and simultaneously reduces both the 2Fe-2S cluster and heme b_H (Zhu et al. 2007). The two resulting H^+ are translocated to the IMS. A conformational change in the ISP then allows the electron from the 2Fe-2S cluster to reduce cyt. c_1 whilst the electron from heme b_L is transferred to heme b_H . Heme b_H now reduces the bound

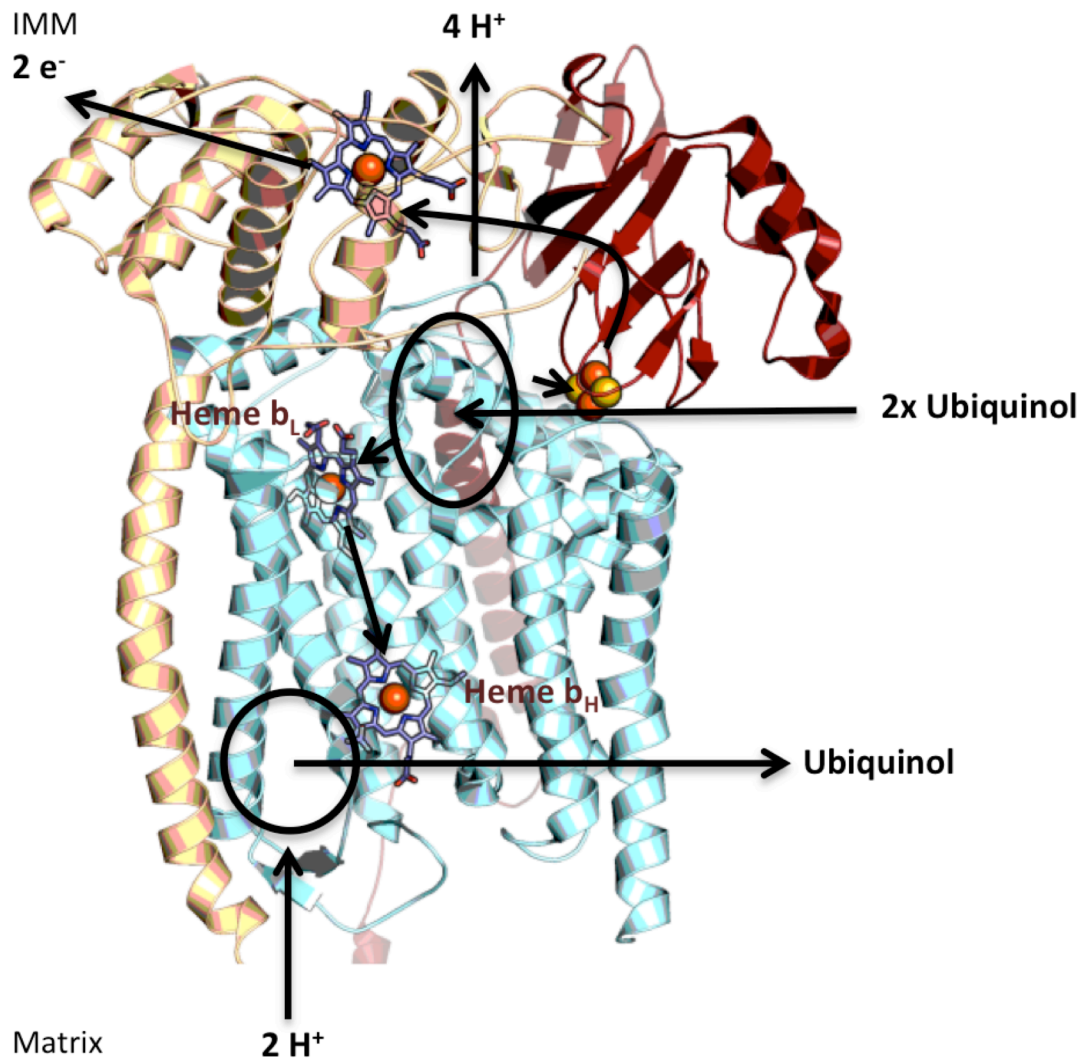


Figure 3.2 | A schematic view of the modified Q-cycle. Cytochrome *b* is in blue, cytochrome *c*₁ is yellow and the Rieske iron-sulphur protein in red. Ubiquinol enters the Q_o site of cytochrome *b* and is reduced to ubiquinone. The released H⁺ are passed into the intermembrane space whilst the resulting electrons are transferred to heme b_L and the 2Fe-2S cluster. The 2Fe-2S cluster then reduces cytochrome *c*₁, which goes into reduce cytochrome *c*. Heme b_L reduces heme b_H which in turn reduced ubiquinone to a semi-ubiquinone intermediate before the next cycle can complete the reaction and produce ubiquinol.

ubiquinone to a semi-ubiquinone intermediate in the Q_i site whilst cyt. *c*₁ reduces a cyt. *c* molecule in the IMS. Cyt. *c* freely diffuses away whilst the semi-ubiquinone present in the Q_i site remains bound for the next cycle to begin. During this following cycle, the semi-ubiquinone present in the Q_i site is fully reduced and diffuses away as a molecule of ubiquinol.

3.1.3 Role and structure of cytochrome *bc*₁ in malaria

The inhibition of cyt. *bc*₁ in *P. falciparum* causes the mitochondrial membrane potential to collapse (Srivastava et al. 1997). This collapse affects multiple downstream metabolic pathways that require the electron transport chain and is lethal to the parasite. The pyrimidine biosynthesis pathway appears to be of particular importance as the parasite lacks the genes for pyrimidine scavenging and it therefore relies solely on *de novo* biosynthesis (Gardner et al. 2002). Pyrimidine biosynthesis requires a constant pool of ubiquinone that is stopped when the ETC is inhibited (Srivastava et al. 1997). The mitochondria produces little ATP and lacks several genes required to encode ATP synthase (Fry et al. 1990; Gardner et al. 2002). The ETC in *Plasmodium spp.* has been suggested to exist solely for the purpose of maintaining reduced ubiquinone (Painter et al. 2007). This has generated controversy (Fisher et al. 2008) but certainly exemplifies its importance.

Cyt. *bc*₁ in *P. falciparum* is predicted to contain at least seven subunits common to all higher cyt. *bc*₁ proteins, though it is possible the other subunits are more diverse and as of yet unidentified (Vaidya & Mather 2009). There is currently no structure of malaria cyt. *bc*₁. *In silico* modelling or yeast models have been used to study individual subunits instead (Kessl, Meshnick, et al. 2007; Kessl et al. 2006; Vallières et al. 2013). *S. cerevisiae* is used as a biological model due to the high sequence identity, particularly of the catalytic subunits (Kessl et al. 2006). Cyt. *b* is the primary subunit of action for the known compounds that target and inhibit cyt. *bc*₁.

3.1.4 Atovaquone antiprotozoal action

Atovaquone (Figure 3.3 1) is a broad-spectrum antiprotozoal clinically approved for use in the treatment of malaria, toxoplasmosis, babesiosis and pneumocystis pneumonia. Atovaquone is the result of rational design against the mitochondria (Gutteridge 1989) and is the only hydroxynaphthoquinone clinically approved. It inhibits the *P. falciparum* cyt.

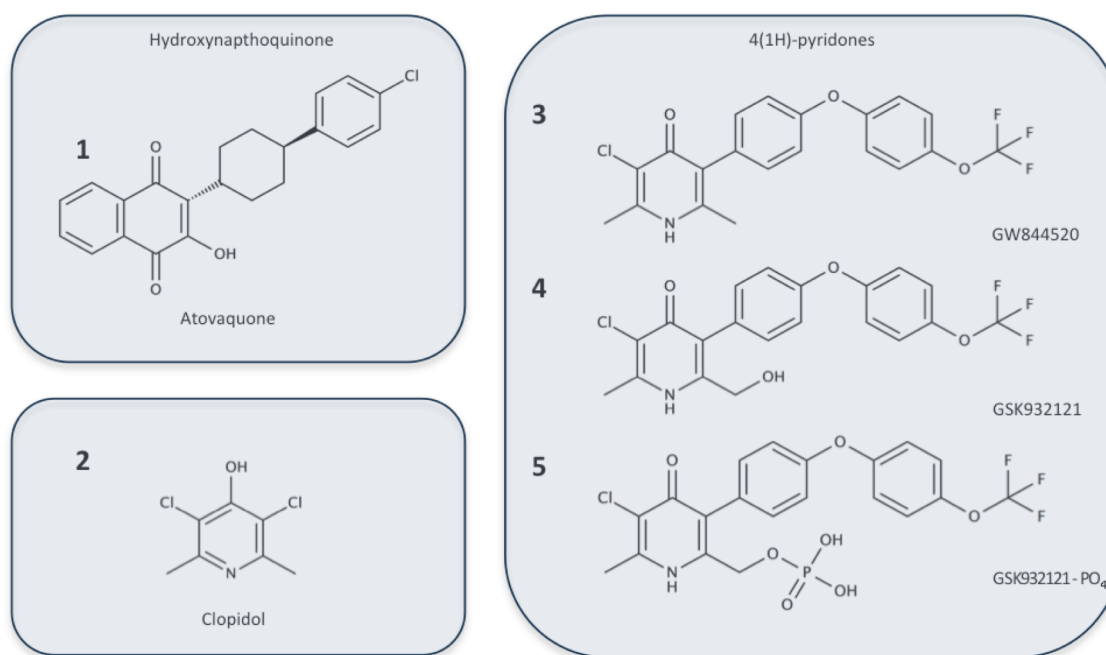


Figure 3.3 | The structures of atovaquone and several 4(1H)-pyridones. The 4(1H)-pyridones displayed here were developed by GSK after initial findings of clopidols antimalarial activity.

*bc*₁ complex at 1000 fold lower concentrations than that of rat and similar mammalian cyt. *bc*₁ complexes (Fry & Pudney 1992). Upon binding it collapses the mitochondrial membrane potential (Srivastava et al. 1997) killing the parasite. However, it suffers from poor bioavailability due to its low water solubility and high protein binding (Dressman & Reppas 2000).

During its development, it was noted that recrudescence occurred with high frequency due to single point mutations in cyt. *b* (Looasreesuwon et al. 1999). For this reason several drugs were considered as a partner compound and proguanil was found to act synergistically with atovaquone (Canfield et al. 1995). The resulting combination was initially marketed as Malarone™ by GSK and made available in 1998 but the price of the combination treatment is prohibitive in developing countries. Malarone is favoured as a highly effective prophylactic treatment with low levels of side effects (Radioff et al. 1996) accounting for half of antimalarial prescriptions in the U.S.A (Barton et al. 2010). Recently the patent owned by GSK has

expired and multiple generic formulations are now available at reduced cost. This raises the a long-term fear that the spread of atovaquone resistance will rise.

Atovaquone, a ubiquinone antagonist, is a nanomolar Q_o site inhibitor of protozoa (Siregar et al. 2015). Recent crystallographic work and direct analysis on parasite enzymes have verified the Q_o site as the site of action (Birth et al. 2014; Siregar et al. 2015). The Q_o site is a relatively large and conserved domain formed by cyt. *b* that shows a high degree of flexibility. The Q_o site contains the PEWY motif on a loop located on the IMS side of cyt. *bc*₁ that is well conserved across phyla (Crofts et al. 1999; Kao & Hunte 2014). Q_o site inhibitors can be categorised according to how they bind within the Q_o site (Esser et al. 2004). These are either heme distal, close to the docking of ISP, or heme proximal, having no effect on ISP mobility (Esser et al. 2004). Atovaquone has recently been co-crystallised with *S. cerevisiae* cyt. *bc*₁ confirming that it binds the Q_o site in the distal position (Birth et al. 2014).

Despite being partnered with proguanil as a combination treatment, resistance to atovaquone has spread rapidly amongst *P. falciparum* in Africa. By far the most frequent mutations *in vivo* are Y268S and less frequently Y268N, though many others have been detected *in vitro* including M133I and L271F (Korsinczky et al. 2000; Syafruddin et al. 1999). The Y268S point mutation reduces atovaquone inhibition by several orders of magnitude whilst also affecting the catalytic turnover of cyt. *bc*₁ (Fisher et al. 2012; Korsinczky et al. 2000).

The exact mechanism of proguanil synergy is unknown. When administered as a monotherapy, proguanil is processed into cycloguanil, a DHFR inhibitor. When administered in combination with atovaquone, it appears that the proguanil in its native form inhibits dihydroorotate dehydrogenase (DHODH) located within the *Plasmodium* mitochondria. DHODH catalyses the only mitochondrial step in pyrimidine biosynthesis and

uses the $\Delta\Psi_m$ as an electron sink. It appears that proguanil acts to lower the effective concentration of atovaquone required to collapse the potential across the IMM (Srivastava & Vaidya 1999).

3.1.5 Drug development targeting cytochrome *bc*₁

A lot of work has been carried out attempting to target the enzymes of the *P. falciparum* ETC (Painter et al. 2010; Nixon, Pidathala, et al. 2013; Stocks et al. 2014). The Q_o site of cyt. *bc*₁ is currently the most well characterised target of the ETC and several classes of drug have been developed against it. Atovaquone does not have ideal pharmaceutical properties and attempts are being made to generate new hydroxynaphthoquinones that could overcome resistance (Schuck et al. 2013). Studies were attempted using several different compounds in this work. The following is a description of each of the different classes attempted.

3.1.5.1 4(1H)-Pyridones

The pyridones have been developed since continuing from work in 1960's that identified the antimalarial effects of clopidol (Markley et al. 1972) (Figure 3.3 2) and that the effect was on the ETC within the mitochondria (Fry & Williams 1984). Clopidol has been shown to have activity against atovaquone resistant strains of *P. falciparum*, which led researchers to believe it bound in the Q_o site in a novel manner (Barton et al. 2010). Structure activity relationships (SARs) were carried out on a series of derivatives of clopidol modified on the hypothesis that it was acting as a ubiquinone antagonist. The addition of a lipophilic side chain and the halogenation of the pyridone group at position 3 increased the potency of the compound 200 fold compared to clopidol *in vivo* and 1000 fold *in vitro* (Yeates et al. 2008). The pyridone group has also been extensively modified into (1H-pyridin-4-ylidene)amines showing strong antimalarial activity (Rodrigues et al. 2009). The pyridones show activity against both blood and liver stage parasites.

The 4(1H)-pyridone GW844520 (Figure 3.3 3) was developed by GSK and went through preclinical trials showing an apparent selectivity of *P. falciparum* cyt. *bc*₁ over the mammalian and a nanomolar IC₅₀ (Xiang et al. 2006). However, it had to be withdrawn due to histopathological complications, thought likely due to its high lipophilicity and non-linear dosage (Bueno et al. 2012). GSK932121 (Figure 3.3 4) was developed from GW844520 by the addition of an hydroxymethyl at C6 (Bueno et al. 2011). It proved potent against multi-drug resistant *P. falciparum* in a mouse model (Jiménez-Díaz et al. 2009) with improved bioavailability and was taken forward to phase I clinical trials. A prodrug (Figure 3.3 5) was developed in parallel with the addition of a phosphate ester group and was progressed into preclinical analysis. Acute toxicity was found when the prodrug was administered to rats, which was thought to be due to the inhibition of mammalian cyt. *bc*₁ by the parent drug. This was confirmed when GSK932121 was administered intravenously (Bueno et al. 2012).

3.1.5.2 Quinolones

The antimalarial activity of quinolones as a class of inhibitors has been known since work done on endochin (Figure 3.4 6) in 1948 and their effect on toxoplasmosis since 1951 (Gingrich & Darrow 1951). Initial work on these compound suffered due to the lack of suitable biological models and knowledge of the parasite biochemistry. More recent work has led to the synthesis of a series of compounds known as endochin-like quinolones (ELQs) (Winter et al. 2011). These compounds have been shown to have high IC₅₀s but suffer from low solubility and bioavailability (Winter et al. 2011; Winter et al. 2009; Cross et al. 2010). ELQs have been shown to impede parasite growth by inhibition of cyt. *bc*₁ and affect both the liver and blood phase of *P. falciparum*. They have recently been shown to bind both the Q_o and the Q_i site depending on the functional groups attached (Stickles, Justino de Almeida, et al. 2015).

Endochin was rapidly metabolised and so suffered from rapid clearance. The addition of a diphenylether functional group, from GSKs

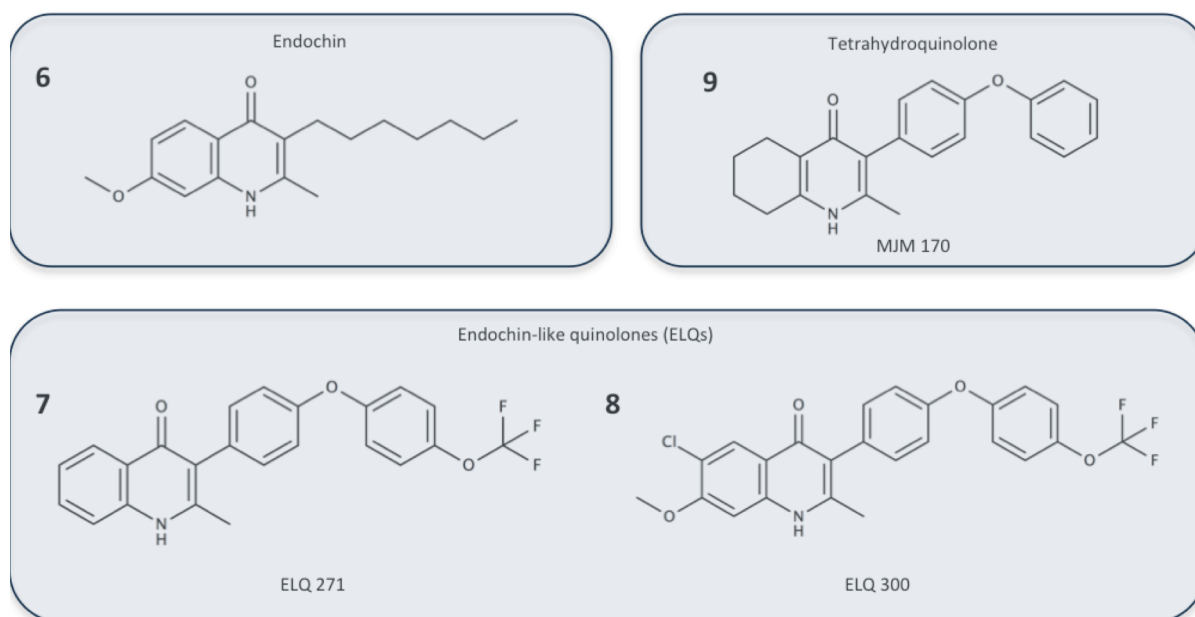


Figure 3.4 | The chemical structure of endochin and related quinolones. The removal the octyl aryl chain from endochin and subsequent replacement with the diphenyl ether increased ELQ potency dramatically. The planar region was removed in MJM 170 to improve solubility and has also improved efficacy against *P. falciparum* and *T. gondii*.

4(1H)-pyridone program, in place of the lipid chain improved this and resulted in compounds such as ELQ 271 and ELQ 300 (Figure 3.4 7 and 8) (Nilsen et al. 2014). ELQ 300 is a particularly potent antimalarial that shows no signs of cross-reactivity with atovaquone and is effective against drug resistant strains of malaria (Nilsen et al. 2013). ELQ 271 is highly efficacious against *T. gondii* and is suspected to bind *cyt. bc₁* (Doggett et al. 2012).

Tetrahydroquinolones

MJM 170 (Figure 3.4 9) is a novel tetrahydroquinolone primarily developed to target the *Q_i* site of *cyt. bc₁* in *T. gondii*, and also shows an effect against *Plasmodium spp.* (unpublished data). MJM 170 was developed based on the 4(1H)-quinolone scaffold ELQ 271, which has previously been shown to be an effective antimalarial and have a mild effect on cysts formation in toxoplasmosis (Doggett et al. 2012). Due to the low solubility of this compound, work was carried out by Prof. Colin Fishwick and colleagues at the

University of Leeds to improve it and to also to improve efficacy against tissue cysts (McPhillie et al, unpublished).

2-aryl quinolones

The bisaryl quinolones were developed from a program designed to target the *P. falciparum* NADH:ubiquinone reductase (*Pf*NDH₂) (Pidathala et al. 2012). Many of the compounds tested from this synthesis possessed IC₅₀s in the nM region and a high selectivity for the *Pf*NDH₂. Some of the compounds also showed activity against cyt. *bc*₁ in the low nanomolar range. Drugs with multiple targets are often beneficial and show a reduced rate of resistance (Csermely et al. 2005).

The initial bisaryl compounds suffered from poor solubility and so further work was carried out, introducing heterocycles in to the aryl side chain (Leung et al. 2012). Several of these new compounds also maintained activity against both *Pf*NDH₂ and cyt. *bc*₁ including the compound SL-2-25 (Figure 3.5 10). These compounds have been previously docked in the Q₀ site

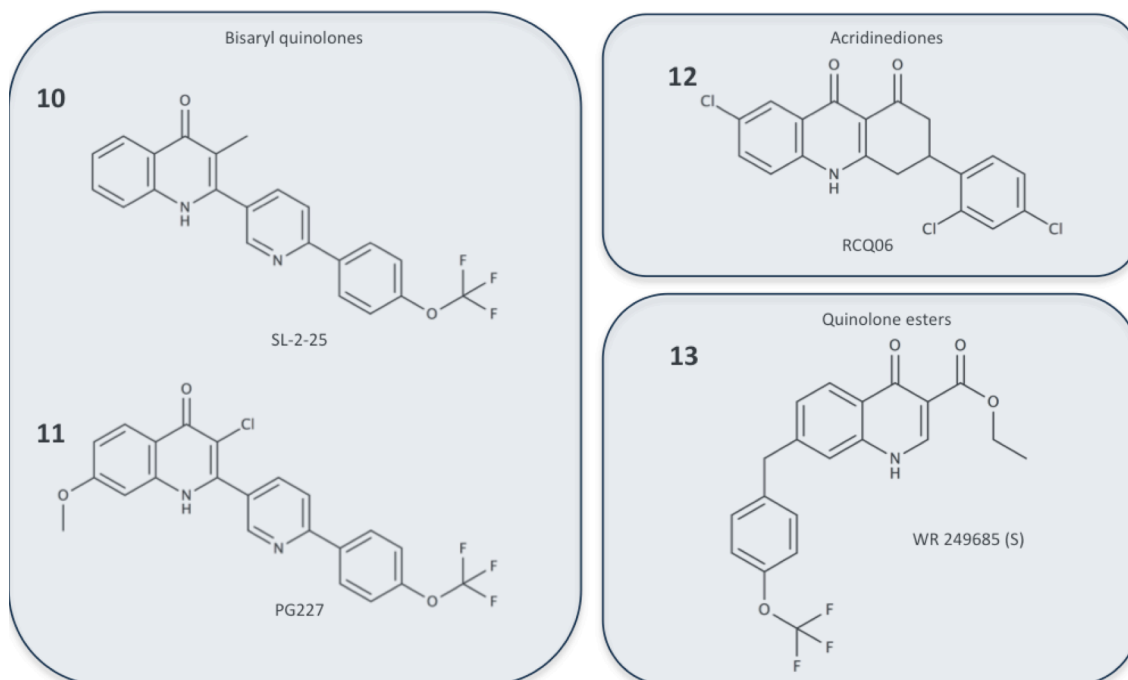


Figure 3.5 | Structures of several further compounds shown to bind cyt. *bc*₁.

of cyt. *bc*₁ (Biagini et al. 2012). PG227 (Figure 3.5 **11**) was developed at the University of Liverpool from SL-2-25 by the addition of a methyl ether as a lead compound.

Quinolone esters

The quinolone esters were produced from the quinolone scaffold and demonstrated good cLogP values (Cowley et al. 2012). RCQ06 (Figure 3.5 **12**) proved a highly effective antimalarial and has an IC₅₀ of 0.46 nM against *P. falciparum* (Cowley et al. 2012). Docking simulations have suggested it is a Q_o site inhibitor and work on *P. falciparum*-like yeast appear to confirm this (Vallières et al. 2013; Nixon, Pidathala, et al. 2013). Unfortunately, the introduction of the Y279S mutation that renders atovaquone resistance, also reduces RCQ06 efficacy. RCQ06 also inhibits bovine cyt. *bc*₁.

3.1.5.3 Acridinediones and acridones

Acridines, acridones and acridinediones were initially investigated due to their ability to bind to heme and prevent biocrystallisation. Several of the compounds also inhibited *P. falciparum* growth through other methods (Dorn et al. 1998). They were further developed into acridinediones which showed an affect on parasite O₂ consumption and cross-resistance with atovaquone (Suswam et al. 2001). Work done at the Walter Reed Army Institute of Research resulted in compound WR 249685 (S enantiomer) (Figure 3.5 **13**) which was shown to be a potent inhibitor (IC₅₀ = 3 nM) of the parasite cyt. *bc*₁ Q_o site and collapse the parasite membrane potential (Biagini et al. 2008).

Acridone compounds were studied for their hemozoin inhibition but the a chemical intermediate with potent antimalarial properties was discovered (Winter et al. 2006). These novel acridones were then shown to act both through hemozoin inhibition and to inhibit cyt. *bc*₁ (Kelly et al. 2009; Barton et al. 2010).

3.1.6 Binding of novel compounds to cytochrome *bc*₁

Previous work studying the binding of both the pyridones and quinolones to *cyt. bc*₁ has been based on homology modelling, docking or mutation studies. These methods are not without their merit but can provide unreliable information. No work has previously been done to determine how the compounds that are toxic may bind and inhibit mammalian *cyt. bc*₁. A deeper understanding of the drug binding to mammalian *cyt. bc*₁, when used in the context of differences between mammalian and protozoan complexes, could be used to inform further drug development. Ideally this would increase selectivity whilst maintaining efficacy against the parasite. In this work protein crystallography has been used to visualise the binding of antimalarial compounds to bovine *cyt. bc*₁. Bovine *cyt. bc*₁ has been used as a mammalian model due to its high sequence identity to the human form of the protein (Figure 3.6). Bovine heart tissue was used as it is relatively easy to acquire. Due to the high number of mitochondria present in cardiac tissue, the large amounts of native protein required for crystallisation can be readily obtained.

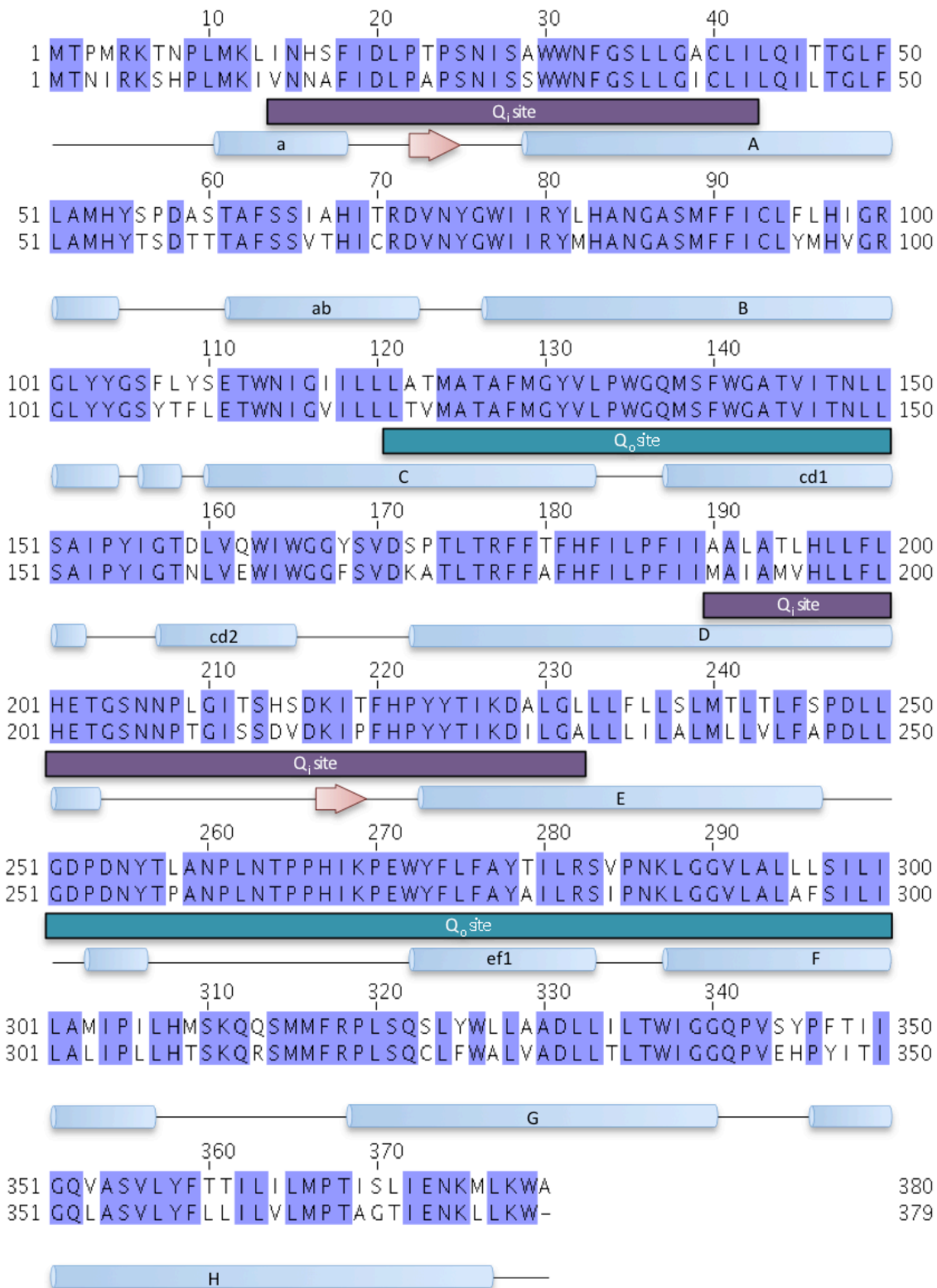


Figure 3.6 | Alignment between human (above) and bovine (below) cytochrome *b* amino acid sequences. The proteins have 79 % sequence identity with the remaining residues also being well conserved. Both the Q_o (green) and Q_i (purple) binding sites are particularly well conserved. Secondary structure is shown in cartoon representation below the appropriate sequence and is labelled according to name.

3.2 Results

3.2.1 Modified purification of cytochrome *bc*₁

First attempts to purify and co-crystallise cyt. *bc*₁ with various ligands were carried out using the same techniques as Iwata et al (Iwata et al. 1998). After solubilisation, the protein was applied to DEAE-sepharose as reported and eluted along a gradient of 150 mM – 350 mM NaCl. This yielded an incomplete separation of cytochrome *c* oxidase from cyt. *bc*₁. This was subsequently modified in line with other recorded purifications of cyt. *bc*₁ (Huang et al. 2005) so that after the protein was loaded onto a column equilibrated with 250 mM NaCl, it was eluted along a gradient of 250 mM to 500 mM NaCl (Figure 3.5a). Later experiments were also carried out using less DDM (0.3 % became 0.01 %). This resulted in more stable protein and also appeared to increase the reproducibility of crystallisation.

Hydroxyapatite has been used to purify the cyt. *bc*₁ complexes of various organisms previously (Ricchio et al. 1977; Berry et al. 1991). In earlier purification attempts it was successfully used to remove the large amount of cytochrome *c* oxidase that had not separated using DEAE-sepharose. In later purifications, when using a gradient of 250 – 500 mM NaCl, this step was no longer necessary and was removed.

Size exclusion chromatography was carried out on a HiPrep 16/60 Sephacryl S-300 HR gel filtration column (GE Healthcare) and resulted in highly pure bovine cyt. *bc*₁ (Figure 3.5b). Size exclusion helped to remove some of the remaining cyt. *bc*₁-cyt. *c* oxidase complex and any aggregates that had formed. Ligands were added after gel filtration to two-fold molar excess from a dimethyl sulfoxide (DMSO) solubilised stock and excess ligand was removed by buffer exchange. This was done to increase the reproducibility of crystallisation.

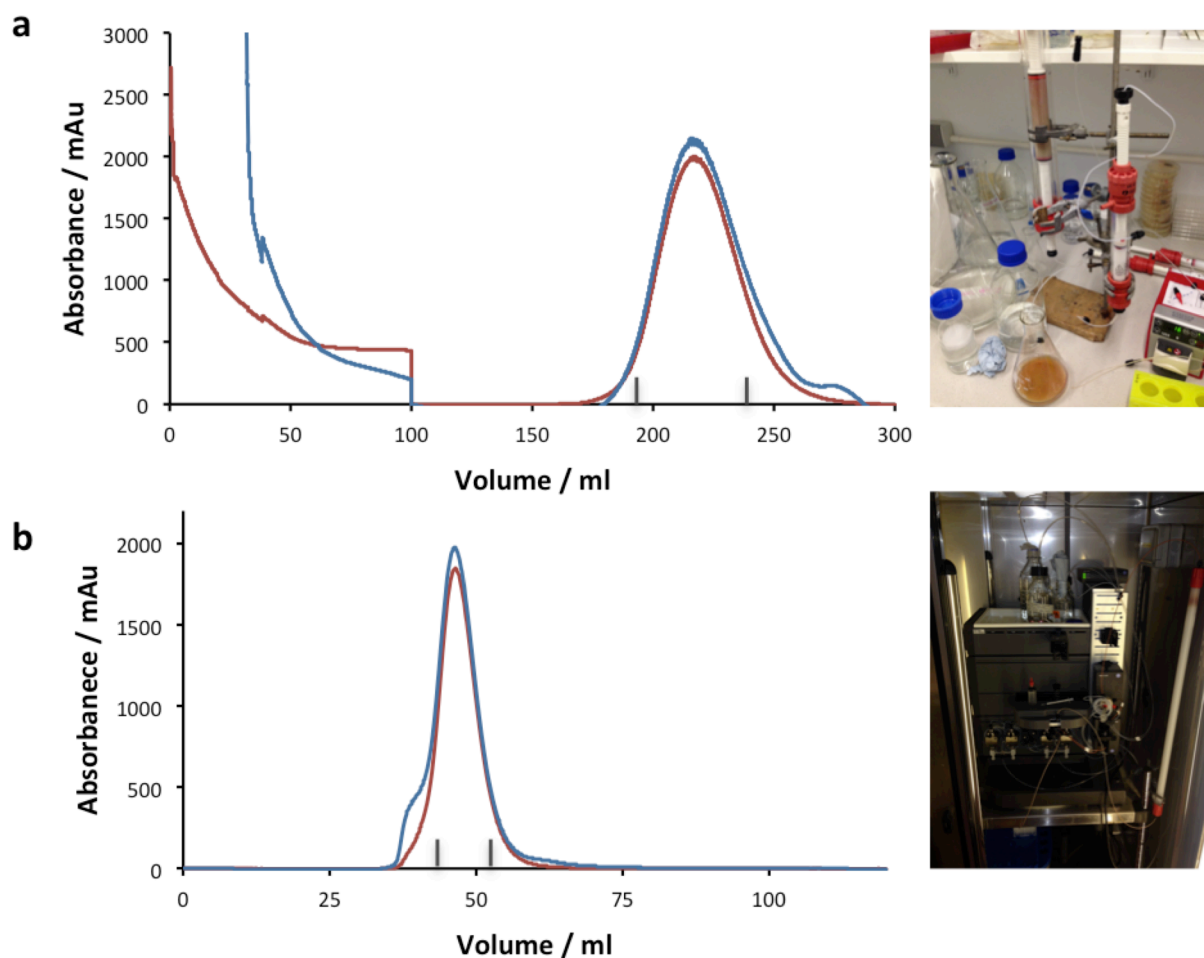


Figure 3.7 | Chromatographic purification of bovine cytochrome bc_1 . 280 nm absorbance is shown in blue, 415 nm absorbance is shown in red. Fractions collected are indicated between the grey lines. **a** DEAE-sepharose removes the majority of the solubilised mitochondrial proteins as flow through leaving a large peak of cyt. bc_1 and a small amount of other contaminants including residual cytochrome c oxidase. The column is shown being loaded with solubilised protein with cyt. bc_1 bound at the top. **b** Size-exclusion chromatography on a Sephacryl-S300 gel filtration column is used to remove the majority of residual cytochrome c oxidase, supercomplex and aggregates. The protein is seen flowing down the column located in a cold cabinet as a single red band inset.

PEG fractionation was used as a final purification step in later work that improved the quality, size and reproducibility of the cyt. bc_1 crystals. PEG fractionation has previously been used prior to crystallisation to remove any residual contaminants (Huang et al. 2005). This worked particularly well to remove cytochrome c oxidase present in residual supercomplex with only a slight loss of cyt. bc_1 yield (Figure 3.8) (Table 3.2).

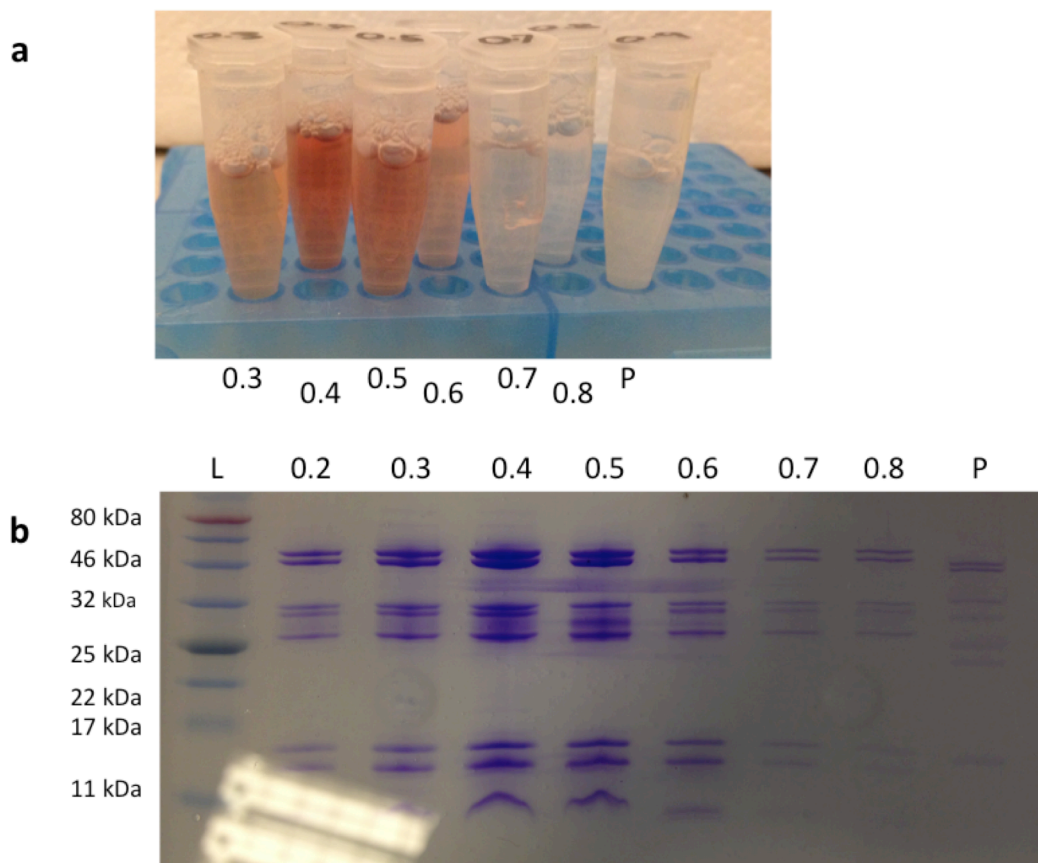


Figure 3.8 | A typical result from PEG fractionation. Numbers indicate the relative volume of precipitant buffer added to cyt. *bc*₁ containing solution. **a** Resuspended cyt. *bc*₁ produced from precipitate pellet. Each time an increased volume of PEG4000 is added, a new fraction of cytochrome *bc*₁ precipitates and can be pelleted by centrifugation. The pellet of pure cyt. *bc*₁ is then resuspended. **b** SDS-PAGE of the resulting resuspended PEG fractions. The fractions containing pure cyt. *bc*₁ are pooled together for crystallisation. Fraction P remained soluble after all cyt. *bc*₁ had precipitated and largely consisted of cytochrome *c* oxidase.

Table 3.2 | Typical yield of cytochrome *bc*₁ throughout the purification process. Numbers displayed to nearest whole number.

Purification step	Total protein / mg	Cytochrome <i>bc</i> ₁ / mg	Yield	Purity
Mitochondria	1680	-	-	-
Detergent solubilised mitochondria	946	95	100 %	9 %
DEAE-sepharose	72	62	65 %	86 %
S300-sephacryl	40	38	40 %	94 %
PEG fractionation	35	34	36 %	96 %

3.2.2 Crystallisation

Crystallisation was initially highly irreproducible and inconsistent. Crystal screening was carried out around known conditions (Iwata et al. 1998) in the hanging drop format and successful conditions were then replicated using large volume sitting drops in an attempt to increase crystal size. Screening took place across a pH range 6 – 7.5 and PEG4000 concentrations were altered from 5 % to 14 %. Micro-seeding using crystal seeds from successful hits helped to increase reproducibility in initial trays by providing nuclei for further crystal growth. The crystallographic structures presented in this work are all from the space group $P 6_5$. Screening was also carried out using varying amounts of the detergent 6-O-(N-Heptylcarbamoyl)-methyl- α -D-glucopyranoside (HECAMEG), glycerol, DMSO, varying protein concentration and using PEG3350 as the precipitant. Crystal trials were attempted using protein solubilised in the detergent decyl- β -D-malsolein (DM) around conditions demonstrated favourable for DDM solubilised protein but yielded no positive hits.

Attempts were made to reproduce the higher resolution $P 2_1 2_1 2_1$ crystal form as reported by Huang et al (Huang et al. 2005) but ultimately failed. Several crystals were grown using variations around the condition but when tested they belonged to the $P 6_5$ space group too. These conditions required an unusual 1:0.9:0.1 ratio of protein:resevoir:additive in the hanging drop. Screening was attempted with altered precipitant concentration (5-13 % PEG3350) and a variety of protein concentrations (30-50 mg/ml).

LCP crystallisation was also attempted with cyt. *bc*₁. Protein was screened mixed using two different lipids, at two temperatures across 14 different commercial screens. Crystal hits were achieved at both room temperature and 4 °C using the MemgoldI and MemgoldII screens (Molecular Dimension) with MAG9.9 (monoolein) (Figure 3.9). Crystals were harvested and tested at the synchrotron but no diffraction was observed.

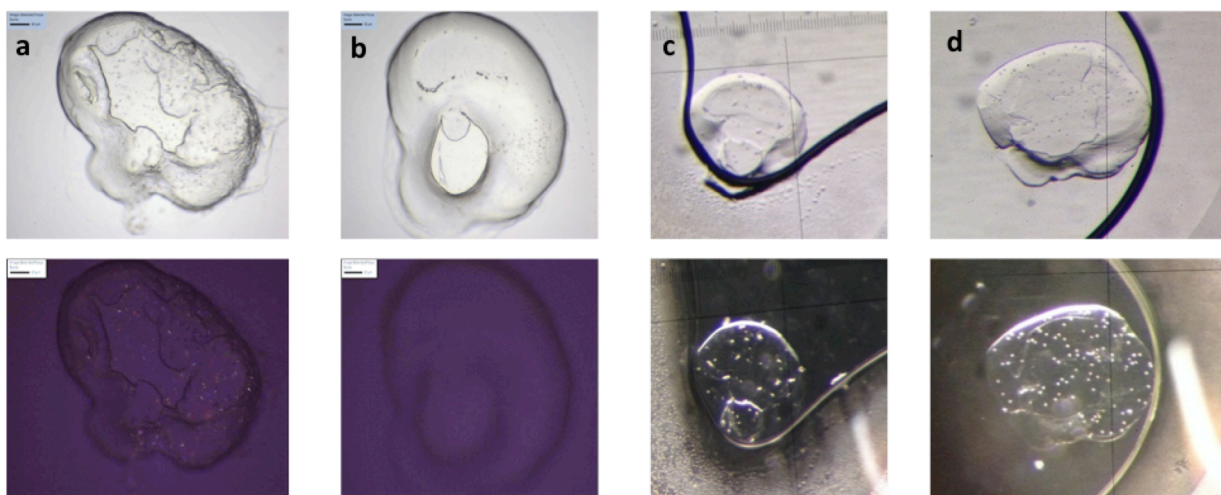


Figure 3.9 | Crystals hits using lipidic cubic phase *cyt. bc₁*. All crystals were grown in batch with monoolein lipid (MAG9.9). **a** Room temperature crystals grown with 0.001 M cadmium chloride/0.03 M magnesium chloride, 0.1 M MES (pH 6.5) and 30 % (v/v) PEG400 (Memgold II, #D11). **b** Room temperature crystals grown using 0.05 M magnesium chloride, 0.1 M glycine (pH 9.0) and 22 % (v/v) PEG400 (Memgold I, #D8). **c** Crystals grown at 4 °C using 0.2 M magnesium chloride/0.1 M potassium chloride, 0.025 M sodium citrate (pH 4.0) and 33 % (v/v) PEG 400 (Memgold I, #G5). **d** Crystals grown at 4 °C in 0.2 M lithium sulphate 0.1 M sodium citrate (pH 3.5) and 28 % (v/v) PEG 400 (Memgold I, #H4).

3.2.3 Cryoprotection and crystal screening

Crystals were screened on the home source before transport to the synchrotron for further analysis. Using the home source, cryoprotectants such as glycerol, sucrose, DMSO, PEG400, paratone-N-oil and sodium malonate were screened and attempts were made to optimise for use with *cyt. bc₁* crystals. A maximum resolution of 20 Å was observed for crystals using PEG400 as a cryoprotectant whilst crystals in sucrose, paratone-N-oil and malonate all failed to yield substantial diffraction. Glycerol and DMSO both appeared to provide good diffraction with little difference observed between the two across multiple crystals examined. Soaks of 30 seconds or more in cryoprotectant proved to be beneficial in reducing the mosaicity of the crystal over shorter periods of time.

3.2.4 Attempted binding of antimalarial compounds

Several antimalarial compounds were attempted in crystallisation but failed to yield a crystallographic structure. Cyt. *bc*₁ formed crystals in the presence of PG227 (Figure 3.5 11), a suspected Q_i site binding ligand, that diffracted beyond 3 Å. The crystals were produced using the Iwata method and over one hundred crystals were tested. High yielding resolution failed to be reproduced however and so no structure is yet available.

Multiple attempts were made with SL-2-25 (Figure 3.5 10) were attempted for co-crystallisation but did not produce any diffracting crystals. Trials were also attempted with the acridinedione WR 249685 that resulted in crystals that consistently diffracted to 6 Å. ELQ 300 (Figure 3.4 8) was also tested with bovine cyt. *bc*₁ and resulted in diffracting crystals but the diffraction from these never exceeded 8 Å.

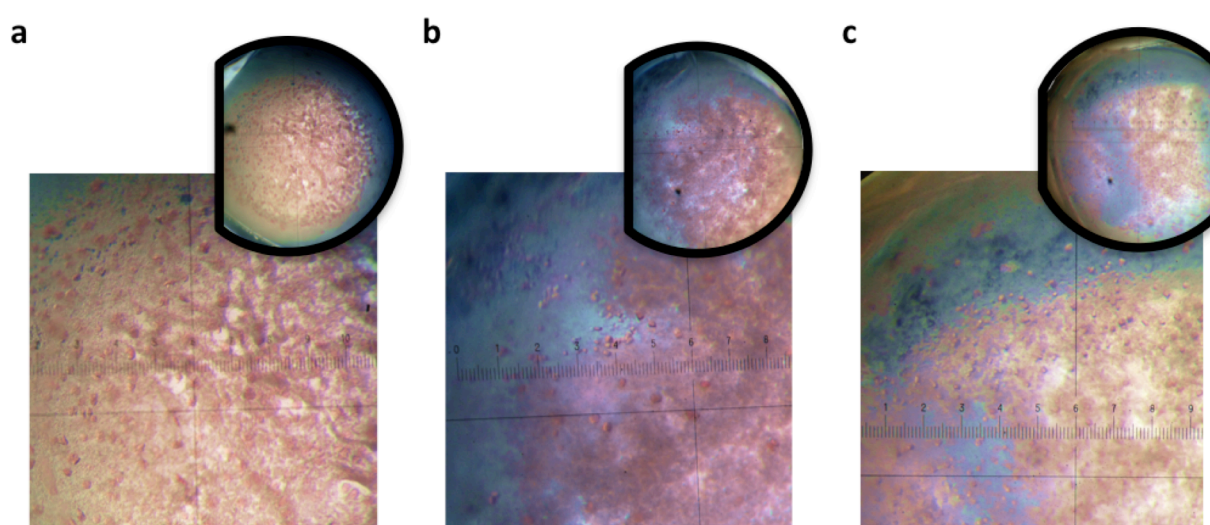


Figure 3.10 | Cytochrome *bc*₁ sitting drop crystal hits in complex with 4(1H)-pyridones. All crystals were grown at 4 °C with an initial protein concentration of 30 mg/ml. **a** Cytochrome *bc*₁ crystals with GW844520 grown with 10 % PEG4000 as a precipitant reaching a maximum size of ca. 20 µm. **b** Crystals of cytochrome *bc*₁ in complex with GW844520 using 12 % PEG4000 growing to a maximum size of ca. 50 µm. **c** Cytochrome *bc*₁ in complex with GSK932121 shown crystallised in 12 % PEG4000 grown to maximum size of ca. 50 µm.

3.2.5 Binding of 4(1H)-pyridones GW844520 and GSK932121

Crystals containing either GSK932121 or GW844520 (Figure 3.4 3 and 4) were grown to full size over the course of a week (Figure 3.10). Data collection and refinement statistics are in Table 3.3. No electron density peaks were present in the Q_o site of cyt. bc_1 but a strong positive peak in the F_o-F_c difference map was visible within the Q_i site for both GW844520 and GSK932121 (Figure 3.11). The Q_i binding site is formed by residues of transmembrane helices A, D and E and helix a located within the

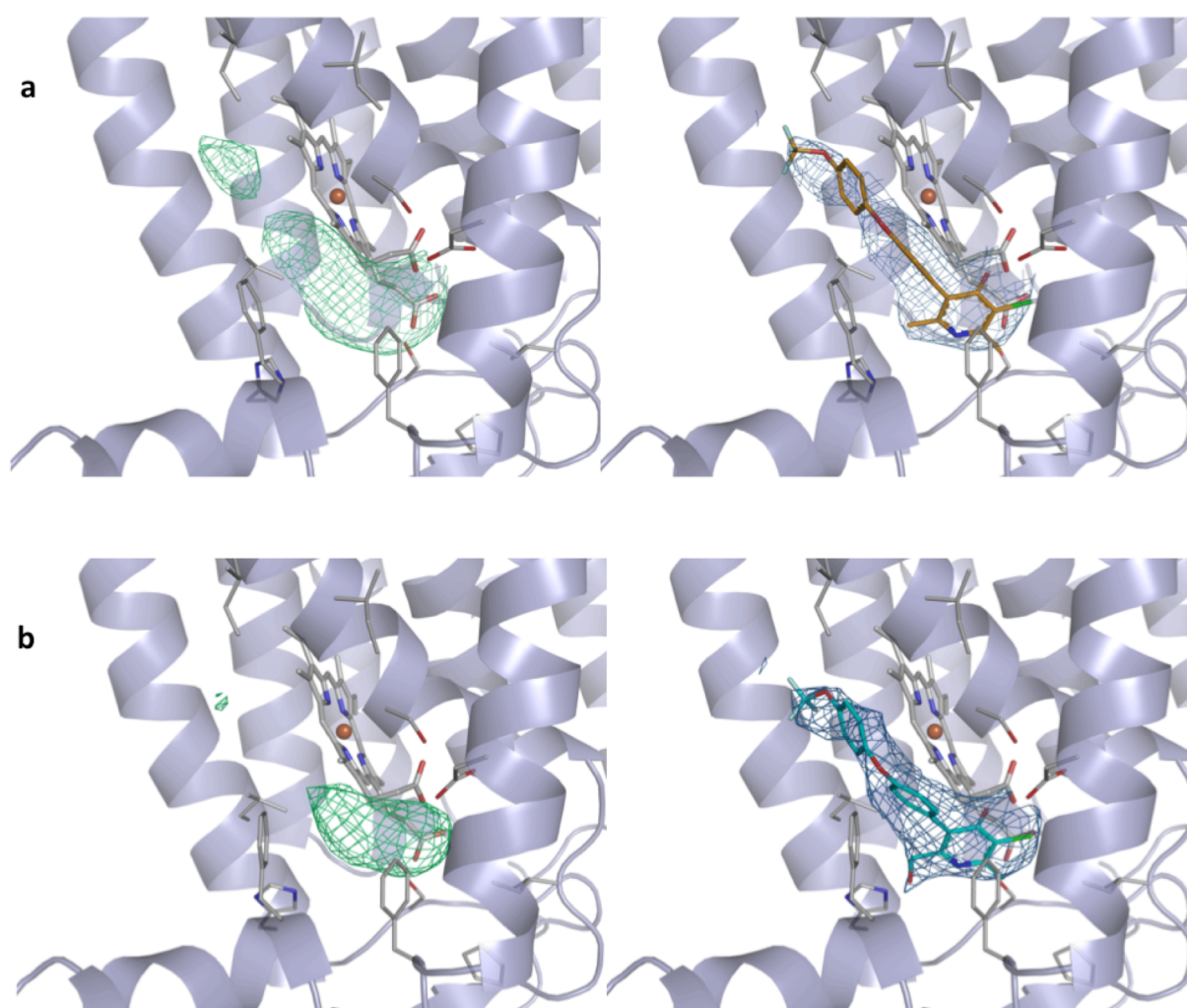


Figure 3.11 | Binding of 4(1H)-pyridones to bovine cytochrome bc_1 . a GW844520 (orange) bound to cyt. bc_1 . An initial F_o-F_c map contoured at 3σ in green followed by the refinement of the ligand into the Q_o site. Blue $2F_o-F_c$ map is contoured at 1σ . b GSK932121 (cyan) bound to cyt. bc_1 . The green F_o-F_c map is at 3σ is positioned in the Q_i site as with GW844520 and after refinement with the ligand present the $2F_o-F_c$ electron density map surrounds the compound well at 1σ .

Table 3.3 | Crystallographic statistics for cytochrome *bc*₁ structures in complex with the 4(1H)-pyridones GW844520 and GSK932121.

	bc₁-GW844520	bc₁-GSK932121
Data collection		
Space group	P 6 ₅	P 6 ₅
Cell dimensions		
<i>a, b, c</i> (Å)	129.9, 129.9, 722.2	129.65, 129.65, 720.12
α, β, γ (°)	90, 90, 120	90, 90, 120
Resolution (Å)	50 - 3.55 (3.68-3.58)	50 - 4.09 (4.25-4.09)
<i>R</i> _{sym} (%)	23 (85)	14 (50)
<i>I</i> / σ <i>I</i>	7.01 (1.83)	6.03 (1.78)
Completeness (%)	100 (100)	80.7 (51.5) [†]
Redundancy	8 (7)	3.2 (2.6)
Refinement		
Resolution (Å)	50 - 3.55	50 - 4.09
No. reflections	81351	50239
<i>R</i> _{work} / <i>R</i> _{free}	24.2/28.4	24/28.4
No. atoms		
Protein	31978	32805
4(1H)-Pyridone	28	29
B-factors (Å²)		
Protein	121.96	123.66
4(1H)-Pyridone	123.6	120.85
R.m.s. deviations		
Bond lengths (Å)	0.007	0.01
Bond angles (°)	1.39	1.89
PDB access codes	4UDE	4UDF

Numbers in parenthesis indicated high resolution shell
r.m.s: root mean square

transmembrane region of cytochrome *b*. It is accessible through a hydrophobic channel which terminates in a cavity of heme b_H and several polar residues. The binding of both GSK932121 and GW844520 appears very similar which is to be expected for such structurally similar compounds. The head group of both molecules binds close to heme b_H whilst the lipophilic tail extends out of the channel away from the heme.

The head of the compound was unambiguously placed in plane according to the omit F_o-F_c density and oriented placing the amine of the pyridone opposite His201 and Ser205 of helix D (Figure 3.12). The carbonyl of both GW844520 and GSK932121 are positioned within 3.5 Å of both Ser35 on loop A and OD1 of Asp228 on loop E which appears to be common amongst compounds that have been visualized within the Q_i site. The chlorine atom at position 3 appears surrounded by aliphatic residues. The diphenyl ether tail was placed in to the density directed towards Met190 and Met194. After refinement with the compounds added to the structure, additional electron density became visible allowing the positioning of the trifluoromethyl tail group in between Met190 and Met194. The phenyl groups of the tail was positioned close to Phe18, Ile43, Leu197 and lie along heme b_H showing the importance of hydrophobic interactions in the binding of these compounds.

The additional hydroxyl group at position 6 on the head of GSK932121 is within close proximity to His201 and Ser205 but cannot be positioned unambiguously at this resolution.

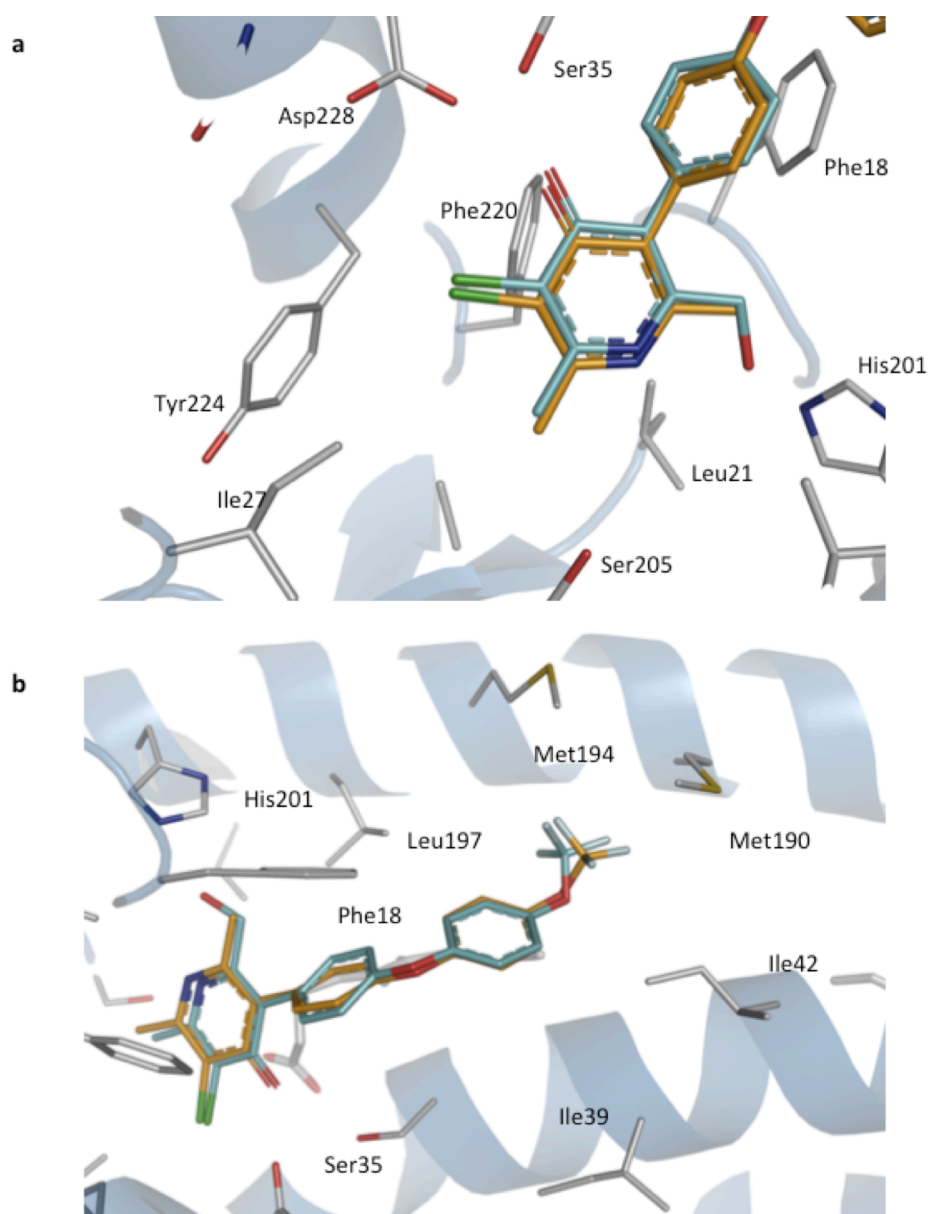


Figure 3.12 | View of the 4(1H)-pyridones overlaid bound in the Q_i site of bovine cytochrome bc_1 . Atoms are colour coded accordingly: oxygen in red, nitrogen in blue, chlorine in green. Carbon atoms in *cyt. b* are grey, in GSK92121 are cyan and GW844520 is displayed as orange. **a** The pyridone head groups of GW844520 and GSK932121 within the Q_i site overlap entirely. The additional hydroxyl moiety of GSK932121 is positioned near His201. **b** Both compounds lie along helices A and D of *cyt. b* with the trifluoromethyl group terminating near Met190 and Met194. The first aryl group from the pyridone forms a stacking interaction with Phe18. Figure produced using Pymol (www.pymol.org).

3.2.6 Binding of MJM 170

Crystals of cyt. *bc*₁ bound to MJM 170 were allowed to grow to full size over the course of upto 2 weeks (Figure 3.13). The structure was solved using the same methods as with the 4(1H)-pyridones and crystallographic statistics are summarised in Table 3.3. A large positive peak in the F_o-F_c map in the Q_i site of cyt. *bc*₁ was present (Figure 3.14) and MJM 170 was modelled in to the density unambiguously. The refined $2F_o-F_c$ electron density map fit well and confirmed MJM 170s status as a Q_i inhibitor. The planar region of the quinolone head group is positioned flat between heme *b*_H and Phe220 whilst the additional ring further extends into the hydrophobic cavity at the apex of

the binding site towards Ala23, Pro24 and Ile27, and Trp31. It potentially forms also a stacking interaction with Tyr224 (Figure 3.15). The polar functional groups of the quinolone are similarly placed to those of the 4(1H)-pyridones. The polar residues Ser35 and Asp228, and the carbonyl of Trp31 surround the carbonyl group on the quinolone whilst the amine is positioned between His201 and Ser205. The tail extends outwards towards the hydrophobic residues Ile39, Ile42 and Leu197 and forms a stacking interaction with Phe18.

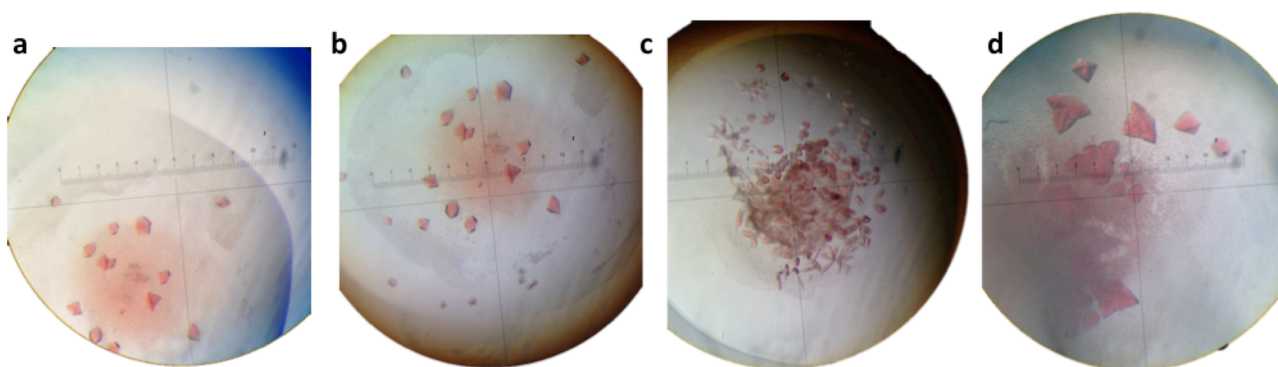


Figure 3.13 | Several examples of cytochrome *bc*₁ crystals grown in complex with MJM 170 at 4 °C. **a** Crystals grown using 8 % PEG4000 with an initial protein concentration of 30 mg/ml in the hanging drop format. **b** Crystals grown using 8 % PEG4000 in a hanging drop experiment with an initial protein concentration of 40 mg/ml. Crystals were seen as large as ca. 200 μ m. **c** Proteins grown using 9 % PEG3350. Crystals grew as rods and grew to ca. 100 μ m. **d** Sitting drop crystallisation of cytochrome *bc*₁ at 40 mg/ml using 8 % PEG4000. Maximum crystals grew larger than 500 μ m.

Table 3.4 | Crystallographic statistics for the structure of cytochrome bc₁ in complex with the novel 4(1H)-quinolone MJM 170.

	Cytochrome MJM170	bc ₁	-
Data collection			
Space group	P 6 ₅		
Cell dimensions			
a, b, c (Å)	129.47, 129.47, 720.29		
α, β, γ (°)	90, 90, 120		
Resolution (Å)	50 – 3.5 (3.56 – 3.50)		
R_{pim}	0.16 (0.82)		
I/σI	5.2 (1.4)		
CC1/2	0.971 (0.331)		
Completeness (%)	99.6 (99.7)		
Multiplicity	9.2 (9.2)		
Refinement			
No. reflections	80,651		
R_{work} / R_{free}	24.13 / 29.13		
No. atoms	31,811		
Protein	30,980		
Other	831		
Average B factors (Å²)			
Protein	93.84		
Other	87.96		
r.m.s deviations			
Bond lengths (Å)	0.010		
Bond angles (°)	1.564		
Ramachandran statistics			
Favoured (%)	95.44		
Allowed (%)	4.56		

Numbers in parenthesis indicated high resolution shell
r.m.s: root mean square

3.2.7 Homology between cytochrome *b* sequences

In order to further improve the compounds discussed so far, it is necessary to understand the differences between the mammalian cyt. *bc*₁ and the cyt. *bc*₁ complexes of both *P. falciparum* and *T. gondii*. A sequence alignment was carried out on the protein sequences using ClustalOmega (Sievers et al. 2011) (Figure 3.16) and homology models were produced using the SWISS-MODEL server (Biasini et al. 2014) (Figure 3.17). The primary sequence alignment shows that these proteins are largely conserved, but that there are several differences. The N-terminal sequence is particularly shorter in *P. falciparum* whilst it appears the C-terminus is reduced in *T. gondii*. There are also several areas of inserted sequence though these largely appear to affect the surface of the protein and are distant from either the Q_i or Q_o site. There are however several smaller differences located in the active sites.

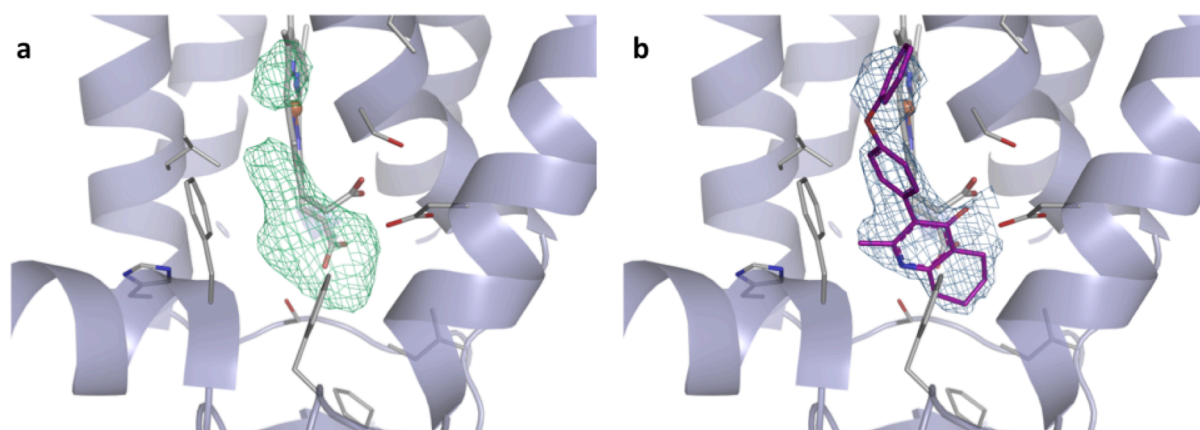


Figure 3.14 | Binding of MJM 170 within the Q_i site. Carbon atoms of cyt. *b* are coloured grey, carbon atoms of MJM170 are coloured purple. **a** The F_o-F_c difference map contoured at 3 σ clearly shows the location of MJM 170 within the Q_i site. **b** When the ligand is refined in the Q_i site, the 2F_o-F_c electron density map, contoured at 1 σ , covers the ligand unambiguously. Figure produced using Pymol (www.pymol.org).

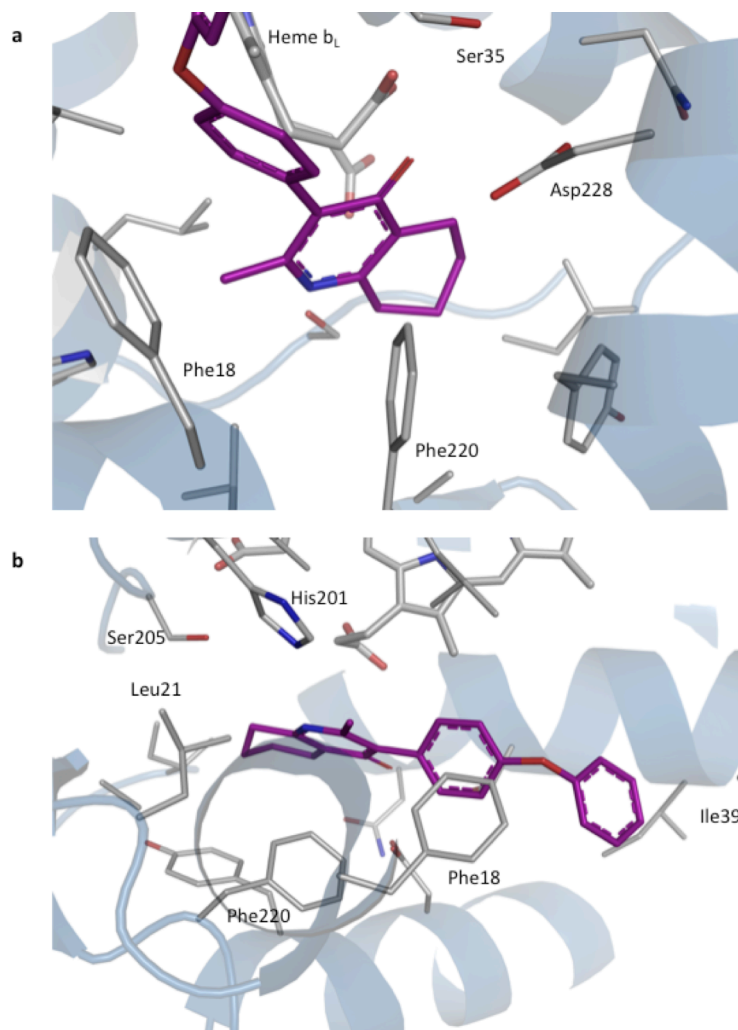


Figure 3.15 | View of MJM 170 bound to cytochrome *b*. **a** The tetrahydroquinolone scaffold is located at the apex of the Q_i site. The additional ring is placed further into the cavity whilst the amine and carbonyl are both positioned as in the 4(1H)-pyridones. **b** A view along the length of MJM 170. The diphenylether group lies along helices A and D as it does in the 4(1H)-pyridone structures. Figure produced using Pymol (www.pymol.org).

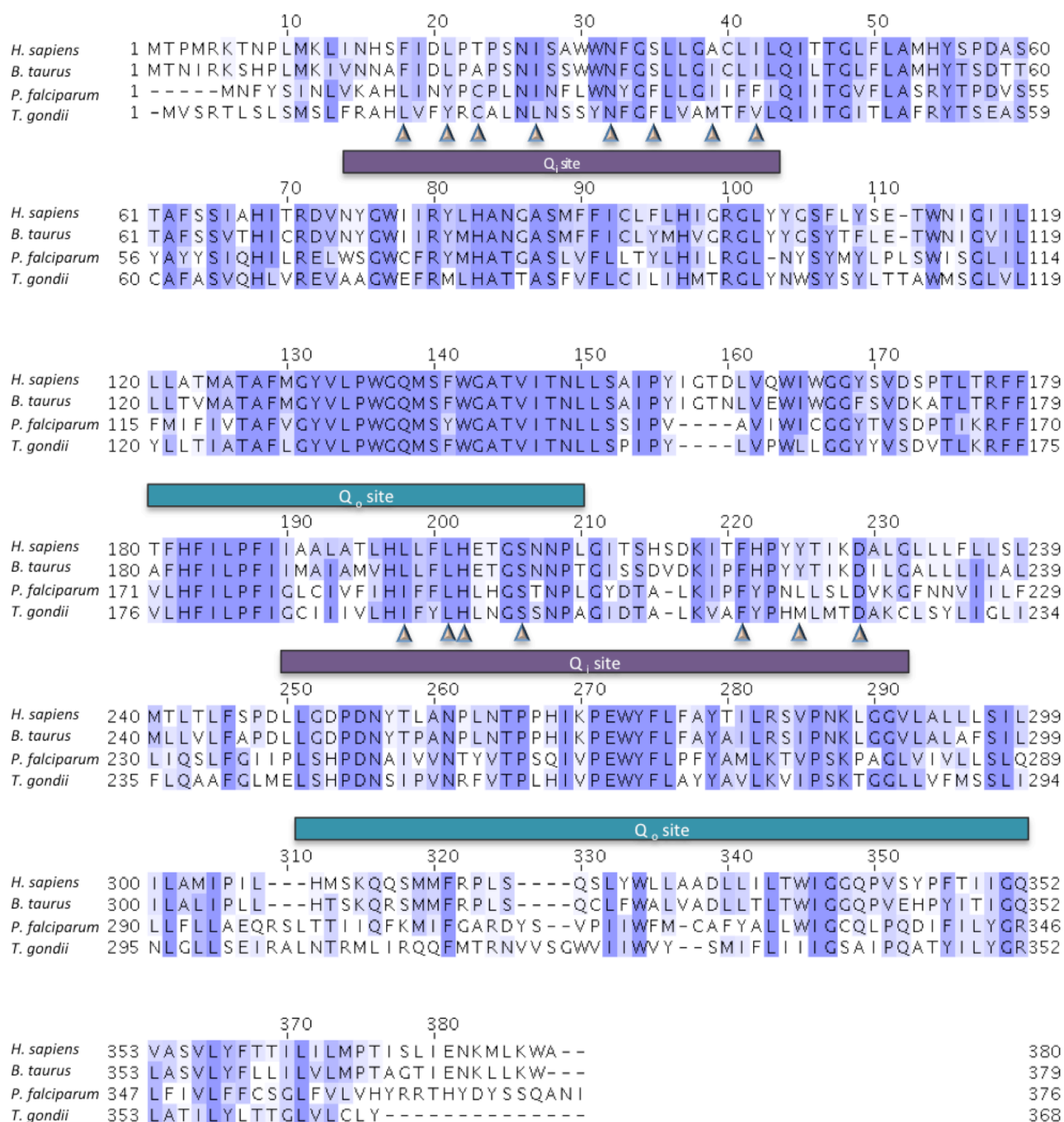


Figure 3.16 | Sequence alignment of mammalian and apicomplexa cytochrome *b* amino acid sequences. Key residues involved in the binding of 4(1H)-pyridones and the tetrahydroquinolone MJM 170 in the Q_i site are identified by triangles. There are several differences in the Q_i site which could be exploited to increase specificity, particularly in the N-terminal region of the domain. Alignment produced using Clustal Omega (Sievers et al. 2011).

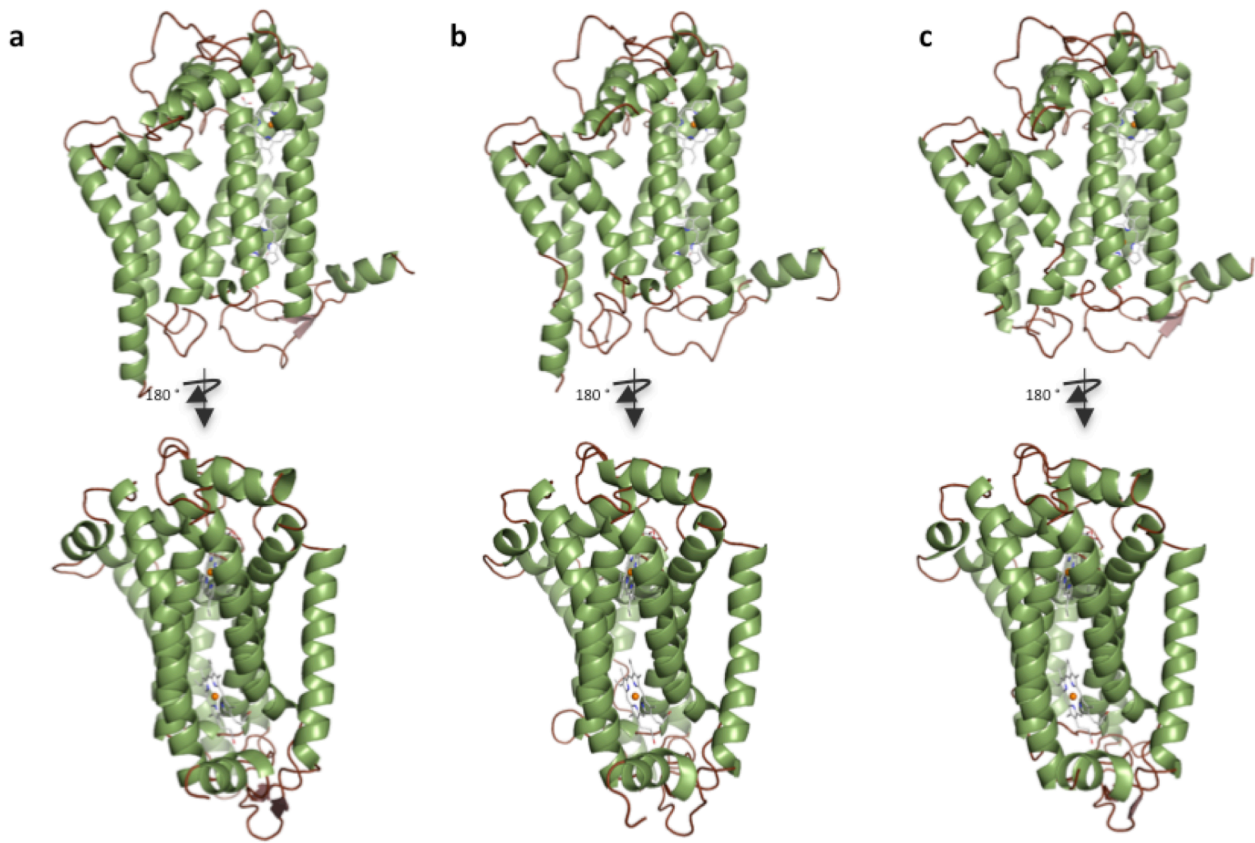


Figure 3.17 | Homology models of cytochrome *b*. **a** Structure of bovine cytochrome *b*. **b** Structure of *P. falciparum* cytochrome *b*. **c** Model of *T. gondii* cytochrome *b*. The overall structure is similar differences in the helix α of the N-terminus can be seen. The helix of *T. gondii* is far shorter than those of bovine and *P. falciparum* (the bovine N-terminus could not be modelled into electron density and therefore looks shorter than it may be). The *P. falciparum* and *T. gondii* models appear to have larger loops than the bovine towards the bottom of the structure which could affect the size of the Q_i binding site as shown at the bottom of the models. Figure produced using Pymol (www.pymol.org).

The homology produced models of *P. falciparum* and *T. gondii* cyt. *b* were aligned to the crystal structure of bovine cyt. *b* with an RMSD 0.649 and 0.547 respectively using the toolkit available in Pymol. This showed a good overall structural consensus except for the shortening of the C-terminal helix in *T. gondii* and increased length of several loops in the apicomplexan cyt. *b*. There are multiple differences of note in the Q_i site that could benefit Q_i drug design (Figure 3.18). The majority of these differences are positioned on helices A and D and include a larger number of phenylalanine residues in this cleft.

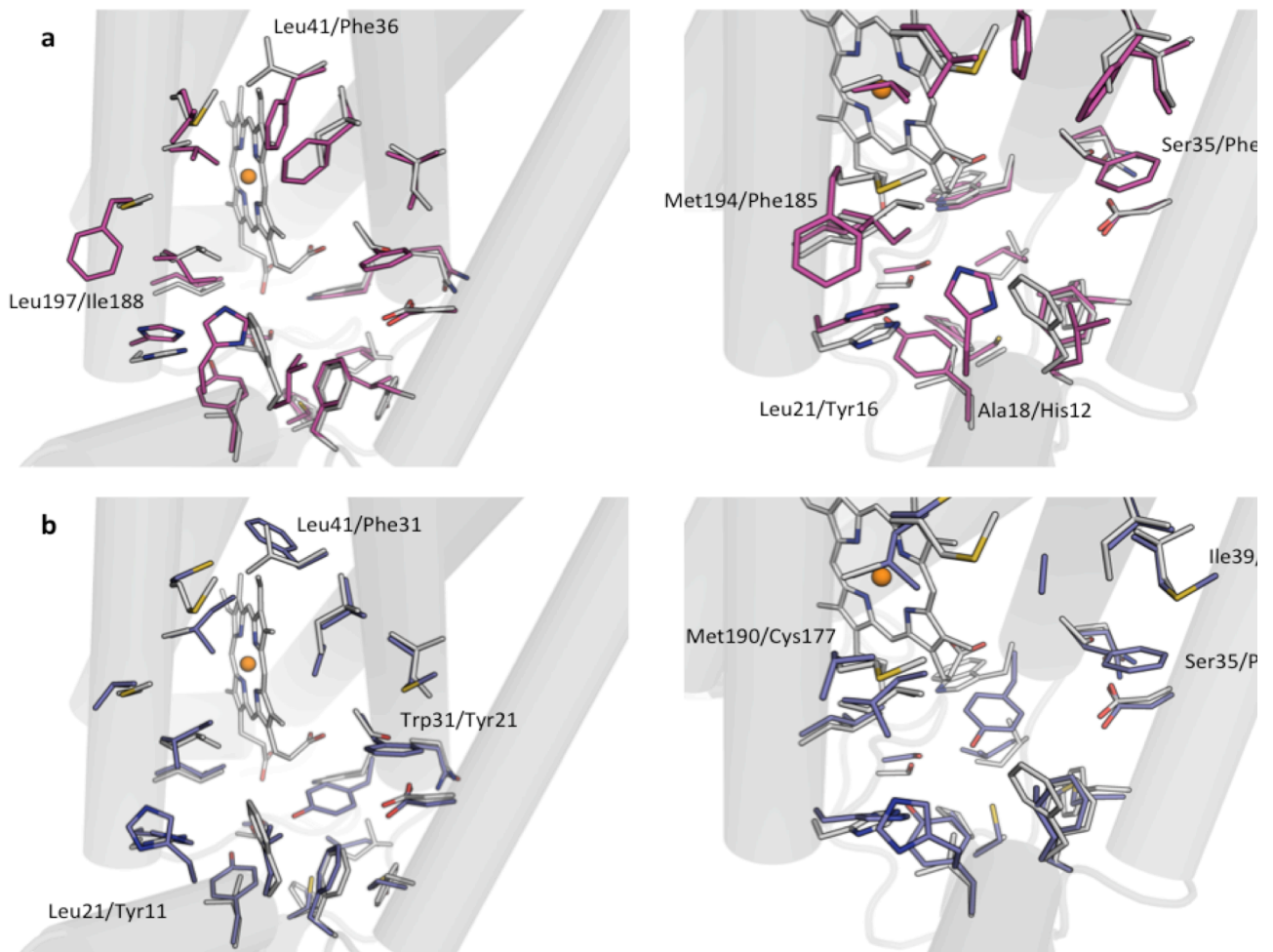


Figure 3.18 | Overlaid Q_i sites of bovine, *P. falciparum* and *T. gondii* cytochrome *b*. **a** Overlaid bovine residues (white) and *P. falciparum* residues (red). **b** Overlaid bovine model with *T. gondii* residues (blue). Figure produced using Pymol (www.pymol.org).

3.3 Discussion

3.3.1 4(1H)-pyridones are Q_i site inhibitors

These crystallographic studies show that both GW844520 and GSK932121 are Q_i site inhibitors of the bovine cyt. *bc*₁ complex. This has revealed the mechanism by which these compounds were able to overcome atovaquone resistance in the Q_o site. This is contrary to previous work suggesting an alternate binding mode within the Q_o site based on mutation and *in silico* studies (Rodrigues et al. 2009). As stated previously, both of these compounds bind in a very similar mode, which is unsurprising due to their high structural homology (Figure 3.19). This suggests that other members of the 4(1H)-pyridone scaffold may also bind the Q_i site. Although

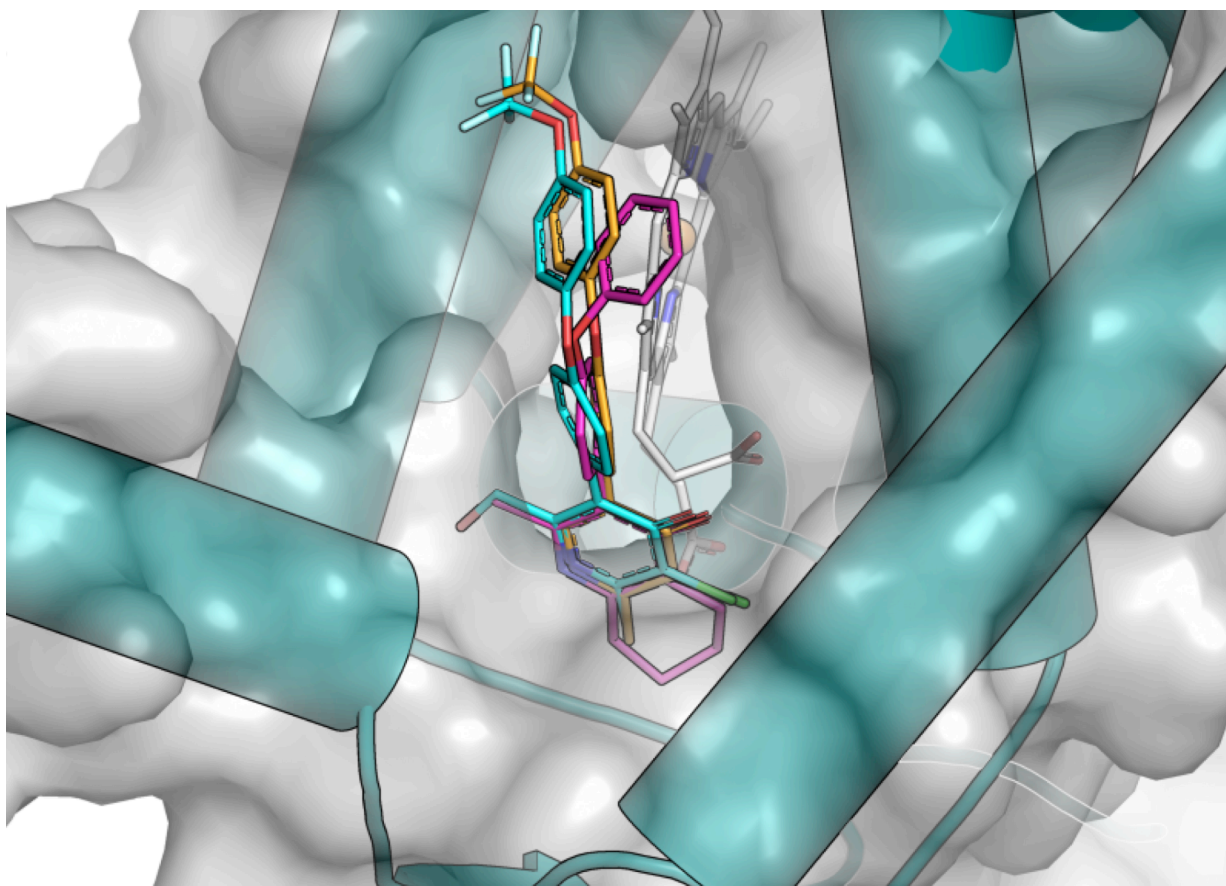


Figure 3.19 | View of GW844520 (orange), GSK932121 (cyan) and MJM 170 (magenta) bound in the Q_i site superposed. The compounds bind in a highly similar mode with the additional ring of the tetrahydroquinolone going deeper into the hydrophobic regions of the Q_i site. The addition of the trifluoromethyl to the 4(1H)-pyridones appears to have caused the diphenyl ether tail to alter position slightly.

the resolution of the structures is low, it is possible to see many details of the binding of the compound, which may help develop novel compounds that bind the Q_i of the parasite complex and not that of the host. Information about the role ordered water molecules play in the binding of the 4(1H)-pyridones is lacking at this resolution. Water has previously been shown to play an important role in the better-studied Q_o site and has been visualised bound to the potent Q_i inhibitor Antimycin within the Q_i site and it is likely to play a role in the binding of these compounds also (Huang et al. 2005; Postila et al. 2013).

The substitution of a methyl group for an alkyl group in GSK932121 is located near His201 (Figure 3.12). It is also in close proximity to the carbonyl group of the peptide on Ala17. This polar environment could provide a strong network of H-bonds, which could help explain the additional efficacy of GSK932121 compared to GW844520 (IC_{50} 2 nM compared to 5 nM respectively (Bueno et al. 2012)). Both His201 and Ser205 are conserved residues and are unlikely to alter position radically in either parasites cyt. *bc1* complex. Ala17 is part of the largely unconserved N-terminal helix α and in both *P. falciparum* and *T. gondii* is replaced by a His residue which could have implications in the binding of both these compounds.

This study has also revealed the cause of compound toxicity, as they are capable of binding mammalian cyt. *bc1*. To confirm this, work was carried out using HEK92 cell grown on galactose. By growing the cells on galactose medium, respiration was forced through the mitochondria, which sensitises these cells to mitochondrial inhibitors and reverses the Crabtree effect (Crabtree 1928; Marroquin et al. 2007). When tamoxifen, a non-mitochondrial inhibitor, is added to the media there is no effect on viability whereas addition of rotenone causes a severe drop in viability (Figure 3.20a and b). Upon the addition of the pyridones, there was also a drop in viability of the cells confirming the toxicity to human cells through interference with the ETC (Figure 3.20c and d) (Capper et al. 2015). This has confirmed that these pyridone compounds are mitochondrial inhibitors within human cells.

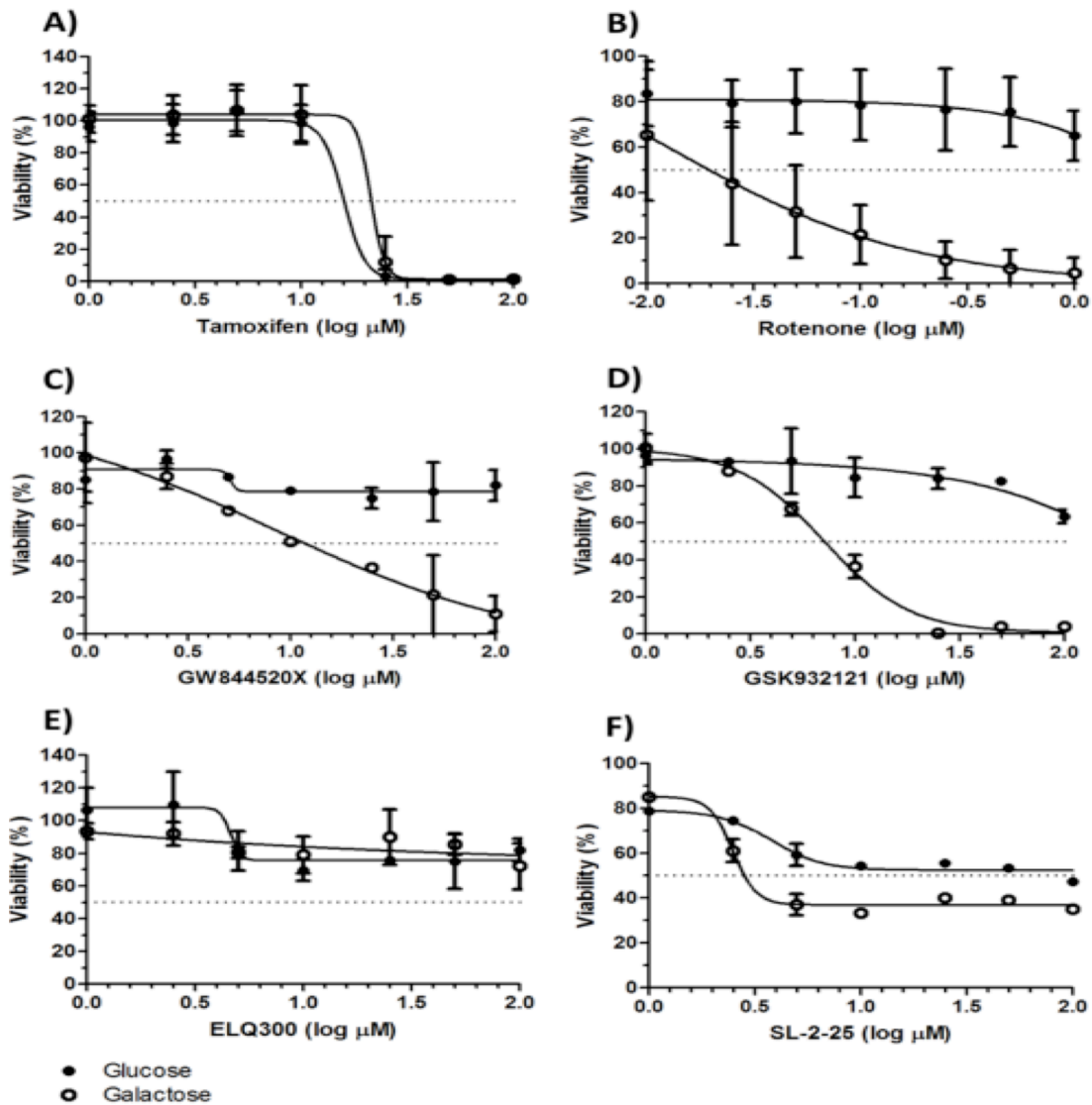


Figure 3.20 | Effects of inhibitors on HEK92 cell viability when grown in different media. **a** Tamoxifen does not act on the mitochondrial ETC and so reduces cell viability regardless of media. **b** Rotenone is a known inhibitor of the complex I and has no effect on viability of cells when grown on glucose as a result of the Crabtree effect. **c** and **d** Both GW844520 and GSK932121 show effect on cell viability when grown on galactose but not when grown on glucose, confirming their mitochondrial inhibition effect on human cells. **e** and **f** ELQ300 and SL-2-25 were tested using the same methods and shown to reduce viability to an extent by targeting the ETC also. Figure adapted from (Capper et al. 2015).

3.3.2 The 4(1H)-quinolone MJM 170 binds the Q_i site

As discussed, MJM 170 was developed as novel tetrahydroquinolone from the endochin-like quinolone scaffold with increased solubility and

efficacy against apicomplexa enzymes (publication under review). Work had already been carried out which suggested that MJM 170 was a Q_i inhibitor based on the 4(1H)-pyridones using yeast mutations in the Q_i site that prevented MJM170 inhibition. The crystallographic structure provides direct evidence of this. Due to the structural similarity between MJM 170 and the 4(H)-pyridones, its binding is similar within the Q_i site. The additional ring of MJM 170 is positioned further towards the end of the Q_i site with the planar region occupying the same space as the pyridones (Figure 3.16). The puckered ring is located in a hydrophobic region that shows variation between the mammalian, *P. falciparum* and *T. gondii* sequences and is a promising region for further drug development. Ala23 lies at the end of the channel and is replaced by Cys13 and Cys18 in *P. falciparum* and *T. gondii* respectively. Met210 or Leu214 substitutes Tyr224, which is placed over the ring. This will remove any stacking interaction that takes place in the protozoa cyt. *b* but remains hydrophobic. Trp26 is replaced by a Tyr residue in the *T. gondii* protein, this could potentially open the Q_i site up towards the apex and allow an additional functional group to be built in to increase specificity.

3.3.3 Future drug development targeting the cytochrome bc₁ Q_i site

Structural information of Q_i site inhibitors has been lacking, which has prevented the development of compounds that target it. Here it has been shown that the Q_i site is a valid target for antiprotozoal compounds and that there are suitable differences in homology between the mammalian protein and those of the protozoa (Figure 3.21). Other recent works have also shone light on the Q_i site as a potential site for antimalarial and antitoxoplasmosis action. It has been shown that subtle changes to the ELQs can alter them from Q_o to Q_i site binding compounds (Stickles, Justino de Almeida, et al. 2015). This identified several important moieties on 4(1H)-quinolone scaffold that determine binding according to mutation studies. *In silico* work carried out docking ELQ 300, a Q_i inhibitor, positions it in a similar manner to MJM 170

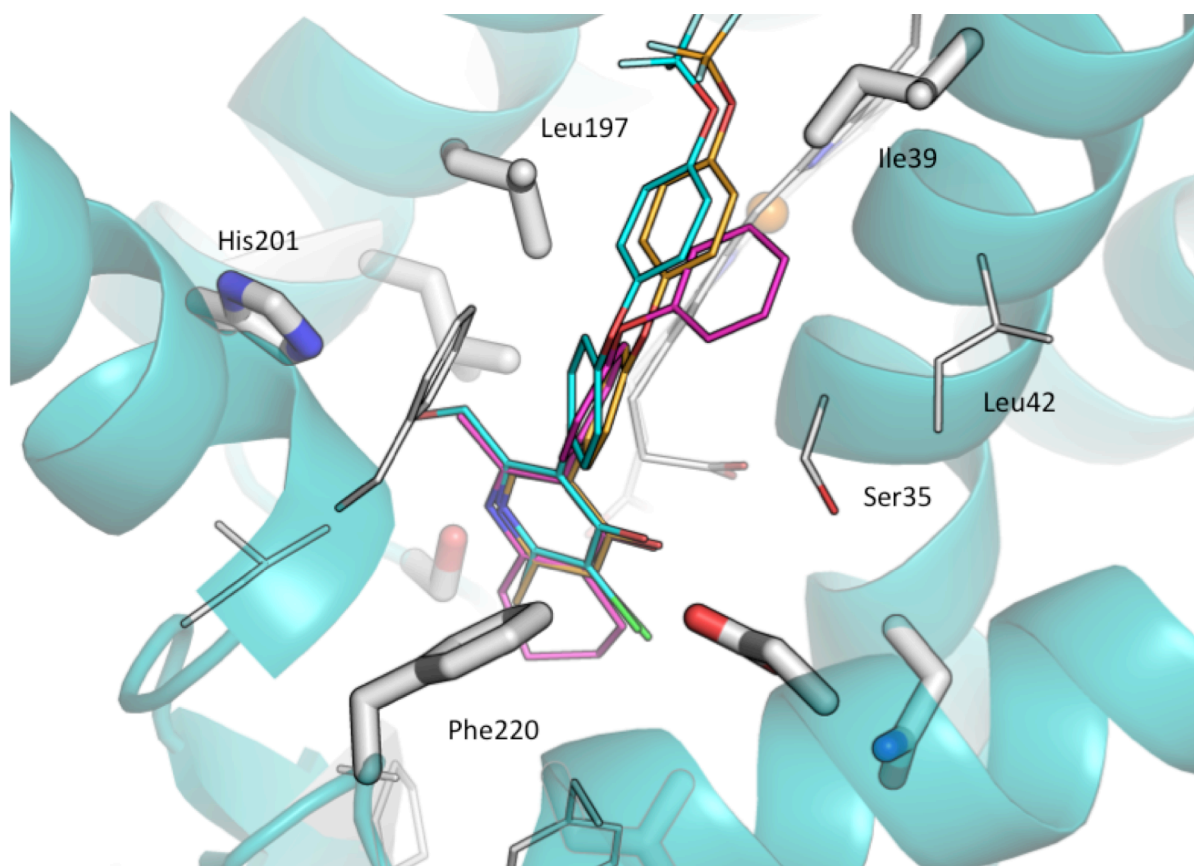


Figure 3.21 | Conservation in the Q_i site of *cyt. b* between parasite and mammalian models. The bovine structure is illustrated with conserved residues emphasised using thick stick amino acids. GW844520 is shown in orange, GSK932121 in cyan and MJM 170 in magenta. Several key residues involved in binding (labelled) are conserved and won't allow for much alteration to the chemical scaffold i.e. Phe220 and His201. Other residues such as Ser35 are altered in the parasite complex and these regions should be targeted to improve specificity in future drug design.

(Stickles, Justino de Almeida, et al. 2015; Capper et al. 2015). This could see the Q_i site become as important a target as the Q_o site.

The hydrophobic diphenyl ether is essential for the strong activity of 4(1H)-pyridones and 4(1H)-quinolones against *cyt. bc₁* (Nilsen et al. 2014; Yeates et al. 2008). Helix a of the N-terminus forms a large number of hydrophobic reactions with this functional group and is largely unconserved between the mammalian and parasites forms. Phe18 is clearly positioned to form stacking interactions with the diphenyl ether moiety in the bovine crystal structure. This residue is replaced with Leu in both parasites (Figure 3.16) (Figure 3.22). Ala17 forms part of the hydrophobic cleft around these

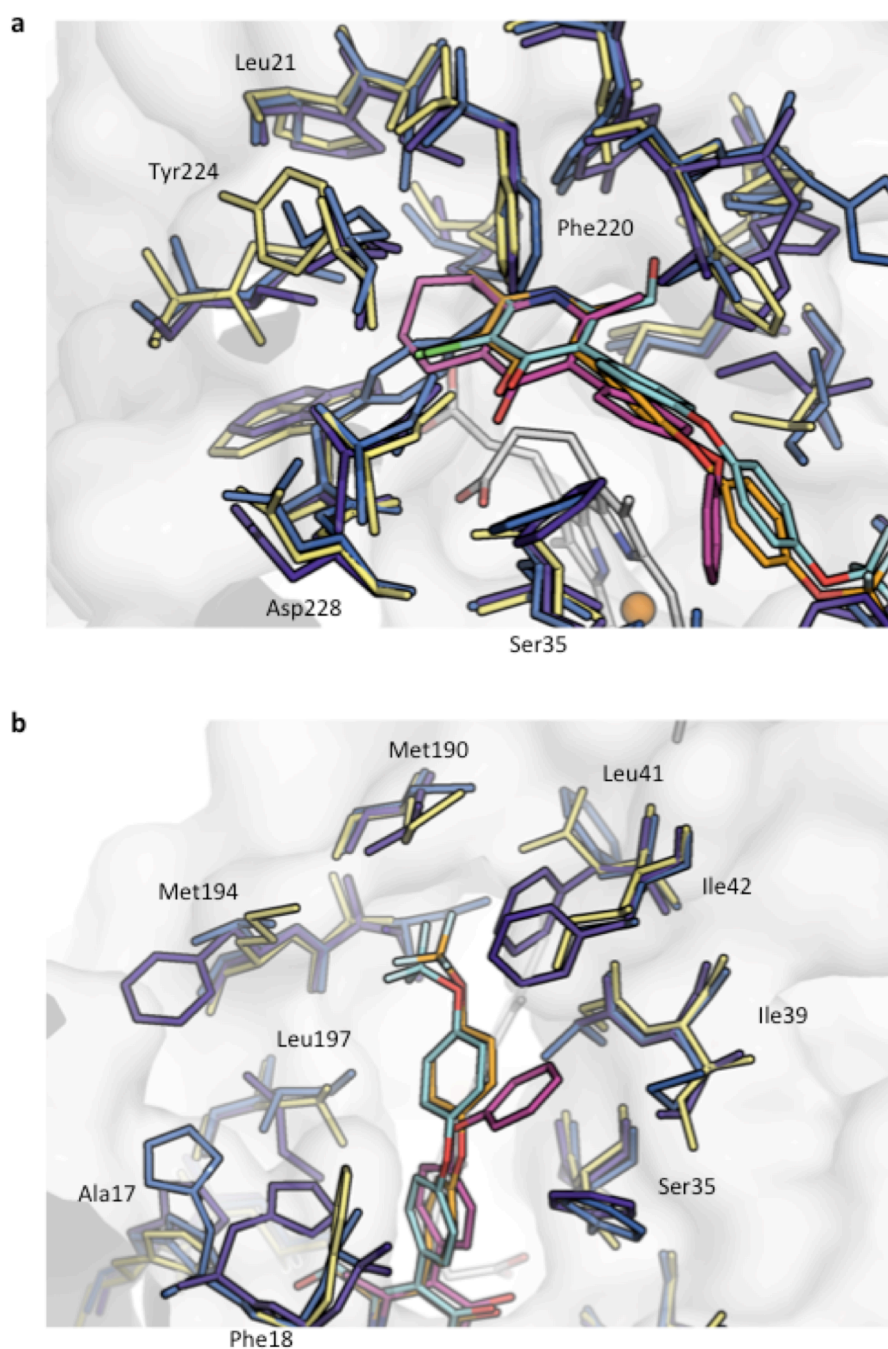


Figure 3.22 | Overlaid homology models of both apicomplexa cytochrome *b* protein over the bovine cytochrome *b* structure. Ligands GW844520, GSK932121 and MJM 170 are coloured in orange, cyan and magenta respectively. Bovine, *P. falciparum* and *T. gondii* cytochrome *b* are yellow, purple and blue each. **a** The overlaid models around the head of each ligand. **b** The aligned models round the diphenyl ether region of each compound.

compounds but is replaced by His in both apicomplexa cyt. *b*. The alteration of these two residues maintains the hydrophobic interactions across the diphenylether in all compounds whilst also providing the possibility for a

polar interaction with a histidine residue. This would improve compound specificity. Pyridines have previously been incorporated into the lipophilic tail during compound development but appeared less effective than their phenyl equivalents (Nilsen et al. 2014).

Ser35, which is located in a hydrophilic pocket surrounding the carbonyl group of both the pyridones and quinolones, is substituted by a Phe residue in both the *P. falciparum* and *T. gondii* homology models. In these models, the phenyl ring of Phe appears to move away from the hydrophilic Asp and Asn residues in that region and has moved in a way that could form stacking interactions with the diphenyl tail. Towards the apex of the cavity, Leu21 and Ala23 in the bovine protein are replaced by Tyr and Cys residues respectively. The change to a Cys residue brings the hydrophobic environment closer to the compounds. The thiol is located above the puckered ring of MJM 170 and towards the methyl group of both 4(1H)-pyridones. The change from Leu21 to Tyr in both parasites leads to a large structural change in the binding site and fills a small pocket around the amine. The hydroxyl group could form interactions here. Tyr224 is replaced by Met210 in *T. gondii* and Leu214 in *P. falciparum*. Both of these residues are more flexible than Tyr224 and could reduce space at the apex forming tighter hydrophobic interactions with the ligands.

Chapter 4 | **Therapeutic effects of rusticyanin**

The merozoite stage of *Plasmodium spp.* is covered in an abundance of surface proteins named merozoite surface proteins. Many of these proteins are thought to have a role in the adhesion to, reorientation on and the invasion of red blood cells and undergo tightly regulated processing (Boyle et al. 2014). These surface proteins have been the subject of vaccine development research and have been shown to be targeted by the immune system upon infection (Fowkes et al. 2010; Richards & Beeson 2009). Antibodies targeting the merozoites are thought to function through opsonisation for phagocytosis by the body's immune system (Bouharoun-Tayoun et al. 1990), by preventing merozoite invasion into the red blood cells (Cohen et al. 1969) and complement-mediated lysis.

4.1 Therapeutic effect of cupredoxins against malaria

Work carried out by Cruz-Gallardo et al (Cruz-Gallardo et al. 2013) demonstrated the therapeutic benefits of cupredoxins in culture with *P. falciparum* parasites. The cupredoxins were studied due to their homology to the immunoglobulin fold. Rusticyanin was the stand-out cupredoxin tested and appeared to have a dramatic effect on parasite growth. It is interesting that holo-rusticyanin showed a strong effect against *P. falciparum* growth whilst the apo protein showed no substantial change. Using isothermal calorimetry (ITC) and NMR studies, rusticyanin was determined to form a strong complex with a 19 kDa fragment of *Plasmodium yoeli* merozoite surface protein 1 (MSP1₁₉). Reduced rusticyanin bound with a K_d of 2 μ M whilst the oxidised form binding was an order of magnitude weaker ($K_d = 25 \mu$ M). Apo-rusticyanin showed no discernible binding. Previously, azurins have been shown to bind MSP1₁₉ less strongly than rusticyanin (Chaudhari et al. 2006).

4.1.1 Merozoite surface protein 1

Merozoite surface protein 1 (MSP1) forms the majority of the surface proteins found on *Plasmodium spp.* merozoites (Kadekoppala & Holder 2010). MSP1 has been shown to have a role in red blood cell binding by the

merozoite in a protein-dependent manner as opposed to sialic acid dependent interactions (Urquiza et al. 1996; Goel et al. 2003). In *P. falciparum* MSP1 is expressed as a ca. 200 kDa polypeptide precursor during schizogony. The polypeptide is highly polymorphous. During maturation, the MSP1 polypeptide is processed into the mature protein through tightly controlled cleavages. The mature complex remains attached to the merozoite surface by a glycosylphosphatidyl inositol (GPI) anchor on the C-terminus. MSP1 is initially cleaved into four polypeptides which remain associated on the membrane of the merozoites through non-covalent interactions during merozoite release (Figure 4.1). The first cleavage is carried out by the serine protease SUB1 (Koussis et al. 2009) which also has a role in the maturation of MSP6, MSP7 and AMA1. This cleavage results in 4 fragments: the largest fragment is an the N-terminal 83 kDa fragment MSP1₈₃, two more fragments MSP1₃₀ and MSP1₃₈, and the C terminal fragment MSP1₄₂. Without this cleavage, merozoites are unable to invade further red blood cells (Koussis et al. 2009). The MSP1 complex also contains protein derived from the surface proteins MSP6 and MSP7 that associated through non-covalent binding (Figure 4.2).

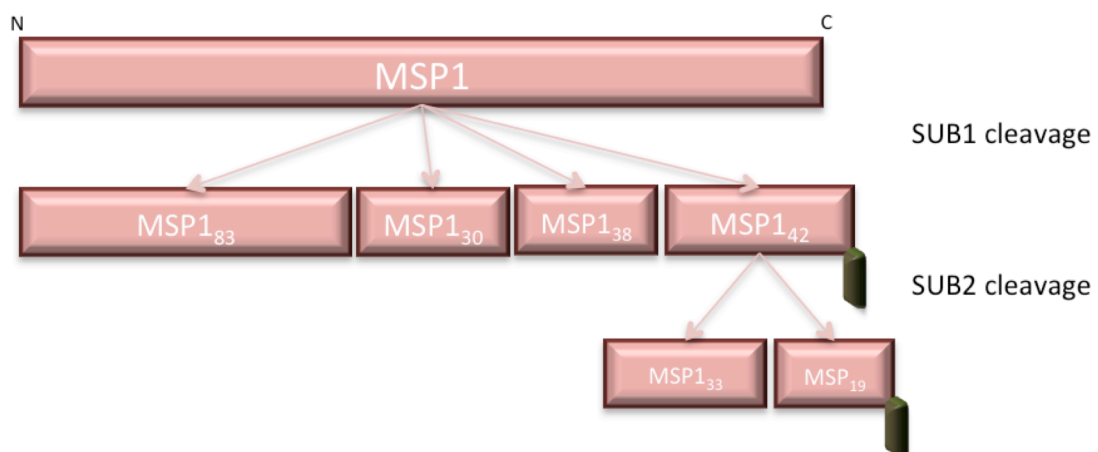


Figure 4.1 | Cleavage of the MSP1 polypeptide. Protein cleavage occurs in two stages. The polypeptide is first cleaved by SUB1 into four proteins that remain bound to each other through non-covalent interactions and bound to the membrane though a C-terminal GPI anchor on MSP1₄₂. A second cleavage is carried out by SUB2 on MSP1₄₂ producing MSP1₃₂ and the C-terminal fragment MSP1₁₉.

Upon the merozoite binding to a RBC, a second proteolytic cleavage step by membrane bound SUB2 cleaves MSP1₄₂ into MSP1₃₃ and MSP1₁₉ (Harris et al. 2005) (Figure 4.1). MSP1₃₃ is a soluble protein that is shed from the membrane and blocks the inflammatory response mediated by S100P (Waisberg et al. 2012). MSP1₁₉ remains attached to the cell membrane by the GPI anchor and enters the red blood cell along with the merozoite (Figure 4.2) (Blackman et al. 1990). Antibodies targeting MSP1₄₂ can prevent this proteolytic cleavage whilst not inhibiting erythrocyte invasion (Blackman et al. 1994). MSP1₄₂ has been the target of vaccine candidates that have entered clinical trials but there has not yet been great success (Ellis et al. 2012). Vaccines have also been developed targeting MSP1₁₉ and have shown promise (Egan et al. 1999; Langermans et al. 2006).

4.1.1.1 MSP1₁₉

MSP1₁₉ has been detected within the food vacuole of differentiated trophozoites within the red blood cells (Drew et al. 2005). It remains on the surface of the food vacuole without further modification and has been

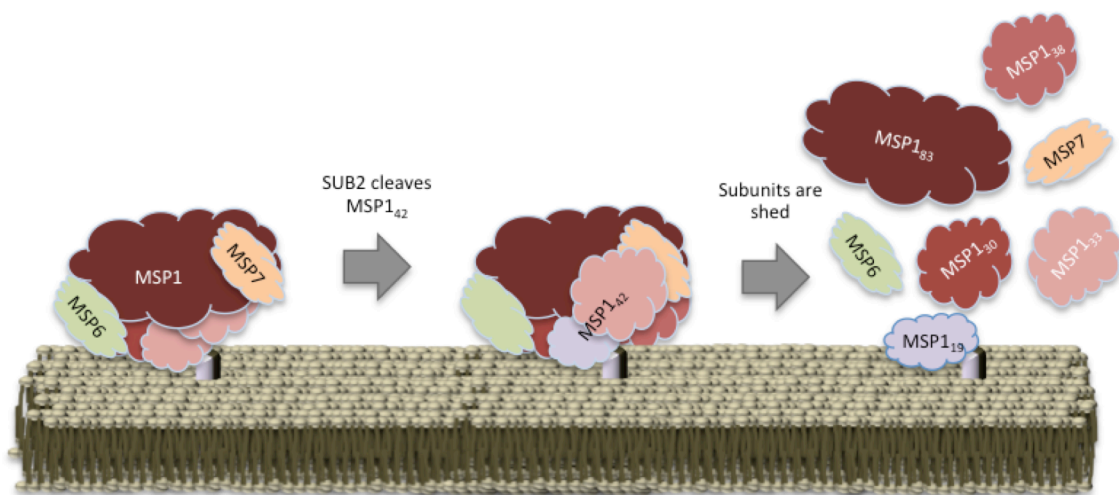


Figure 4.2 | MSP1/6/7 complex and subsequent shedding. The MSP complex is linked to the membrane by a GPI anchor and is held together through non-covalent interactions. After SUB2 cleavage MSP1₃₃ remains attached to the complex through non-covalent interactions. Shortly before invasion, all of the protein sub-units are shed whilst MSP1₁₉ remains attached through the GPI anchor. MSP1₁₉ subsequently enters the RBC and form a part of the parasite food vacuole.

implied to serve a function in the formation of the vacuole itself (Dluzewski et al. 2008). Antibodies targeting MSP1₁₉ have been shown to prevent parasite growth and emphasize its importance in vaccine development against malaria (Egan et al. 1999). Antibodies bound to MSP1₁₉ may also be internalised upon red blood cell invasion (Blackman et al. 1994). Recent work has targeted MSP1₁₉ with small molecules that inhibit invasion (Chandramohanadas et al. 2014).

MSP1₁₉ is a well conserved protein across *Plasmodium spp.* and is formed by the cysteine rich C-terminal region of MSP1. Early sequence analysis indicated that structurally it consisted of two epidermal growth factor (EGF) like domains each containing six cysteines (Figure 4.3) (Holder et al. 1992; O'Donnell et al. 2000). This has since been confirmed by X-ray crystallographic studies in complex with antibodies and NMR in solution on its own (James et al. 2006; Morgan et al. 1999; Babon et al. 2007; Garman et al. 2003). The 96 amino acid structure shows both EGF-like domains connected by a region of hydrophobic interactions (Morgan et al. 1999). Likely due in part to this compact structure and large number of di-sulphide bonds, MSP1₁₉ is resistant to protease degradation which has been suggested as one of the reasons it is able to remain present in the food vacuole (Dluzewski et al. 2008). The EGF-like domains rather than the specific primary sequence appear to be essential for MSP1₁₉ function (O'Donnell et al. 2000; Drew et al. 2004).

4.1.2 Cupredoxins

The cupredoxins are small, soluble copper containing proteins that are possibly evolutionarily linked to immunoglobins (Stevens 2008). They all contain Type-1 copper and appear to be largely involved in electron transfer. Several cupredoxins have previously been shown to have therapeutic effects against several diseases. These include HIV, cancers, toxoplasmosis and malaria (Chaudhari et al. 2006; Chaudhari et al. 2007; Naguleswaran et al. 2008).

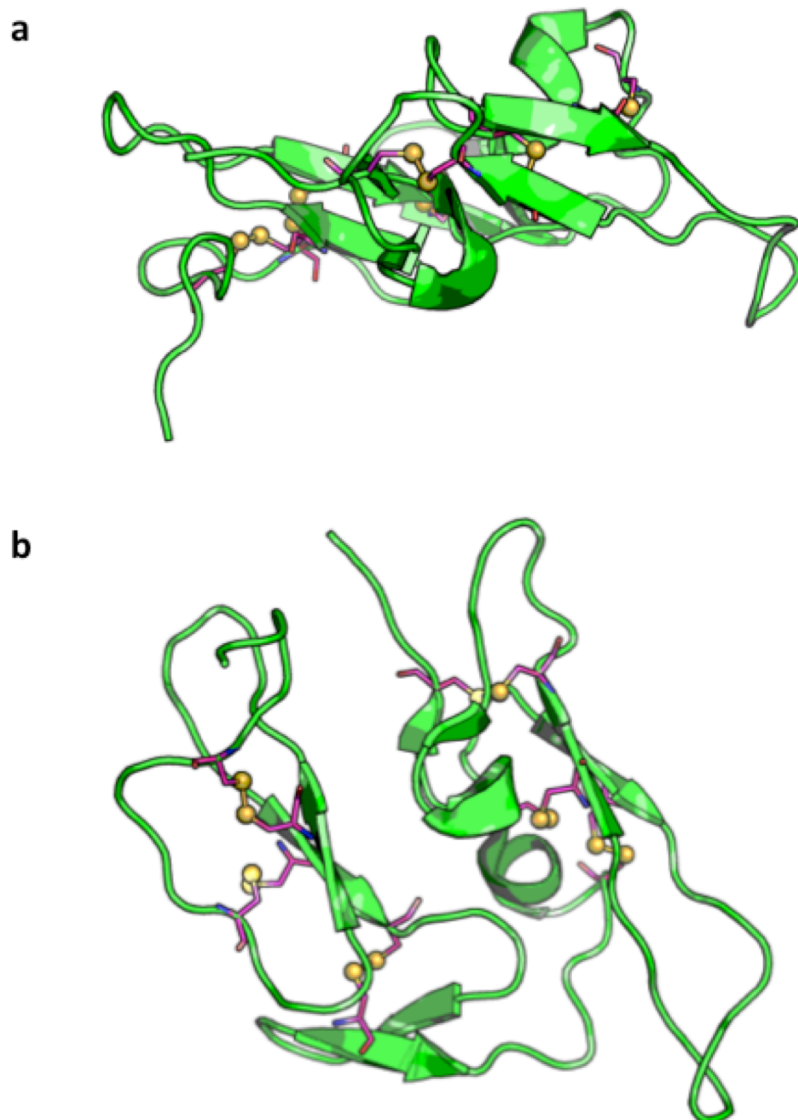


Figure 4.3 | Solution structure of MSP₁₉. Cysteine residues involved in disulphides are drawn in purple sticks with sulphur atoms displayed as yellow spheres. **a** Side view of MSP₁₉ with the membrane facing die at the bottom and the N-terminus in the foreground. **b** Rotated from **a** by 90 ° revealing the membrane facing sound. The C-terminus is located at the top of the protein. Image made from PDB 1OB1 (Garman et al. 2003).

4.1.2.1 Rusticyanin

Rusticyanin is a particularly interesting cupredoxin. It has been isolated from the acidophilic bacteria, *Thiobacillus ferrooxidans*, an organism capable of growth using Fe²⁺ as its only energy source (Ronk et al. 1991). Rusticyanin has two remarkable properties. It has exceptionally high acid

stability with an optimum pH of 2, with detectable activity at pH 0 (Blake II & Shute 1987). Rusticyanin has a redox potential of 680 mV, the highest of the cupredoxins which have more typical redox potentials of ca. 300 mV (Ingledeew & Cobley 1980). It seems likely that these properties play a role in the antimalarial properties reported. Structural studies of rusticyanin have been performed using both X-ray crystallography and NMR (Figure 4.4) (Djebli et al. 1992; Walter et al. 1996; Kanbi et al. 2002; Barrett et al. 2006; Harvey et al. 1998; Botuyan et al. 1996). Further studies have also been carried out to study the type-1 copper environment using EXAFS (Barrett et al. 2006).

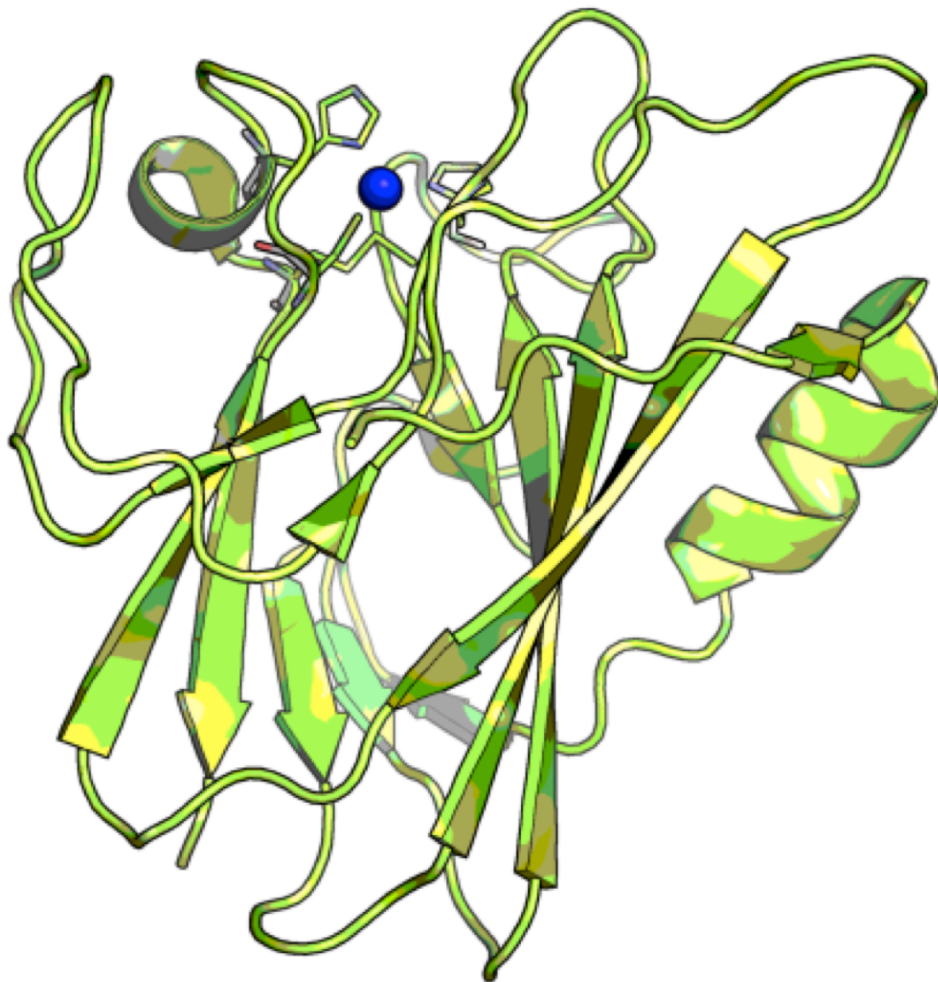


Figure 4.4 | Structure of the cupredoxin rusticyanin. The Type I copper site residues are shown as sticks with a blue copper atom. A β -barrel sandwich lies at the core of the protein with 2 helices and regions of random coil surrounding it. Image made using PDB 2CAK (Barrett et al. 2006).

It is possible to alter both the acid stability and redox potential of rusticyanin through mutagenesis (Hall et al. 1998). Several of these mutants have been studied previously and are well characterised (Table 4.1) (Barrett et al. 2006; Hall et al. 1998; Kanbi et al. 2002). It seems likely that the unique properties of rusticyanin provide it with the antimalarial properties described (Cruz-Gallardo et al. 2013). These mutants provide an excellent tool to probe the MSP₁₉ – rusticyanin complex and determine the mechanism by which it acts.

4.2 Results

4.2.1 Rusticyanin expression and purification

Rusticyanin expression and purification was carried out as previously reported (Hall et al. 1998). SEC was carried out during the first purifications and yielded a single protein peak of rusticyanin (Figure 4.5). This showed that there was no need for gel filtration in subsequent work. To test for long-term storage, protein was flash frozen in liquid nitrogen with or without the

Table 4.1 | Table demonstrating different rusticyanin mutants and their altered biochemical properties.

	Redox potential / mV	Acid stability
Native	667	Excellent
Met148Leu	798	Poor
Met148Gln	563	Excellent
Met148Glu	551	Good
Met148Lys	550	Poor
Ser86Asn	590	Moderate
Ser86Asp	623	Good
Ser86Gln	664	Moderate
Ser86Leu	702	Poor (becomes apo)

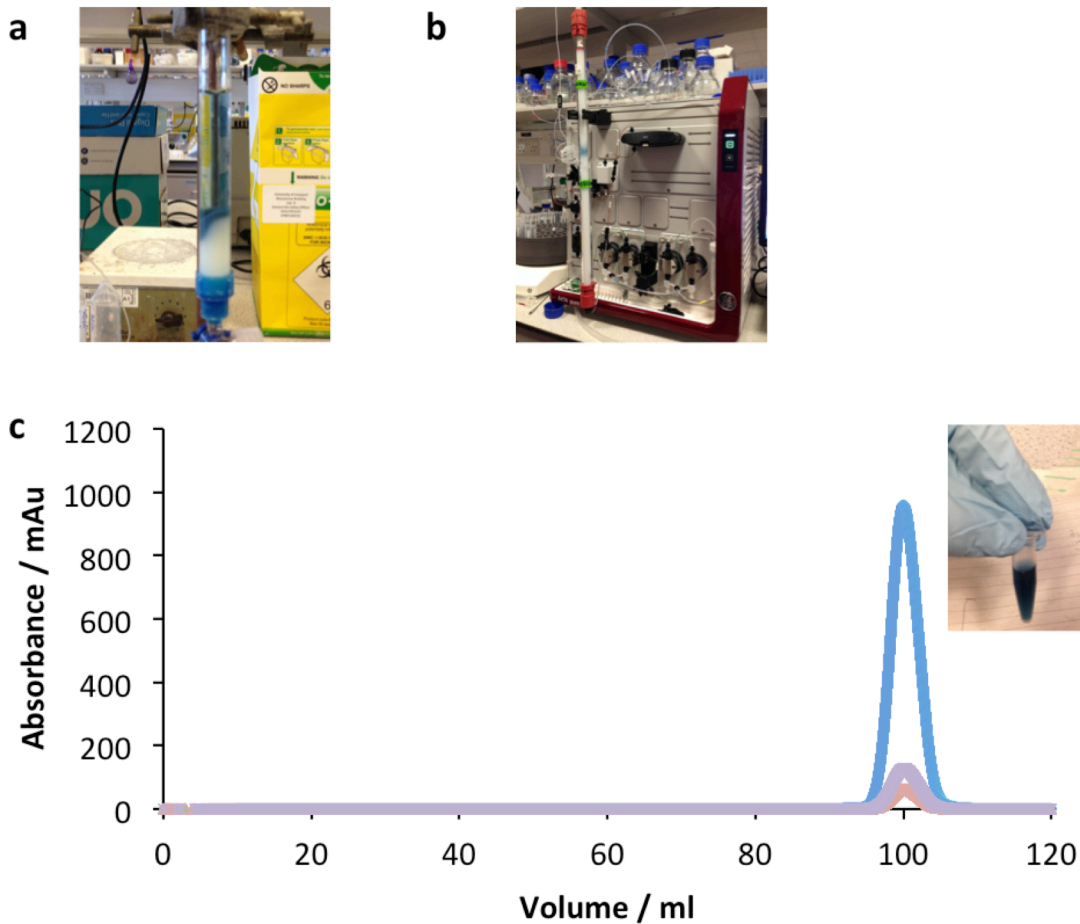


Figure 4.5 | Purification of rusticyanin. **a** Rusticyanin bound to SP-sepharose during the purification. **b** SEC purification of rusticyanin took place at room temperature and was easily tracked due to the distinct blue colour. **c** The chromatogram from rusticyanin SEC using Sephacryl 200 reveals a large single peak after SP-sepharose purification indicating no need for repeating this step in future work. 280 nm absorbance is shown in blue, 254 nm in pink and 592 nm absorbance in red.

addition of 10 % glycerol. SEC revealed that the protein frozen with the addition of glycerol remained entirely soluble whilst some of the protein frozen without glycerol has aggregated.

4.2.2 Rusticyanin crystal structure

Crystallisation was done according to previous crystallography reports (Djebli et al. 1992) and produced large clusters of rusticyanin crystals (Figure 4.6). Previous reports of the native protein crystal structure

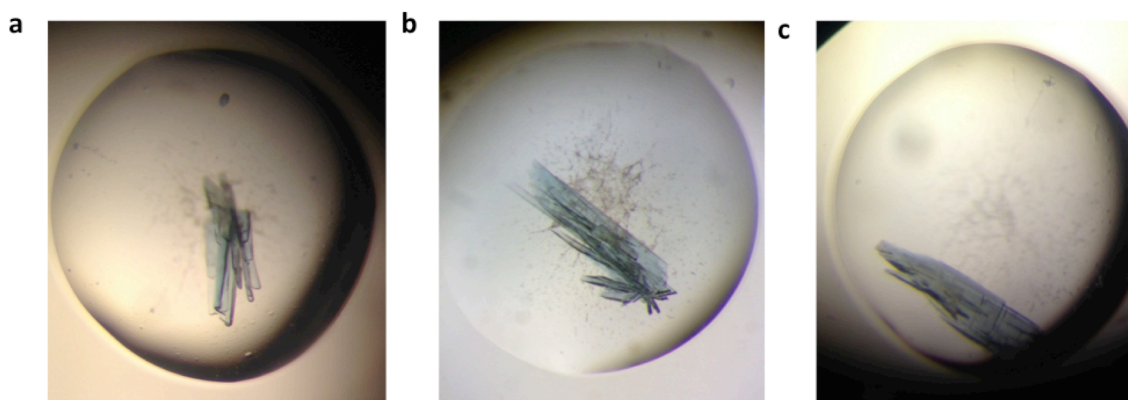


Figure 4.6 | Typical rusticyanin crystals in 3 μ l drops. **a** Protein added 1:1 with precipitant containing 22 % PEG8000. Crystals took 10 days to reach maximum size. **b** Crystals grew in 24 % PEG8000 at a protein : precipitant ratio of 2:1. **c** Protein was set 2:1 with precipitant solution containing 25.5 % PEG8000 and crystal grew to maximum length of 500 μ m.

have been carried out at room temperature and data collected to 1.27 \AA (Barrett et al. 2006). A full dataset was collected to 1.1 \AA (Table 4.2). The crystal appeared to diffract further and reflections were visible to 0.9 \AA but a full dataset to this resolution could not be collected due to spot overlap. Density was well defined for the entire structure with only Ala2 and Lys155 proving difficult to model entirely (Figure 4.7). The structure deviated from the previously published native structure very little with an RMSD of 0.208 \AA when all atoms were aligned using Pymol (www.pymol.org).

4.2.3 Expression and purification of MSP₁₉

MSP₁₉ was expressed in *Pichia pastoris* and secreted by the yeast into the cell media through a secretion signal encoded in the plasmid pPIC9K (Invitrogen). Selection for multi-copy integrants produced a strain resistant to 0.75 mg/ml G418-disulphide indicating the presence of 2-3 copies of the MSP₁₉ encoding gene. Expression was initially carried out by inducing with 0.5 % methanol in BMMY but it was later found that 0.1 % increased the yield. After deglycosylation and Ni²⁺ affinity chromatography and SEC, a single peak of pure *P. falciparum* MSP₁₉ remained (Figure 4.8).

Table 4.2 | Tale of crystallographic statistics for native rusticyanin.

Rusticyanin - native	
Data collection	
Space group	P 2 ₁
Cell dimensions	
a, b, c (Å)	32.02, 59.60, 36.79
α, β, γ (°)	90, 106.1, 90
Resolution (Å)	30 – 1.1 (1.12 – 1.10)
R_{pim}	0.05 (0.258)
I/ σI	6.3 (1.7)
CC_{1/2}	0.991 (0.797)
Completeness (%)	89.0 (93.6)
Multiplicity	2.9 (2.7)
Refinement	
No. reflections	68,741
R_{work} / R_{free}	12.25 / 15.07
No. atoms	1,474
Protein	1,265
Other	209
Average B factors (Å²)	
Protein	12.15
Other	27.6
r.m.s deviations	
Bond lengths (Å)	0.009
Bond angles (°)	1.482
Ramachandran statistics	
Favoured (%)	100

Numbers in parenthesis indicated high resolution shell
r.m.s: root mean square

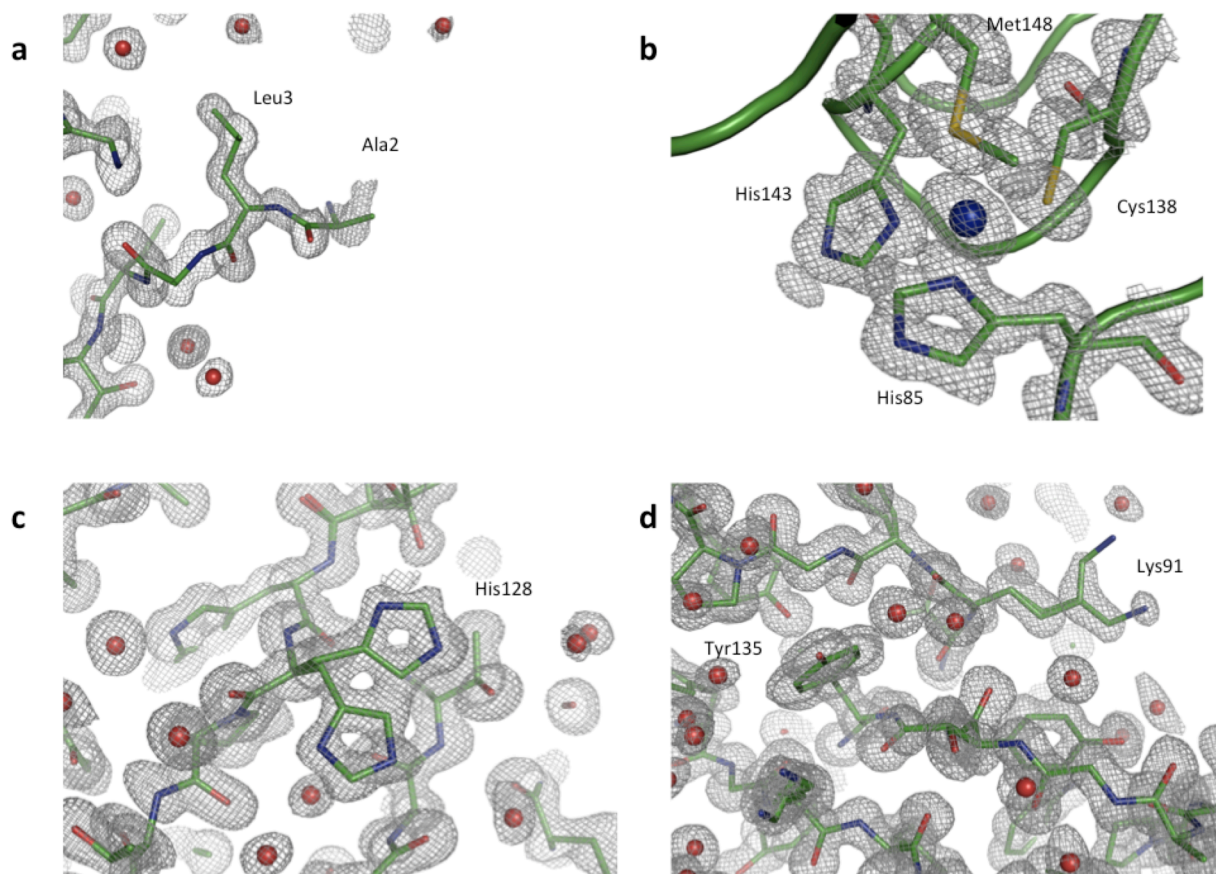


Figure 4.7 | High resolution electron density of rusticyanin. Water molecules are represented by red spheres. Copper is represented as a blue sphere. The $2F_o - F_c$ electron density map is drawn at 1σ . **a** The N-terminal region of rusticyanin shows continuous density but the first residue Ala2 can not be unambiguously placed. **b** The type I copper site shows good agreement with previous structures of native rusticyanin. **c** and **d** Multiple conformations of various residues are visible within the density but are entirely located on the surface of the protein forming crystal contacts.

4.2.4 Binding of rusticyanin to MSP1₁₉

Rusticyanin was reduced using ascorbic acid to support binding to MSP1₁₉ as reported (Cruz-Gallardo et al. 2013). When run on gel filtration, the oxidised protein did not appear to form a complex as demonstrated by the two distinct peaks (Figure 4.9 a). MSP1₁₉ and excess reduced rusticyanin were incubated prior SEC analysis and a small peak of potential protein complex eluted ahead of residual rusticyanin (Figure 4.9 b). The same quantity of rusticyanin was run as a control down the same column and yielded a single peak (Figure 4.9 c). MSP1₁₉ had previously been shown to

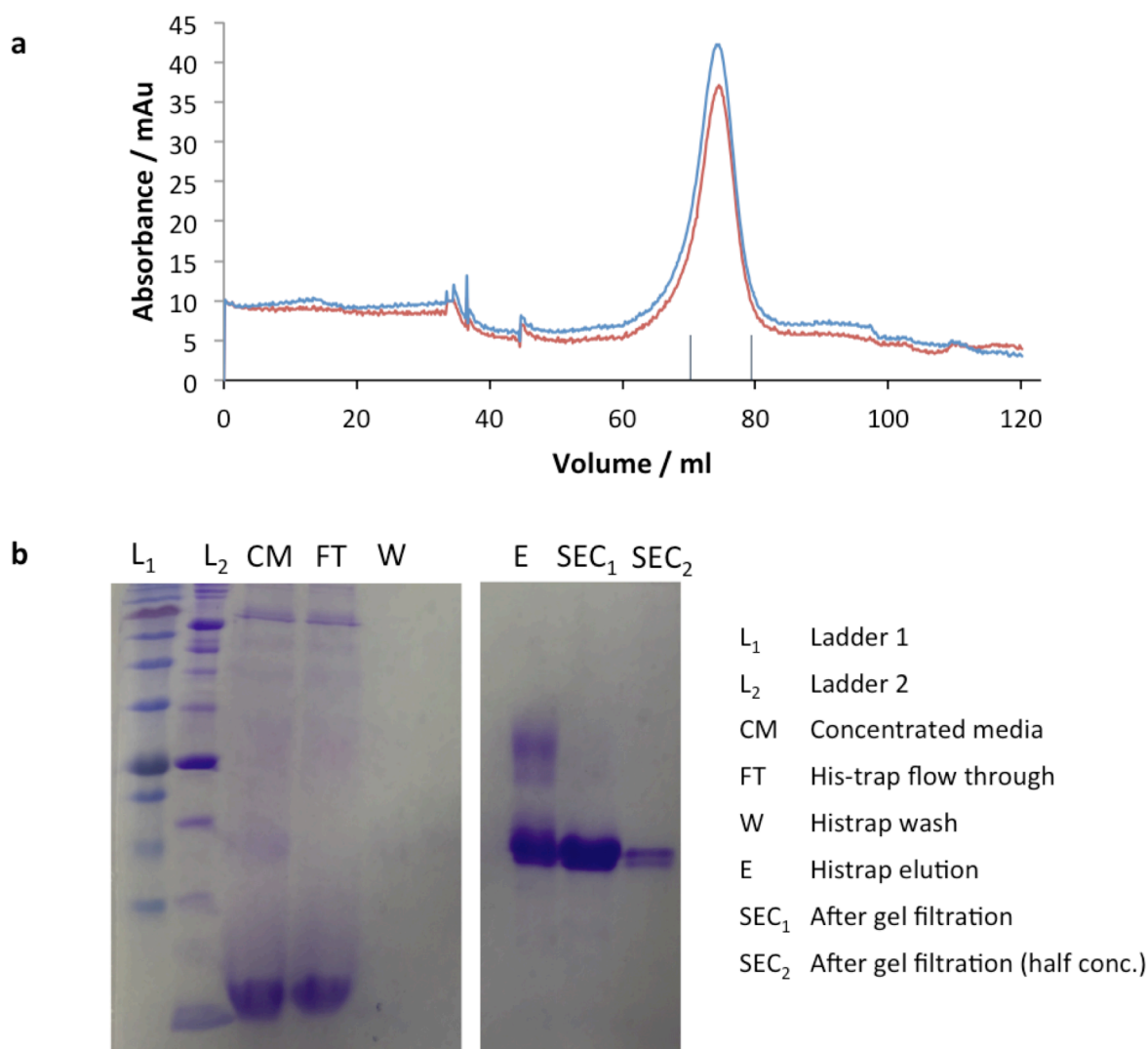


Figure 4.8 | Purification of *P. falciparum* MSP1₁₉. **a** Chromatogram of MSP1₁₉ gel filtration. 280 nm absorbance shown in blue, 254 nm absorbance shown in red. SEC on Superdex 200 16/600 pg column revealed a single peak of MSP1₁₉. The brackets indicate the region collected for further work. **b** SDS-PAGE confirms the presence of MSP1₁₉ throughout purification. MSP1₁₉ runs at ca 17 kDa under reducing conditions and is clearly pure after gel filtration.

run slower than rusticyanin on a large column indicating that the peak ahead of rusticyanin could be due to complex formation. The presence of both rusticyanin and MSP1₁₉ were confirmed using coomassie stained SDS-PAGE and western blot analysis using a selective antibody for the 6xHis tag engineered onto MSP1₁₉ (Figure 4.10).

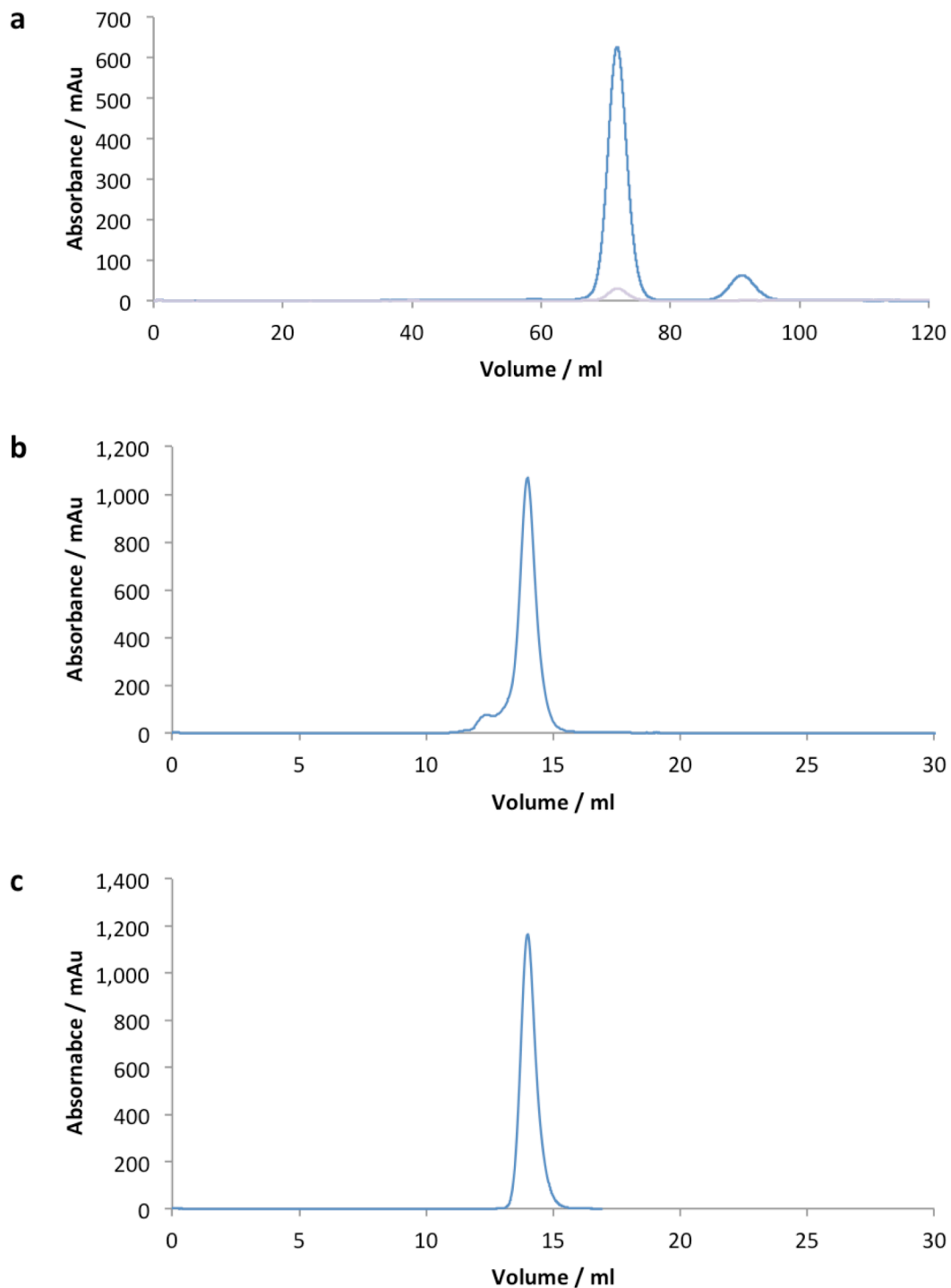


Figure 4.9 | Size-exclusion chromatography demonstrating MSP1₁₉-rusticyanin complex formation. Blue line represents absorbance at 280 nm, the pink line represents absorbance at 592 nm. **a** Oxidised rusticyanin and MSP1₁₉ run down a Sephacryl S75 16/60 gel filtration column separately resulting in a large peak of rusticyanin first followed by a small peak containing MSP1₁₉. **b** Reduced rusticyanin added to excess and MSP1₁₉ form a complex on an S75 10/30 gel filtration column followed by a larger rusticyanin peak. **c** Reduced rusticyanin ran by itself as a control down an S75 10/30 gel filtration column.

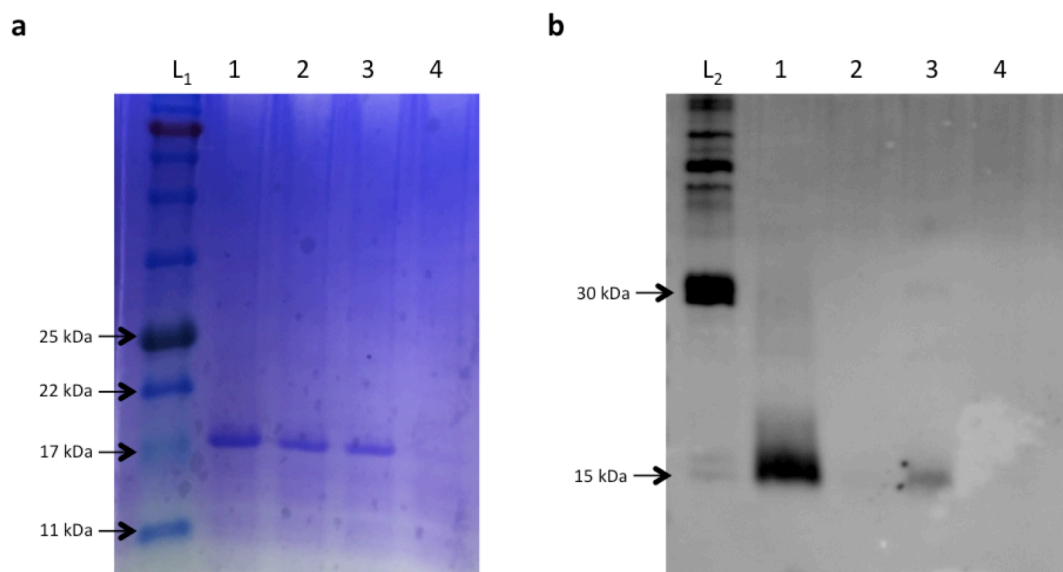


Figure 4.10 | SDS-PAGE and western blot analysis of MSP₁₁₉-rusticyanin complex. **a** Coomassie stained SDS-PAGE reveals rusticyanin presence. L₁ neb colour plus protein ladder, 1 rusticyanin control, 2 and 3 sample from rusticyanin peak in Figure 4.9b, 4 sample from shoulder previous to rusticyanin peak. **b** Western blot using an anti-6xHis antibody confirms the presence of MSP₁₁₉ in the complex peak. L₂ 6xHis protein ladder (Qiagen), 1 MSP₁₁₉ control, 2 pre-shoulder sample, 3 sample from shoulder, 4 sample form rusticyanin peak.

4.2.5 Crystal screening of MSP₁₁₉-rusticyanin complex

Several commercial crystallisation screens were used across two concentrations of the protein complex. A crystallisation robot was used to make the most of the protein available and screen as many conditions as possible. There have been no crystals hits from current conditions.

4.3 Discussion

4.3.1 Structure of rusticyanin

The structure of rusticyanin has been well characterised by previous crystallographic and NMR studies. The structure presented here is to a new high resolution of 1.1 Å as opposed to previous crystal structures for native published to 1.29 Å (Barrett et al. 2006). The diffraction from these crystals

did reach a higher resolution (visible spots were seen to 0.9 Å) but data of reasonable completeness could not be collected. With further optimisation of crystal conditions, it seems reasonable to expect to collect a future dataset beyond 0.9 Å.

4.3.2 Purification of complex

An excess of rusticyanin was added to MSP1₁₉ in an attempt to produce the protein complex. Attempts to complex *P. falciparum* MSP1₁₉ with both oxidised and reduced rusticyanin on gel filtration resulted in differing absorbance profiles indicating complex formation is some how redox controlled. This would further explain why apo-rusticyanin has no effect on parasite growth *in vivo* (Cruz-Gallardo et al. 2013). Further tests need to be ran to confirm the presence of protein complex. ITC analysis should be carried out to verify the initial papers findings. An increased resolution of the complex when using gel filtration would increase the purity of future protein purified, which could in turn also assist crystallisation.

4.3.3 Crystal trials on complex

There are currently no hits from crystal trials. Previous examples of antibodies that have been co-crystallised with *Plasmodium knowlesi* MSP1₁₉ have been carried out at room temperature and so initial trials carried out with rusticyanin were also done at room temperature (Pizarro et al. 2002). Future trials could be carried out at 4 °C in the hope that this stabilises the complex long enough for crystallisation to take place. Due to limited protein, a small amount of initial trays were set at low concentration. Further screening will take place and explore more conditions at a higher concentrations. Due to the need for reduced rusticyanin to form protein complex, the addition of a reducing agent to the reservoir in crystal trials may prove beneficial and should be attempted.

Chapter 5 | **General discussion and summary**

5.1 Cytochrome bc_1 as a drug target

In this work, the importance of structural studies in drug design has clearly been reiterated. The crystallographic studies carried out on cyt. bc_1 in complex with two key drug classes in the search of novel antimalarials has revealed that the presumed site for binding was incorrect. This has also confirmed the reason for the failure of GSKs 4(1H)-pyridones during development. The identification of the Q_i site as the site of action for these compounds will allow future antimalarial programs targeting cyt. bc_1 to be better directed, and make use of structural information to inform rational drug design. Future *in silico* work should also be targeted against the Q_i site as well as the Q_o site.

Atovaquone is a successful prophylactic drug and has demonstrated the validity of cyt. bc_1 as a drug target despite its use as a monotherapy quickly leading to rapid resistance mutations emerging within the Q_o site. It is yet to be seen if the Q_i site will yield mutations at an equivalent rate but the prospect of developing compounds against this site is promising and studies have shown that resistance to endochin-like quinolones (ELQs) thought to target the Q_i site are less prone to resistance than atovaquone (Stickles, Ting, et al. 2015). The prospect of multiple cyt. b targeting compounds in a medical treatment is also interesting. It is possible that by targeting both quinone binding sites simultaneously rates of resistance would be decreased. Synergy between the 4(1H)-quinolones and clodolol, from which the 4(1H)-pyridones have been developed, has previously been reported (Xiang et al. 2006) and recent screening to uncover novel antimalarials has identified Q_i site inhibitors that work in synergy with atovaquone (Lukens et al. 2014).

5.2 Further directions for cytochrome bc_1

Bovine cyt. bc_1 should continue to be used for research into antimalarial compounds that show signs of cross-species specificity. The large quantity of protein that can be readily purified and crystallised is of

great benefit to further studies. Crystallography has been used with great effect here to identify the correct binding mode of several potential next-generation drugs, and should continue to be used for this. As discussed in the body of this work, the insight gained from these structural studies can further instruct drug design to prevent binding to the mammalian enzyme. Improved resolution should be attempted to increase our knowledge of binding within the Q_i site of the current compounds which could identify more precisely the importance of various compound functional groups and elucidate the importance of water molecules, if any, for the binding of the next generation of compounds. To achieve this resolution, work to produce highly diffracting cyt. bc_1 crystals in the $P 2_1 2_1 2_1$ space group should be pursued. Dehydration appears to have a positive affect on cyt. bc_1 crystals and has been shown to improve diffraction quality of other protein crystals previously (Sanchez-Weatherby et al. 2009; Bowler et al. 2006; Huang et al. 2005). To achieve reproducible dehydration to an optimum degree, the use of HC1 at DLS could prove beneficial. This could potentially increase the resolution of diffraction from these crystals.

Future work developing novel inhibitors against cyt. bc_1 would greatly benefit from direct structural information from both of the parasite's proteins. Direct visualisation of both the Q_o and Q_i site of *P. falciparum* or *T. gondii* cyt. b would reveal the exact binding mode of these anti-parasitic compounds and characterise the differences in structure between the bovine and apicomplexa proteins. This would allow drug design to capitalise on these differences. For example, if various ELQ's could be crystallised bound to both of these sites, it should explain why it is that certain functional groups are required to differentiate between Q_o and Q_i inhibitors and identify which of these are most effective. The growth of these parasites is a labour intensive process and the amount of protein that could be purified would be fairly small. However, thanks to the techniques developed whilst working on bovine cyt. bc_1 in crystal production and data collection, it is possible that protein crystals can be produced and data collected.

Another option for the further study and evaluation of these compounds is using a parasite model. Yeast has been used extensively in the production of *P. falciparum* models for the study of compound binding and resistance. This has involved a series of mutations within *cyt. b* to make the binding sites more parasite like (Vallières et al. 2013). This is however an incomplete model. With the increased demonstration of genome editing techniques such as CRISPR/cas9 (Dicarlo et al. 2013) it may be possible to switch entire subunits of *cyt. bc₁*. This could be first attempted by simply replacing the mitochondrial DNA encoded *cyt. b* with that of *P. falciparum* and *T. gondii*. For a further degree of reliability, work could be continued to replacing further subunits of *cyt. bc₁* and produce stable *cyt. bc₁* of parasites within the yeast mitochondria. A yeast model that could be made to express parasite protein would be a huge improvement over native growth due to the ease with which large amounts could be grown.

Studies to determine mutation rates in the Q_i site could provide further support for this site as a principle target in the development of antimalarials. The synergy between Q_o and Q_i inhibitors is an interesting prospect for future combination therapies.

5.3 Rusticyanin in complex with MSP1₁₉

In this thesis, initial studies on the MSP1₁₉-rusticyanin complex have been carried out. The purification of both rusticyanin and MSP1₁₉ have successfully resulted in pure protein and initial attempts to produce the complex have been attempted on gel filtration. Further studies on this native complex will form the basis for future work. Crystal screens of the complex have not yet yielded any hits, but with time and more screening, it may be possible to produce a crystal of the complex. This will reveal in-depth structural information about the binding interface between the proteins.

5.4 Further directions for rusticyanin and MSP1₁₉

The work set out here is preliminary to further exploration of the antimalarial properties of rusticyanin. Further studies on the complex could be carried out using a variety of biophysical techniques. The exact binding of MSP1₁₉ to rusticyanin has not yet been fully explored and only a model based on docking algorithms and NMR data has been suggested (Cruz-Gallardo et al. 2013). As MSP1₁₉ has previously been crystallised in the presence of Fab antibody fragments (Fabs), it is possible that the rusticyanin-MSP1₁₉ complex will also be amenable to crystallisation. This would elucidate the exact binding mode of the complex. Although no success has been seen from current crystals screens, through further experiments, it may prove possible to produce diffracting crystals. In addition to X-ray crystallography, the complex can be further probed using smalls angle X-ray scattering with on-line size-exclusion chromatography (SEC-SAXS). This will produce low resolution structures which can then accurately identify the positions of both MSP1₁₉ and rusticyanin.

The next stages of work will involve the production of various mutants, in order to alter their redox potential and acid stability. The complex formed between these proteins to MSP1₁₉ can then be studied using a variety of biophysical techniques in order to determine how these altered properties vary the strength of the complex formed. The antimalarial properties of the mutants could then be studied in parasite culture. This would provide insight into the mechanism by which rusticyanin kills *Plasmodium* and could help instruct future therapeutics or vaccine development.

Properties developed using MSP1₁₉ and rusticyanin could also prove beneficial in the development of treatments targeting toxoplasmosis. It has been shown that azurins bind the surface protein SAG1 (Surface Antigen 1) of *T. gondii* (Naguleswaran et al. 2008). SAG1 is also a GPI anchored surface protein that has been shown important for binding to host cells (Mineo &

Kasper 1994). Further studies could be carried out using the mutated versions of rusticyanin on this important target (Liu et al. 2006).

5.5 Final remarks

The prospects for the eradication of malaria appear to be improving. With ongoing research into all avenues of malaria control there are a multitude of new drugs being developed with a variety of targets (Wells et al. 2015; Burrows et al. 2013). The success of the recent vaccine development could assist in producing herd immunity amongst children in some of the worst affected places (RTS 2015). Although generally asymptomatic, the long-term effects of toxoplasmosis are still relatively poorly understood. Patients who are immunocompromised also suffer greatly and children can be born with disabling conditions. As it affects large numbers of people in tropical countries and developing economies, treatment of acute sickness is a large burden. Cyt. *bc*₁ has been the target of a large body of work to develop drugs against both of these apicomplexa parasitic diseases. Targeting the Q_i site, or both the Q_o and Q_i site simultaneously, could provide a novel avenue for drug development and provide more tools to combat both of these diseases.

Chapter 6 | **Materials and Methods**

6.1 Cytochrome *bc*₁

6.1.1 Isolation of crude mitochondria

Fresh bovine heart was carried from the abattoir to the laboratory on ice immediately after slaughter. All subsequent work was carried out at 4 °C. Fatty tissue and connective tissue were removed from the heart using a sharp knife leaving behind cubes of lean muscle tissue. Muscle tissue was combined with ice-cold homogenisation buffer (250 mM sucrose, 20 mM K₂HPO₄, 2 mM succinic acid, 0.5 mM EDTA) at a ratio of 2 L of buffer to 500 mL of tissue. The resulting mixture was homogenised in a waring blender for 10 cycles of 30 sec on, 30 sec off. The pH of the homogenate was altered to 7.5 using filtered 2 M Tris and phenylmethanesulfonyl fluoride (PMSF) was added to a final concentration of 0.1 mM. The solution was centrifuged at 1500 g for 20 mins at 4 °C to remove remaining tissue. The supernatant was filtered through doubled muslin cloth and the flow through centrifuged at 24,000 g for 20 mins at 4 °C. The pellets were resuspended in wash buffer 1 (50 mM KPi pH 7.5, 0.1 mM PMSF) before being centrifuged again under the same conditions. The washed crude mitochondria were then taken and flash frozen in liquid nitrogen before storage at -80 °C or taken through to the next stage of purification.

6.1.2 Solubilisation of membrane proteins

Pellets were thawed in cold water at 4 °C and resuspended in 140 mL wash buffer 2 (50 mM KPi (pH 7.5), 250 mM NaCl, 3 mM NaN₃, 0.1 mM PMSF). An aliquot was taken to determine protein concentration by BCA assay (Pierce, as per instructions) and the remainder of the solution was spun at 42k rpm in a T647.5 rotor (ca. 200,000 g) for 1 hour at 4 °C. The supernatant was discarded and the resulting pellet was resuspended in 140 mL of the same wash buffer. n-Dodecyl β -D-maltoside (Generon) (DDM) was added at a ratio of 1 mg detergent to 1 mg of protein and allowed to mix for 30 mins. A colour change was visible if lysis occurred successfully. The solution was centrifuged at 200,000 g under the same conditions as before.

The resulting supernatant contained soluble cytochrome *bc*₁ and was used for purification.

6.1.3 Purification of cytochrome *bc*₁

6.1.3.1 DEAE-sepharose purification of cytochrome *bc*₁

The solubilised protein solution was applied to a DEAE-sepharose CL-6B column ca. 50 mL pre-equilibrated in 50 mM KPi (pH 7.5), 250 mM NaCl, 3 mM NaN₃ and 0.03 % DDM for weak anion exchange. The column was then washed with 2 CV of the same buffer before the bound proteins were eluted along a gradient of 250 - 500 mM NaCl. Initial purification efforts were carried out on a gradient of 150 - 350 mM NaCl but yielded incomplete separation of cyt. *bc*₁ from cytochrome *c* oxidase. In later purification efforts for cyt. *bc*₁ bound to MJM 170 solubilised protein was applied to a DEAE-sepharose CL-6B column ca. 50 ml pre-equilibrated with 50 mM KPi (pH 7.5), 250 mM NaCl, 0.5 mM EDTA, 0.01 % DDM and eluted along a gradient of 250 – 500 mM.

6.1.3.2 Hydroxyapatite purification of cytochrome *bc*₁

Fractions containing cyt. *bc*₁ were pooled from DEAE-sepharose purification and diluted two-fold with 50 mM KPi, 3 mM NaN₃, 0.03 % DDM and applied to a hydroxyapatite column ca. 15 mL pre-equilibrated in the same diluent buffer. The bound protein was washed with 5 CV before eluting along a gradient from 50 - 1000 mM KPi (pH 7.5) and fractions containing cytochrome *bc*₁ were pooled. This stage of purification was removed in later purifications.

6.1.3.3 Size exclusion chromatography of cytochrome *bc*₁

Protein from either DEAE-sepharose or hydroxyapatite was concentrated to ca. 500 µL using an Amicon Ultra-15 Centrifugal filter MWCO 100 kDa (Millipore). The concentrated solution was applied to a HiPrep Sephacryl-S300 HR column (ca. 120 ml) pre-equilibrated in 25 mM KPi (pH

7.5), 100 mM NaCl, 3 mM NaN₃, 0.015 % DDM and ran at 0.5 ml/min. The single peak containing pure homodimeric cyt. *bc*₁ was collected.

Later purification attempts were carried out using the same column pre-equilibrated in 20 mM MOPS-KOH (pH 7.2), 100 mM NaCl, 0.5 mM EDTA, 0.01 % DDM under the same conditions.

6.1.3.4 Compound binding prior to crystallisation

The compounds used tended to be hydrophobic and so were kept as 10 mM stocks solubilised in 100 % DMSO. After gel filtration, cyt. *bc*₁ was either diluted or concentrated to 5 μM and compounds were added to a two-fold molar excess. The protein was allowed to incubate with the compounds for 30 mins at 4 °C.

6.1.3.5 PEG fractionation of cytochrome *bc*₁

Cytochrome *bc*₁ solution was mixed with increasing volumes of a PEG precipitation buffer (100 mM MES-KOH (pH 6.4), 0.5 mM EDTA, 10 % PEG4000) relative to the protein solution volume as previously reported (Huang et al. 2005). After each addition of precipitation buffer, the solution was left to incubate on ice for 20 mins before being spun at 13,000 g at 4 °C. The pellet of precipitated cytochrome *bc*₁ was resuspended in gel filtration buffer. Fractions were analysed by SDS-PAGE for their purity and then combined. The resulting solution was buffer exchanged into 25 mM KPi (pH 7.5), 0.01 % DDM, 3 mM NaN₃ or 20 mM Tris-HCl (pH 7.5), 0.5 mM EDTA, 0.1 % Undecyl β -D-maltoside (UM) (Generon) with an Amicon Ultra-15 Centrifugal filter MWCO 100 kDa (Millipore) prior to crystallisation. Final buffer choice was made dependent on the method of crystallisation to be employed.

6.1.4 Determining the concentration of cytochrome *bc*₁

Cyt. *bc*₁ was diluted in assay buffer (50 mM KPi (pH 7.5), 0.5 mM EDTA) and absorbance was recorded at 280 nm and 415 nm to determine purity. The sample was fully oxidised by the addition of potassium ferricyanide crystals and the absorbance was measured at 562 nm and 575 nm. The same sample was then fully reduced using powdered sodium dithionite and the absorbance at 562 nm and 575 nm was recorded again. Using the sodium dithionite reduced minus ferricyanide oxidised readings, the concentration of cytochrome *b* could then be determined with $\epsilon_{562-575} = 28.5 \text{ mMcm}^{-1}$ (Yu et al. 1974). Alternatively the concentration of cyt. *bc*₁ was determined from just the dithionite reduced sample difference spectrum using $\epsilon_{562-600} = 70 \text{ mMcm}^{-1}$ (Huang et al. 2005).

6.1.5 Crystallisation of cytochrome *bc*₁

Multiple methods were used to attempt cytochrome *bc*₁ crystallisation. All crystals trays were set up in a cold room at 4 °C or on a bed of ice. Crystal drops were set using VDX plates with sealant and 22 mM siliconized glass cover slips (Hampton Research).

6.1.5.1 Initial crystallisation

Initial crystals were grown by screening protein at 30 mg/ml in KPi buffer with DDM. The hanging drop format was used with 2 μl drops of 1:1 protein against precipitant. Conditions were screened across 50 mM KPi (pH 6.0 – 7.4), 100 mM NaCl, 6 – 14 % PEG4000, 3 mM NaN_3 with no additional 6-O-(N-Heptylcarbonyl)-methyl- α -D-glucopyranoside (Generon) (HECAMEG), 0.16 % HECAMEG or 1.6 % HECAMEG. Crystals appeared amongst precipitate overnight and took 1 – 2 days to reach maximum size. Successful conditions were replicated in larger sitting drops with 10 or 20 μl volumes though results were inconsistent.

6.1.5.2 Micro-seeding

A micro-seed stock was produced from successful crystal drops by crushing the crystal with a probe and then subjecting them to vortexing in the presence of a seed bead (Hampton Research). The seed stock was then serially diluted in precipitant solution from the drop (D'Arcy et al. 2007). Seed stocks were either used fresh or after being stored at – 20 °C.

Crystal drops incorporating seeds were set 1:0.75:0.25 (protein : precipitant : seeds) using 30 mg/ml cyt. *bc*₁ in KPi buffer with DDM. Drops were set against the same reservoir solutions as in initial trials but crystals appeared with far more reproducibility and slightly larger size.

6.1.5.3 Refined crystallisation

Protein from PEG fractionation proved purer and more reliable in crystallisation. After being exchanged into final buffer containing 25 mM KPi (pH 7.5), 100 mM NaCl, 0.01 % DDM and 3 mM NaN₃, protein was screened in the hanging drop format at concentrations of 20 mg/ml, 30 mg/ml, 40 mg/ml and 50 mg/ml. The protein was screened against varying concentrations of PEG4000 after the addition of 1.4 % HECAMEG directly to the protein solution. Changes in pH appeared to have little effect on crystallisation and so was kept constant at pH 6.8. 40 mg/ml yielded the largest crystals against 8 or 9 % PEG4000.

Different additives were screened against these conditions in an attempt to improve diffraction: glycerol, sucrose, DMSO, PEG400 and MgCl₂. These were added to the reservoir solution at various concentrations from a stock solution before being added to the drop.

6.1.5.4 Lipidic cubic phase crystal screening

Cyt. *bc*₁ in complex with ligands at 30 mg/ml in KPi buffer with DDM was used for LCP screening. 9.9 MAG (monoolein) and 7.8 MAG lipids were used for screening. Protein solution was mixed 2:3 against lipid using two

Hamilton syringes and a connecting barrel until mixture was clear. This could be assisted by cooling the connector with ice. A Gryphon LCP robot (ARI) was used to set sandwich plates in duplicate for monitoring at 4 °C or room temperature. 100 nl drops were used against 6 nl precipitant solution from 14 commercially available screens.

6.1.5.5 Crystallisation in Undecyl Maltoside

Crystallisation was attempted following conditions by Huang et al. (2005). Protein from PEG fraction used in a final buffer of Tris-HCl (pH 7.5), 0.5 mM EDTA, 0.1 % UM. Hexyl β -D-glucopyranoside (Generon) (HG) was added as solution in the same buffer from a 2.5 M stock to a concentration of 375 mM. The mixture was left to incubate on ice for at least 30 minutes prior to setting crystal trays. Protein was set at concentrations of 20 mg/ml, 30 mg/ml and 40 mg/ml against precipitant solutions of 100 mM sodium cacodylate (pH 6.2 – 6.8), 20 mM MgCl₂, 3 mM NaN₃, 10 % glycerol and 5 – 10 % PEG3350. Trials were set as hanging drops 1:0.9:0.1 protein to well solution to a minor precipitant. The minor precipitant was condition #31 from the commercial kit Crystal Screen II (Hampton Research) and consisted of 100 mM HEPES pH 7.5 and 20 % Jeffamine 600. Crystals appeared overnight and continued to grow for several days.

6.1.6 Crystal freezing

All crystal manipulation took place at 4 °C. Crystals were fished from drops using nylon loops on magnetic pins for cryo-crystallographic data collection (Hampton Research). Crystal loop size was best matched against the size of the crystal to limit the amount of solvent left on the drop, and therefore limit background noise associated with solvent scatter. Crystals were picked from the drop and placed in prepared cryoprotectants that had been cooled to 4 °C. Crystals were allowed to soak for several seconds in the cryoprotectant before being fished out and quickly plunged into liquid nitrogen. Loops were then either stored long-term in cryovials on canes or placed into PUCKs for transport to the synchrotron.

6.1.7 Data collection of cytochrome bc_1 crystals

6.1.7.1 Screening on FRE+ home source

Crystals were transported on canes and kept submerged in liquid nitrogen at all time for diffraction screening on a rotating copper anode FRE+ X-ray source. Data were recorded on a MAR CCD225. Crystals were disposed of if there was a lack of diffraction or weak diffraction. Successful crystals were placed back on canes and stored before being transferred to PUCKs for synchrotron beamtime. Typically one in ten crystals screened would warrant further investigation at the synchrotron.

6.1.7.2 Data collection for cytochrome bc_1

Crystals were transferred to synchrotrons on loops in PUCKs and shipped using a dry shipping dewar. Data were collected on Proxima1, Soleil, St-Aubin, France and I02, I04, I04-1 and I24, Diamond Light Source (DLS), Oxfordshire, UK. Data were consistently measured using X-rays of wavelength 0.9868 Å. Attempts were made to fit beam size to the crystal when available except for on I24. All crystals were kept in a cryostream maintained at 100 K. Data were recorded using Pilatus 6M detectors allowing rapid data collection using fine slicing when appropriate. Approximately 1 in 10 crystals from screening would diffract to a resolution between 3 – 3.5 Å.

Data collection of cytochrome bc_1 – pyridones

Data were collected on I04 at DLS and Proxima1 at Soleil from multiple crystals until radiation damage diminished data quality and resolution. Diffraction spots could be seen to 3.2 Å. Frames were recorded over 0.5 ° oscillation and 0.2 s exposures with the X-ray beam at 20 % transmission. Crystals tended to survive no more than 30 – 40 ° of data before severe radiation damage was an issue.

Data collection of cytochrome bc_1 – MJM 170

Data were collected using I24 at DLS. Multiple datasets were collected from single crystals making use of the micro-focus beam. Overlapping 20 ° wedges of data were collected at points on the crystal before translation and further collection. Up to 10 datasets were collected from each crystal. Data were collected with 0.2 ° oscillation, 0.1 s exposure and 60 % beam transmission.

6.1.8 Data reduction and structure refinement

The methods used in data reduction and structural refinement were common for all datasets. Data for cyt. bc_1 in complex with the pyridones GW844520 and GSK932121 was indexed, scaled and merged using Denzo and Scalepack in the HKL2000 suite (Otwinowski & Minor 1997). Datasets for cyt. bc_1 in complex with MJM 170 was indexed using iMosflm (Leslie & Powell 2007; Battye et al. 2011) and merged using BLEND (Foadi & Aller 2013) before being scaled with Aimless (Evans & Murshudov 2013) in the CCP4 suite (Collaborative Computational Project 1994; Winn et al. 2011). Initial phases were produced using molecular replacement in Molrep (Vagin & Teplyakov 1997) using PDB 1PPJ with the ligands removed as a model. Rigid body refinement was carried out in Refmac5 (Murshudov et al. 2011) prior to restrained refinement. Restrained refinement was carried out using NCS restraints and additional secondary structure restraints generated by Prosmart (Nicholls et al. 2012). Regions that were observed to be missing were deleted and replaced and no definitive density could be placed for the Rieske iron-sulphur protein for a single cyt. bc_1 monomer. Phospholipids were built into the electron density where appropriate and extended as far as the density allowed. Ligands were built using JLigand (Lebedev et al. 2012) and placed in strong positive peaks of the Fo-Fc density map. Subsequent steps of manual model refinement in Coot (Emsley & Cowtan 2004) and automated restrained refinement were carried out until reaching a final model. The models were validated using ProCheck (Laskowski et al. 1993). Statistics are summarised in tables 3.3 and 3.4.

6.2 Rusticyanin

6.2.1 Rusticyanin expression

A pET21d plasmid containing the rusticyanin gene from *Thiobacillus ferrooxidans*, the result of many years research, was kindly supplied by Dr. John Hall.

Escherichia coli BL21(DE3) (Novagen) were transformed using the heatshock method to enable protein expression. A 50 μ L aliquot of chemically competent cells was taken from -80 °C and thawed on ice. The cells were then incubated with plasmid DNA for 20 mins on ice before being placed in a 42 °C water bath for 45 s and then put back on ice for 10 mins. 200 μ L of Super Optimal broth with Catabolite repression media (SOC) was added to the cells which were then incubated at 37 °C in a shaking incubator for one hour. The cells were then plated on to LB-agar (lysogeny broth) plates containing 100 μ g/ml ampicillin (Amp) as a selective marker. The plates were incubated overnight at 37 °C to allow clone growth. 5 mL LB (100 μ g/ml Amp) were inoculated with transformants and allowed to grow overnight at 220 rpm, 37 °C. The 5 mL cultures were then transferred to 500 mL LB (100 μ g/ml amp) in 2 L baffled flasks at 37 °C shaking at 220 rpm until the broth reached $OD_{600} = 0.6$. Protein expression was induced with 1 mM isopropyl β -D-1-thiogalactopyranoside (IPTG) and left to continue growing for 5 hours at 37 °C. The culture was then spun at 5000 g for 10 mins in a centrifuge to collect the cells, which were resuspended in 100 ml of 10 mM H_2SO_4 before being centrifuged again under the same conditions. Cell pellets were stored at -20 °C.

6.2.2 Rusticyanin purification

Cell pellets were thawed at room temperature and resuspended in 15 ml of 10 mM H_2SO_4 per 500 ml of culture. Cells were lysed by sonication on ice with a 50 % duty ratio for 10 mins. The resulting lysate was clarified by spinning at 21,000 rpm for 1 hr at 4 °C in a SS-34 rotor; the supernatant was

collected. Ammonium sulphate was added to the supernatant to 60 % saturation and left to incubate at 4 °C for 1 hr before being spun at 21,000 rpm for 1 hr at 4 °C in the SS-34 rotor. The resulting pellet was discarded and further ammonium sulphate was added to the supernatant until saturation before being spun under the same conditions. The pellet was collected and resuspended in 10 ml 100 mM sodium acetate (pH 4) before being dialysed against 2 L of 100 mM sodium acetate (pH 4) overnight at 4 °C using Snakeskin™ dialysis tubing MWCO 10 kDa (Pierce) whilst being agitated.

10 mM CuSO₄ was added from 1 M stock to the dialysis solution and left at 4 °C for 1 hour. Protein was removed from the dialysis tubing and loaded on a 3 ml SP-sepharose column (GE Healthcare), pre-equilibrated in 100 mM sodium acetate (pH 4), and washed with 100 mM sodium acetate (pH 4), 200 mM NaCl. Salt was increased in 50 mM steps to 500 mM and fractions were collected. Rusticyanin containing fractions, notable for their blue colouration, were pooled and concentrated to 1 ml using an Amicon Ultra-15 Centrifugal filter MWCO 10 kDa (Millipore) before being injected onto a HiLoad Superdex 200 pg 16/60 column (GE Healthcare) pre-equilibrated in 100 mM sodium acetate buffer (pH 4), 150 mM NaCl and run at 0.5 ml/min. Rusticyanin was the only peak and protein containing fractions were collected and concentrated as before. Protein was either stored at 4 °C for short term use or supplemented with 10 % glycerol prior to storage at -20 °C.

6.2.3 Rusticyanin crystallisation and freezing

Protein was dialysed against 10 mM H₂SO₄ overnight at 4 °C before being concentrated to 10 mg/ml for crystallisation. Crystal trays were set using 2 µl hanging drops (1:1) against a well solution of 100 mM sodium citrate (pH 4.5 – 5), 200 mM LiCl, 23 – 26 % PEG8000. Crystals took approximately 1 week to appear and took up to two weeks to reach maximum size. Crystals were then fished using nylon loops and dipped in

paratone oil (Hampton Research) as a cryoprotectant before being flash frozen in liquid nitrogen for storage and subsequent data collection.

6.2.4 Rusticyanin data collection

Data for rusticyanin were collected on I24 at DLS at 100 K. Data were collected with a wavelength of 0.9868 Å with the beam at 50 % transmission. Frames were measured with 0.15 ° oscillation using 0.2 s exposure and recorded on a Pilatus 6M detector. A small satellite crystal was present in the loop and led to overlaps in some places.

6.2.5 Rusticyanin data reduction and structure refinement

Data was indexed in $P 2_1$ using iMosflm (Battye et al. 2011; Leslie & Powell 2007) with the unit cell 32.02, 59.60, 36.79 and 90, 106.1, 90. The resulting data was then scaled with aimless to 1.1 Å resolution (Evans & Murshudov 2013). Rigid body refinement was used with the new data using the model PDB:2CAK. Waters and ligands were removed to create an initial model for use with the new data. Restrained refinement was subsequently carried out using Refmac5 (Murshudov et al. 2011). Alternating rounds of manual model building and multiple cycles of restrained refinement were carried out whilst slowly increasing the high resolution limit of the data used. Waters were added in Coot and then monitored in refinement using coot:watertidycoot (Emsley et al. 2010). B-factors were refined anisotropically and alternate rotamers for residues were placed as required. Statistics are summarised in table 4.2.

6.3 MSP119

6.3.1 MSP1₁₉ cloning

The sequence for MSP1₁₉, corresponding to 1526 – 1621 of Uniprot entry P04933, was codon optimised for *Pichia pastoris* expression and ordered from Genscript inserted in the SnaBI restriction site of pPIC9K

(Invitrogen). An N-terminal 6x His tag was added with the DNA sequence CACCATCATCATCAC. The plasmid was amplified using *E. coli* Stellar Competent cells (Clontech). The cells were transformed with the plasmid using the same protocol as used in section 6.2.1. A 10 ml LB culture with 100 µg/ml Amp was inoculated with a transformant and grown overnight in a shaking incubator at 37 °C, 220 rpm overnight. The culture was centrifuged at 5000 g for 10 mins to collect the cell pellet and plasmid DNA was isolated using a Qiagen miniprep kit as per protocol.

Pure plasmid DNA was linearised using the restriction enzyme SacI-HF (neb). 1.5 µg of DNA, 1 x Cutsmart buffer and 1 µl of the SacI-HF enzyme were incubated in 50 µl total volume and left for 1 hr at 37 °C. The digested production was cleaned up using the Clontech PCR clean-up kit as per protocol.

6.3.2 Transformation of *P. pastoris* and screening

Electrocompetent *P. pastoris* SMD1168 (Invitrogen) were thawed from -80 °C on ice and transferred to an electroporation cuvette with 2.0 mm gap on ice. 50 – 100 ng of linearised DNA was added to the cells and allowed to incubate for 2 mins. The electroporation cuvette was then placed in a GenePulser II (BioRad) and subjected to a pulse at charging voltage 1500 V, resistance 200 Ω and capacitance at 25 µF. After the pulse the cuvette was placed back on ice and 1 ml of 1 M sorbitol was added. The cells were then taken from the cuvette and plated on to minimal dextrose media plates (MD) to select for yeast transformed with pPIC9K. Plates were placed in an incubator at 29.4 °C for several days until colonies appeared.

Cells were scraped from the MD plates and transferred in filtered water on to yeast extract, peptone, dextrose media (YPD) supplemented with the G418 antibiotic. Cells were first transferred to 0.25 mg/ml G418 plates and left to grow at 29.4 °C until colonies appeared. As colonies appeared they were transferred to higher and higher concentrations of G418 to select for

yeast with a higher number of integrants. High-copy number integrants were selected and stored at – 80 °C.

6.3.3 *MSP1₁₉* expression

A 100 ml starter culture of the yeast was grown in buffered glycerol-complex media (BMGY) at 29.4 °C and 260 rpm overnight. The culture was spun down at 1500 g for 10 mins and transferred to a 500 ml culture of BMGY. The 500 ml culture was grown as before until it reached OD₆₀₀ of 3. The cells were then spun down at 1500g for 10 mins before being resuspended in buffered methanol-complex media (BMMY) for induction. Cells were grown for 4 days at 29.4 °C and 260 rpm. 0.5 % v/v methanol was added each day to account for evaporation and maintain both the carbon source and induction.

6.3.4 *MSP1₁₉* purification

Cells were spun down at 1500 g for 10 mins and the supernatant was filtered into sterile containers. The yeast pellet was discarded. The supernatant was pH'd to 7.2 using KOH and concentrated using a 400 ml stirred cell using ultrafiltration discs MWCO 3 kDa (Millipore) under pressure of 5 kPa. 5000 units of glycerol free PNGaseF (neb) were added to the concentrated solution in order to deglycosylate the protein. The reaction was left to run at 37 °C for four days. Successful deglycosylation was determined by differences in protein migration on an 15 % SDS-PAGE.

After deglycosylation, 5 M NaCl was added to the protein to a final concentration of 300 mM. The resulting solution was applied to a 5 ml HisTrap FF column (GE healthcare) pre-equilibrated in 20 mM NaPi (pH 6.5), 300 mM NaCl, 20 mM imidazole. The column was washed with two CVs of the same buffer and the bound protein was eluted using 250 mM imidazole. The eluted protein was concentrated using an Amicon Ultra-15 Centrifugal filter MWCO 3500 Da (Millipore). The concentrated protein was then further purified and buffer exchanged using a 16/60 Superdex S75 column PG (GE

Healthcare) pre-equilibrated in 10 mM NaPi (pH 6.5), Fractions corresponding to MSP1₁₉ were collected for further work.

6.4 MSP1₁₉-rusticyanin complex

6.4.1 Complex purification

Rusticyanin was reduced using a small amount ascorbic acid removing the blue colour and producing colourless protein. The resulting rusticyanin was then dialysed against 10 mM NaPi (pH 6.5) to remove residual ascorbic acid before complex formation.

Rusticyanin was added to MSP1₁₉ to excess and left to bind at room temperature overnight. The protein mixture was then added to a Superdex 75 10/50 GL pre-equilibrated in 10 mM NaPi (pH 6.5) and ran at a flow rate of 0.5 ml/min. Fractions were collected for further analysis.

6.4.2 MSP1₁₉-rusticyanin complex crystal trials

Crystal trays were set using an Innovadyne™ Screenmaker 96+8 robot. Drops were set 1:1 protein to precipitant with a total volume of 200 nl against a reservoir volume of 80 µl. Protein was screened at concentrations of 10 mg/ml and 5 mg/ml. The commercial screens Structure I+II (Molecular Dimensions), PEGRx HT™ (Hampton Research) and Midas™ (Molecular Dimensions) were chosen for initial screening. Trays were set up and left at room temperature to monitor crystal growth.

References

- Agnandji, S.T. et al., 2014. Efficacy and Safety of the RTS,S/AS01 Malaria Vaccine during 18 Months after Vaccination: A Phase 3 Randomized, Controlled Trial in Children and Young Infants at 11 African Sites. *PLoS Medicine*, 11(7).
- Alex, A.A. & Millan, D.S., 2012. Chapter 5 Contribution of Structure-Based Drug Design to the Discovery of Marketed drugs. In *Drug Design Strategies: Quantitative Approaches*. London: Royal Society of Chemistry, pp. 108–163.
- Allan, D.R. et al., 2015. Status of the crystallography beamlines at Diamond Light Source. *The European Physical Journal Plus*, 130(56), pp.1–20.
- Alonso, P.L. et al., 1991. The effect of insecticide-treated bed nets on mortality of Gambian children. *The Lancet*, 337(8756), pp.1499–1502.
- Alphey, L. et al., 2002. Malaria control with genetically manipulated insect vectors. *Science*, 298(5591), pp.119–121.
- Althoff, T. et al., 2011. Arrangement of electron transport chain components in bovine mitochondrial supercomplex I1III2IV1. *The EMBO journal*, 30(22), pp.4652–4664.
- Antoine, T. et al., 2013. Rapid kill of malaria parasites by artemisinin and semi-synthetic endoperoxides involves ROS-dependent depolarization of the membrane potential. *The Journal of Antimicrobial Chemotherapy*, 69(4), pp.1–12.
- Araujo, F.G. et al., 1992. In vitro and in vivo activities of the hydroxynaphthoquinone 566C80 against the cyst form of *Toxoplasma gondii*. *Antimicrobial Agents and Chemotherapy*, 36(2), pp.326–330.
- Ariey, F. et al., 2014. A molecular marker of artemisinin-resistant *Plasmodium falciparum* malaria. *Nature*, 505(7481), pp.50–5.
- Babon, J.J. et al., 2007. Structural studies on *Plasmodium vivax* merozoite surface protein-1. *Molecular and Biochemical Parasitology*, 153(1), pp.31–40.
- Baird, J.K., 2007. Neglect of *Plasmodium vivax* malaria. *Trends in Parasitology*, 23(11), pp.533–539.
- Bakheet, T.M. & Doig, A.J., 2009. Properties and identification of human protein drug targets. *Bioinformatics*, 25(4), pp.451–457.
- Barrett, M.L. et al., 2006. Atomic resolution crystal structures, EXAFS, and quantum chemical studies of rusticyanin and its two mutants provide insight into its unusual properties. *Biochemistry*, 45(9), pp.2927–39.
- Bartoloni, A. & Zammarchi, L., 2012. Clinical aspects of uncomplicated and severe malaria. *Mediterranean Journal of Hematology and Infectious Diseases*, 4(1).
- Barton, V. et al., 2010. Inhibiting *Plasmodium* cytochrome bc1: A complex

- issue. *Current Opinion in Chemical Biology*, 14(4), pp.440–446.
- Battye, T.G.G. et al., 2011. iMOSFLM: a new graphical interface for diffraction-image processing with MOSFLM. *Acta Crystallographica Section D: Biological Crystallography*, 67(Pt 4), pp.271–81.
- Benedict, M.Q. & Robinson, A.S., 2003. The first releases of transgenic mosquitoes: An argument for the sterile insect technique. *Trends in Parasitology*, 19(8), pp.349–355.
- Berdoy, M., Webster, J.P. & Macdonald, D.W., 2000. Fatal attraction in rats infected with *Toxoplasma gondii*. *Proceedings. Biological sciences / The Royal Society*, 267(1452), pp.1591–1594.
- Berman, H.M. et al., 2000. The Protein Data Bank. *Nucleic Acids Research*, 28(1), pp.235–242.
- Berry, E.A., Huang, L. & DeRose, V.J., 1991. Ubiquinol-Cytochrome c Oxidoreductase of Higher Plants. *The Journal of Biological Chemistry*, 266(15), pp.9064–9077.
- Biagini, G.A. et al., 2008. Acridinediones: selective and potent inhibitors of the malaria parasite mitochondrial bc1 complex. *Molecular Pharmacology*, 73(5), pp.1347–1355.
- Biagini, G.A. et al., 2012. Generation of quinolone antimalarials targeting the *Plasmodium falciparum* mitochondrial respiratory chain for the treatment and prophylaxis of malaria. *Proceedings of the National Academy of Sciences of the United States of America*, 109(21), pp.8298–8303.
- Biasini, M. et al., 2014. SWISS-MODEL: Modelling protein tertiary and quaternary structure using evolutionary information. *Nucleic Acids Research*, 42(W1), pp.252–258.
- Bibby, J. et al., 2012. AMPLE: a cluster-and-truncate approach to solve the crystal structures of small proteins using rapidly computed ab initio models. *Acta Crystallographica Section D: Biological Crystallography*, D68, pp.1622–1631.
- Bignami, A. & Marchiafava, E., 1894. On summer-autumnal fevers. In *Two Monographs on Malaria and the Parasites of Malarial Fevers*. The New Sydenham Society London, pp. 1–393.
- Bilderback, D.H., Elleaume, P. & Weckert, E., 2005. Review of third and next generation synchrotron light. *Journal of Physics B: Atomic, Molecular and Optical Physics*, 38, pp.S773–S797.
- Bill and Melinda Gates Foundatin, 2007. Bill and Melinda Gates Call for New Global Commitment to Chart a Course for Malaria Eradication. *Press release*. Available at: <http://www.gatesfoundation.org/Media-Center/Press-Releases/2007/10/Chart-a-Course-for-Malaria-Eradication/> [Accessed August 4, 2015].
- Birth, D., Kao, W.-C. & Hunte, C., 2014. Structural analysis of atovaquone-inhibited cytochrome bc1 complex reveals the molecular basis of

- antimalarial drug action. *Nature Communications*, 5(May), p.4029.
- Black, M.W. & Boothroyd, J.C., 2000. Lytic cycle of *Toxoplasma gondii*. *Microbiology and molecular biology reviews : MMBR*, 64(3), pp.607–623.
- Blackman, M.J. et al., 1990. A single fragment of a malaria merozoite surface protein remains on the parasite during red cell invasion and is the target of invasion-inhibiting antibodies. *The Journal of experimental medicine*, 172(1), pp.379–382.
- Blackman, M.J. et al., 1994. Antibodies inhibit the protease-mediated processing of a malaria merozoite surface protein. *The Journal of experimental medicine*, 180(1), pp.389–393.
- Blake, C.C.F. et al., 1965. Structure of Hen Egg-White Lysozyme. *Nature*, 206, pp.757–761.
- Blake II, R.C. & Shute, E.A., 1987. Respiratory Enzymes of *Thiobacillus ferrooxidans*. *The Journal of Biological Chemistry*, 262(31), pp.14983–14969.
- Blundell, T.L., 1996. Structure-based drug design. *Nature*, 384(6604 Suppl), pp.23–26.
- Blundell, T.L., Jhoti, H. & Abell, C., 2002. High-throughput crystallography for lead discovery in drug design. *Nature Reviews Drug discovery*, 1(1), pp.45–54.
- Blundell, T.L. & Johnson, L.N., 1976. *Protein Crystallography*, New York: Academic Press, New York.
- Blundell, T.L. & Patel, S., 2004. High-throughput X-ray crystallography for drug discovery. *Current Opinion in Pharmacology*, 4(5), pp.490–496.
- Botuyan, M. V et al., 1996. NMR solution structure of Cu(I) rusticyanin from *Thiobacillus ferrooxidans*: structural basis for the extreme acid stability and redox potential. *Journal of molecular biology*, 263(5), pp.752–767.
- Bouharoun-Tayoun, H. et al., 1990. Antibodies that protect humans against *Plasmodium falciparum* blood stages do not on their own inhibit parasite growth and invasion in vitro, but act in cooperation with monocytes. *The Journal of experimental medicine*, 172(6), pp.1633–1641.
- Bowler, M.W. et al., 2006. Reproducible improvements in order and diffraction limit of crystals of bovine mitochondrial F1-ATPase by controlled dehydration. *Acta Crystallographica Section D: Biological Crystallography*, 62(9), pp.991–995.
- Boyle, M.J. et al., 2014. Sequential processing of merozoite surface proteins during and after erythrocyte invasion by *Plasmodium falciparum*. *Infection and Immunity*, 82(3), pp.924–936.
- Bragg, W.L., 1913. The diffraction of Short Electromagnetic Waves by a Crystal. *Proceedings of the Cambridge Philosophical Society*, 17, pp.43–57.
- Braun, H. & Schmitz, U.K., 1995. Are the 'core' proteins of the mitochondrial bc1 complex evolutionary relics of a processing protease? *Trends in*

- Biochemical Sciences*, (20), pp.171–175.
- Breman, J.G., 2001. The ears of the hippopotamus: Manifestations, determinants, and estimates of the malaria burden. *American Journal of Tropical Medicine and Hygiene*, 64(1-2 SUPPL.), pp.1–11.
- Brunger, A.T., 1992. Free R value: a novel statistical quantity for assessing the accuracy of crystal structures. *Nature*, 355, pp.472–475.
- Bueno, J.M. et al., 2012. Exploration of 4(1H)-pyridones as a novel family of potent antimalarial inhibitors of the plasmodial cytochrome bc1. *Future medicinal chemistry*, 4(18), pp.2311–23.
- Bueno, J.M. et al., 2011. Potent antimalarial 4-pyridones with improved physico-chemical properties. *Bioorganic and Medicinal Chemistry Letters*, 21(18), pp.5214–5218.
- Burrows, J.N. et al., 2013. Designing the next generation of medicines for malaria control and eradication. *Malaria journal*, 12, p.187.
- Caffrey, M. & Cherezov, V., 2009. Crystallizing membrane proteins using lipidic mesophases. *Nature Protocols*, 4(5), pp.706–31.
- Caminade, C. et al., 2014. Impact of climate change on global malaria distribution. *Proceedings of the National Academy of Sciences of the United States of America*, 111(9), pp.3286–91.
- Canfield, C.J., Pudney, M. & Gutteridge, W.E., 1995. Interactions of Atovaquone with Other Antimalarial Drugs against Plasmodium falciparum in Vitro. *Experimental Parasitology*, 80, pp.373–381.
- Capper, M.J. et al., 2015. Antimalarial 4(1H)-pyridones bind to the Qi site of cytochrome bc1. *Proceedings of the National Academy of Sciences of the United States of America*, 112(3), pp.755–760.
- Carpenter, E.P. et al., 2008. Overcoming the challenges of membrane protein crystallography. *Current Opinion in Structural Biology*, 18(5), pp.581–586.
- Carrington, H.C. et al., 1951. A Metabolite of ‘Paludrine’ with High Antimalarial Activity. *Nature*, 168, p.1080.
- Carter, R. & Mendis, K.N., 2002. Evolutionary and Historical Aspects of the Burden of Nalaria. *Clinical Microbiology Reviews*, 15(4), pp.564–594.
- Chandra, G. et al., 2008. Mosquito control by larvivorous fish. *Indian Journal of Medical Research*, 127(1), pp.13–27.
- Chandramohanadas, R. et al., 2014. Small Molecule Targeting Malaria Merozoite Surface Protein-1 (MSP-1) Prevent Host Invasion of Divergent Plasmodial Species. *The Journal of infectious diseases*, 1.
- Chareonviriyaphap, T., Bangs, M.J. & Ratanatham, S., 2000. Status of malaria in Thailand. *Southeast Asian Journal of Tropical Medicine and Public Health*, 31(2), pp.225–237.
- Chaudhari, A. et al., 2006. Azurin, Plasmodium falciparum Malaria and

- HIV/AIDS. *Cell Cycle*, 5(15), pp.1642–1648.
- Chaudhari, A. et al., 2007. Cupredoxin-cancer interrelationship: Azurin binding with EphB2, interference in EphB2 tyrosine phosphorylation, and inhibition of cancer growth. *Biochemistry*, 46(7), pp.1799–1810.
- Chayen, N.E. & Saridakis, E., 2008. Protein crystallization: from purified protein to diffraction-quality crystal. *Nature Methods*, 5(2), pp.147–153.
- Cherezov, V., Abola, E. & Stevens, R.C., 2010. Toward drug design: recent progress in the structure determination of GPCRs, a membrane protein family with high potential as pharmaceutical targets. *Methods in Molecular Biology*, 654, pp.141–168.
- Cherezov, V., Fersi, H. & Caffrey, M., 2001. Crystallization screens: compatibility with the lipidic cubic phase for in meso crystallization of membrane proteins. *Biophysical journal*, 81(1), pp.225–42.
- Cohen, A.E. et al., 2014. Goniometer-based femtosecond crystallography with X-ray free electron lasers. *Proceedings of the National Academy of Sciences of the United States of America*, 111(48), pp.17122–17127.
- Cohen, S., Butcher, G. a & Crandall, R.B., 1969. Action of malarial antibody in vitro. *Nature*, 223(5204), pp.368–371.
- Collaborative Computational Project, N. 4, 1994. The CCP4 suite: Programs for protein crystallography. *Acta Crystallographica Section D: Biological Crystallography*, 50, pp.760–763.
- Congreve, M. et al., 2003. A 'Rule of Three' for fragment-based lead discovery? *Drug Discovery Today*, 8(19), pp.876–877.
- Congreve, M., Murray, C.W. & Blundell, T.L., 2005. Structural biology and drug discovery. *Drug discovery today*, 10(13), pp.895–907.
- Cowley, R. et al., 2012. The development of quinolone esters as novel antimalarial agents targeting the Plasmodium falciparum bc1 protein complex. *MedChemComm*, 3(39), pp.39–44.
- Cowman, a F. et al., 1988. Amino acid changes linked to pyrimethamine resistance in the dihydrofolate reductase-thymidylate synthase gene of Plasmodium falciparum. *Proceedings of the National Academy of Sciences of the United States of America*, 85(23), pp.9109–9113.
- Crabtree, H.G., 1928. The carbohydrate metabolism of certain pathological overgrowths. *Biochemical Journal*, 22(5), pp.1289–1298.
- Crofts, A.R. et al., 1999. Mechanism of Ubiquinol Oxidation by the bc 1 Complex : Role of the Iron Sulfur Protein and Its Mobility. *Biochemistry*, 38(48), pp.15791–15806.
- Crofts, A.R. et al., 2003. The modified Q-cycle explains the apparent mismatch between the kinetics of reduction of cytochromes c1 and bH in the bc 1 complex. *Journal of Biological Chemistry*, 278(38), pp.36191–36201.
- Crompton, P.D., Pierce, S.K. & Miller, L.H., 2010. Advances and challenges in malaria vaccine development. *Journal of Clinical Investestigation*,

120(12), pp.4168–4178.

- Cross, R.M. et al., 2010. Endochin optimization: structure-activity and structure-property relationship studies of 3-substituted 2-methyl-4(1H)-quinolones with antimalarial activity. *Journal of Medicinal Chemistry*, 53(19), pp.7076–7094.
- Cruz-Gallardo, I. et al., 2013. Antimalarial activity of cupredoxins: the interaction of Plasmodium merozoite surface protein 119 (MSP119) and rusticyanin. *The Journal of Biological Chemistry*, 288(29), pp.20896–907.
- Csermely, P., Ágoston, V. & Pongor, S., 2005. The efficiency of multi-target drugs: the network approach might help drug design. *Trends in Parasitology*, 182, pp.178–182.
- Cushman, D.W. et al., 1977. Design of potent competitive inhibitors of angiotensin-converting enzyme. Carboxyalkanoyl and mercaptoalkanoyl amino acids. *Biochemistry*, 16(25), pp.5484–5491.
- D’Arcy, A., Villard, F. & Marsh, M., 2007. An automated microseed matrix-screening method for protein crystallization. *Acta Crystallographica Section D: Biological Crystallography*, 63(4), pp.550–554.
- Dauter, Z. et al., 1999. Can anomalous signal of sulfur become a tool for solving protein crystal structures? *Journal of molecular biology*, 289(1), pp.83–92.
- Debouck, C., 1992. The HIV-1 protease as a therapeutic target for AIDS. *AIDS Research and Human Retroviruses*, 8(2), pp.153–164.
- Deisenhofer, J. et al., 1985. Structure of the protein subunits in the photosynthetic reaction centre of Rhodospseudomonas viridis at 3Å resolution. *Nature*, 318(6047), pp.618–624.
- Van Delden, C. & Hirschel, B., 1996. Folinic acid supplements to pyrimethamine-sulfadiazine for Toxoplasma encephalitis are associated with better outcome. *The Journal of infectious diseases*, 173(5), pp.1294–1295.
- Dicarlo, J.E. et al., 2013. Genome engineering in Saccharomyces cerevisiae using CRISPR-Cas systems. *Nucleic Acids Research*, 41(7), pp.4336–4343.
- Djebli, A. et al., 1992. Crystallization and Preliminary X-ray Crystallographic of Rusticyanin from Thiobacillus ferrooxidans. *Journal of Molecular Biology*, 277, pp.581–582.
- Dluzewski, A.R. et al., 2008. Formation of the food vacuole in Plasmodium falciparum. A potential role for the 19 kDa fragment of merozoite surface protein 1 (MSP119). *PLoS ONE*, 3(8).
- Doggett, J.S. et al., 2012. Endochin-like quinolones are highly efficacious against acute and latent experimental toxoplasmosis. *Proceedings of the National Academy of Sciences of the United States of America*, 109(39), pp.15936–15941.
- Dondorp, A.M. et al., 2009. Artemisinin Resistance in Plasmodium falciparum

- Malaria. *The New England Journal of Medicine*, 361(5), pp.455–467.
- Dondorp, A.M., Pongponratn, E. & White, N.J., 2004. Reduced microcirculatory flow in severe falciparum malaria: Pathophysiology and electron-microscopic pathology. *Acta Tropica*, 89(3), pp.309–317.
- Dorn, A. et al., 1998. An Assessment of Drug-Haematin Binding as a Mechanism for Inhibition of Haematin Polymerisation by Quinoline Antimalarials. , 55(97), pp.727–736.
- Dressman, J.B. & Reppas, C., 2000. In vitro–in vivo correlations for lipophilic, poorly water-soluble drugs. *European journal of pharmaceutical sciences*, 11(Suppl. 2), pp.S73–S80.
- Drew, D.R. et al., 2004. A Common Cross-species Function for the Double Epidermal Growth Factor-like Modules of the Highly Divergent Plasmodium Surface Proteins MSP-1 and MSP-8. *Journal of Biological Chemistry*, 279(19), pp.20147–20153.
- Drew, D.R., Sanders, P.R. & Crabb, B.S., 2005. Plasmodium falciparum Merozoite Surface Protein 8 Is a Ring-Stage Membrane Protein That Localizes to the Parasitophorous Vacuole of Infected Erythrocytes. *Infection and Immunity*, 73(7), pp.3912–3922.
- Drews, J., 2000. Drug discovery: a historical perspective. *Science*, 287(5460), pp.1960–1964.
- Dubey, J.P. et al., 2012. A review of toxoplasmosis in humans and animals in Ethiopia. *Epidemiology and Infection*, 140(11), pp.1935–1938.
- Dubey, J.P., 1998. Advances in the life cycle of Toxoplasma gondii. *International Journal for Parasitology*, 28(7), pp.1019–1024.
- Dubey, J.P., 2009. History of the discovery of the life cycle of Toxoplasma gondii. *International Journal for Parasitology*, 39(8), pp.877–882.
- Dubey, J.P. et al., 2011. Sporulation and Survival of Toxoplasma gondii Oocysts in Different Types of Commercial Cat Litter. *Journal of Parasitology*, 97(5), pp.751–754.
- Dudkina, N. V. et al., 2010. Structure and function of mitochondrial supercomplexes. *Biochimica et Biophysica Acta - Bioenergetics*, 1797, pp.664–670.
- Duke, E.M.H. & Johnson, L.N., 2010. Macromolecular crystallography at synchrotron radiation sources: current status and future developments. *Proceedings of the Royal Society A: Mathematical, Physical and Engineering Sciences*, 466(2124), pp.3421–3452.
- Edi, C.V.A. et al., 2012. Multiple-insecticide resistance in anopheles gambiae mosquitoes, Southern Côte d'Ivoire. *Emerging Infectious Diseases*, 18(9), pp.1508–1511.
- Egan, A.F. et al., 1999. Human antibodies to the 19kDa C-terminal fragment of Plasmodium falciparum merozoite surface protein 1 inhibit parasite growth in vitro. *Parasite immunology*, 21(3), pp.133–139.

- Elfawal, M.A. et al., 2015. Dried whole-plant *Artemisia annua* slows evolution of malaria drug resistance and overcomes resistance to artemisinin. *Proceedings of the National Academy of Sciences of the United States of America*, p.201413127.
- Elissa, N. et al., 1993. Resistance of *Anopheles gambiae* s.s. to Pyrethroids in Cote D'Ivoire. *Annales de la Societe Belge de Medecine Tropicale*, 73, pp.291–294.
- Ellis, R.D. et al., 2012. Phase 1 Study in Malaria Naïve Adults of BSAM2/Alhydrogel®+CPG 7909, a Blood Stage Vaccine against *P. falciparum* Malaria. *PLoS ONE*, 7(10).
- Emsley, P. et al., 2010. Features and development of Coot. *Acta Crystallographica Section D: Biological Crystallography*, 66, pp.486–501.
- Emsley, P. & Cowtan, K., 2004. Coot: Model-building tools for molecular graphics. *Acta Crystallographica Section D: Biological Crystallography*, 60, pp.2126–2132.
- Enserink, M., 2010. GM Mosquito Trial Alarms Opponents, Strains Ties in Gates-Funded Project. *Science*, pp.1030–1031.
- Esser, L. et al., 2004. Crystallographic studies of quinol oxidation site inhibitors: A modified classification of inhibitors for the cytochrome bc1 complex. *Journal of Molecular Biology*, 341(1), pp.281–302.
- Esser, L. et al., 2006. Surface-modulated motion switch: capture and release of iron-sulfur protein in the cytochrome bc1 complex. *Proceedings of the National Academy of Sciences of the United States of America*, 103(35), pp.13045–13050.
- European Medicines Agency, 2015. First malaria vaccine receives positive scientific opinion from EMA. *Press release*. Available at: http://www.ema.europa.eu/ema/index.jsp?curl=pages/news_and_events/news/2015/07/news_detail_002376.jsp&mid=WC0b01ac058004d5c1 [Accessed August 3, 2015].
- Evans, P.R. & Murshudov, G.N., 2013. How good are my data and what is the resolution? *Acta Crystallographica Section D: Biological Crystallography*, 69(7), pp.1204–1214.
- Ferguson, D.J. et al., 1994. An ultrastructural study of the effect of treatment with atovaquone in brains of mice chronically infected with the ME49 strain of *Toxoplasma gondii*. *International Journal of Experimental Pathology*, 75(2), pp.111–116.
- Fisher, N.E. et al., 2012. Cytochrome b Mutation Y268S Conferring Atovaquone Resistance Phenotype in Malaria Parasite Results in Reduced Parasite bc1 Catalytic Turnover and Protein Expression. *Journal of Biological Chemistry*, 287(13), pp.9731–9741.
- Fisher, N.E. et al., 2008. Malaria-parasite mitochondrial dehydrogenases as targets: too early to write the obituary. *Trends in Parasitology*, 24(1), pp.9–10.

- Fisher, N.E. & Meunier, B., 2008. Molecular basis of resistance to cytochrome bc1 inhibitors. *FEMS Yeast Research*, 8(2), pp.183–192.
- Fleck, S.L., Pudney, M. & Sinden, R.E., 1996. The effect of atovaquone (566C80) on the maturation and viability of Plasmodium falciparum gametocytes in vitro. *Transactions of the Royal Society of Tropical Medicine and Hygiene*, 90, pp.309–312.
- Flegr, J. et al., 2002. Increased risk of traffic accidents in subjects with latent toxoplasmosis: a retrospective case-control study. *BMC infectious diseases*, 2, p.11.
- Flegr, J., 2013. Influence of latent Toxoplasma infection on human personality, physiology and morphology: pros and cons of the Toxoplasma-human model in studying the manipulation hypothesis. *The Journal of Experimental Biology*, 216(1), pp.127–133.
- Flegr, J. et al., 2014. Toxoplasmosis - A global threat. Correlation of latent toxoplasmosis with specific disease burden in a set of 88 countries. *PLoS ONE*, 9(3).
- Florens, L. et al., 2002. A proteomic view of the Plasmodium falciparum life cycle. *Nature*, 419(6906), pp.520–526.
- Foadi, J. & Aller, P., 2013. BLEND : managing , scaling and merging multiple datasets.
- Fontenille, D. & Simard, F., 2004. Unravelling complexities in human malaria transmission dynamics in Africa through a comprehensive knowledge of vector populations. *Comparative Immunology, Microbiology and Infectious Diseases*, 27(5), pp.357–375.
- Fowkes, F.J.I. et al., 2010. The relationship between anti-merozoite antibodies and incidence of Plasmodium falciparum malaria: A systematic review and meta-analysis. *PLoS Medicine*, 7(1).
- Fromme, P. & Spence, J.C.H., 2011. Femtosecond nanocrystallography using X-ray lasers for membrane protein structure determination. *Current Opinion in Structural Biology*, 21(4), pp.509–516.
- Fry, M. & Pudney, M., 1992. Site of Action of the Antimalarial Hydroxynathoquinone, 2-[trans-4-(4'chlorophenyl) cyclohexyl]-3-hydroxy-1,4-napthoquinone (566C80). *Biochemical Pharmacology*, 43(7), pp.1545–1553.
- Fry, M., Webb, E. & Pudney, M., 1990. Effect of Mitochondrial Inhibitors on Adenosinetriphosphate levels in Plasmoidum Falciparum. *Comparative Biochemistry and Physiology*, 96(4), pp.775–782.
- Fry, M. & Williams, R.B., 1984. Effects of decoquinatate and clopidol on electron transport in mitochondria of Eimeria tenella (Apicomplexa: Coccidia). *Biochemical Pharmacology*, 33(2), pp.229–240.
- Gallup, J.L. & Sachs, J.D., 2001. The economic burden of malaria. *American Journal of Tropical Medicine and Hygiene*, 64(1-2 SUPPL.), pp.85–96.

- Gardner, M.J. et al., 2002. Genome sequence of the human malaria parasite *Plasmodium falciparum*. *Nature*, 419(6906), pp.498–511.
- Garman, E., 2003. ‘Cool’ crystals: Macromolecular cryocrystallography and radiation damage. *Current Opinion in Structural Biology*, 13(5), pp.545–551.
- Garman, E. & James, W., 2003. CCP4 study weekend Heavy-atom derivatization CCP4 study weekend. *Acta Crystallographica Section D: Biological Crystallography*, D59, pp.1903–1913.
- Garman, E.F., 2010. Radiation damage in macromolecular crystallography: what is it and why should we care? *Acta Crystallographica Section D: Biological Crystallography*, 66(Pt 4), pp.339–51.
- Garman, S.C. et al., 2003. Structure of the C-terminal domains of merozoite surface protein-1 from *Plasmodium knowlesi* reveals a novel histidine binding site. *The Journal of Biological Chemistry*, 278(9), pp.7264–9.
- Geels, M.J. et al., 2011. European Vaccine Initiative: lessons from developing malaria vaccines. *Expert Review of Vaccines*, 10(12), pp.1697–1708.
- Georgopoulos, G.D., 1954. Extension to chlordane of the resistance to DDT observed in *Anopheles sacharovi*. *Bulletin of the World Health Organization*, 11(4-5), pp.855–864.
- Gething, P.W. et al., 2012. A Long Neglected World Malaria Map: *Plasmodium vivax* Endemicity in 2010. *PLoS Neglected Tropical Diseases*, 6(9).
- Gething, P.W. et al., 2011. Modelling the global constraints of temperature on transmission of *Plasmodium falciparum* and *P. vivax*. *Parasites & vectors*, 4(1), p.92.
- Gingrich, W.D. & Darrow, E.M., 1951. The Effect of Endochin on Experimental Toxoplasmosis. *American Journal of Tropical Medicine and Hygiene*, s1-31(1), pp.12–17.
- Goel, V.K. et al., 2003. Band 3 is a host receptor binding merozoite surface protein 1 during the *Plasmodium falciparum* invasion of erythrocytes. *Proceedings of the National Academy of Sciences of the United States of America*, 100(9), pp.5164–5169.
- Green, D.W., Ingram, V.M. & Perutz, M.F., 1954. The structure of haemoglobin IV. Sign determination by the isomorphous replacement method. *Proceedings of the Royal Society of London. Series A, Mathematical, Physical and Engineering Sciences*, 225, pp.287–307.
- Greenwood, B.M. et al., 2008. Malaria: progress, perils, and prospects for eradication. *The Journal of Clinical Investigation*, 118(4), pp.1266–1276.
- Gregson, A. & Plowe, C. V., 2005. Mechanisms of Resistance of Malaria Parasites to Antifolates. *Pharmacol Rev*, 57(1), pp.117–145.
- Gutteridge, W.E., 1989. Antimalarial drugs currently in development. *Journal of the Royal Society of Medicine*, 82 Suppl 1(17), pp.63–66; discussion 66–68.

- El Hage, S. et al., 2009. Synthesis and antimalarial activity of new atovaquone derivatives. *European Journal of Medicinal Chemistry*, 44(11), pp.4778–4782.
- Hajduk, P.J., Olejniczak, E.T. & Fesik, S.W., 1997. One-dimensional relaxation- and diffusion-edited NMR methods for screening compounds that bind to macromolecules. *Journal of the American Chemical Society*, 119(50), pp.12257–12261.
- Hall, J.F. et al., 1998. Modulating the Redox Potential and Acid Stability of Rusticyanin by Site-Directed Mutagenesis of Ser86. *Biochemistry*, 37(33), pp.11451–11458.
- Harinasuta, T., Suntharasamai, P. & Viravan, C., 1965. Chloroquine-Resistant falciparum Malaria in Thailand. *The Lancet*, 286(7414), pp.655–657.
- Harris, P.K. et al., 2005. Molecular identification of a malaria merozoite surface sheddase. *PLoS Pathogens*, 1(3), pp.0241–0251.
- Harvey, I. et al., 1998. Structure Determination of a 16.8 kDa Copper Protein at 2.1 Å Resolution Using Anomalous Scattering Data with Direct Methods. *Acta Crystallographica Section D: Biological Crystallography*, 54(4), pp.629–635.
- Hauptman, H.A., 1991. The Phase Problem of X-ray Crystallography. *Reports on Progress in Physics*, pp.1427–1454.
- Hay, S.I. & Snow, R.W., 2006. The Malaria Atlas Project: Developing Global Maps of Malaria Risk. *PLoS Medicine*, 3(12), pp.2204–2208.
- Heinemann, U., Illing, G. & Oschkinat, H., 2001. High-throughput three-dimensional protein structure determination. *Current Opinion in Biotechnology*, 12(4), pp.348–354.
- Held, J., Jeyaraj, S. & Kreidenweiss, A., 2015. Antimalarial compounds in Phase II clinical development. *Expert Opinion Investigating Drugs*, 24(3), pp.363–382.
- Helliwell, J.R. et al., 1982. Central data collection facility for protein crystallography, small angle diffraction and scattering at the Daresbury Laboratory Synchrotron Radiation Source (SRS), England. *Journal of Physics E: Scientific Instruments*, 15, pp.1363–1372.
- Helliwell, J.R. & Mitchell, E.P., 2015. Synchrotron radiation macromolecular crystallography: science and spin-offs. *IUCr*, 2(2), pp.283–291.
- Hemingway, J., 2014. The role of vector control in stopping the transmission of malaria: threats and opportunities. *Philosophical transactions of the Royal Society of London. Series B, Biological sciences*, 369(1645), p.20130431.
- Hendrickson, W.A., Horton, J.R. & LeMaster, D.M., 1990. Selenomethionyl proteins produced for analysis by multiwavelength anomalous diffraction (MAD): a vehicle for direct determination of three-dimensional structure. *The EMBO journal*, 9(5), pp.1665–1672.

- Hendrickson, W.A. & Teeter, M.M., 1981. Structure of the Hydrophobic Protein Crammin Determined Directly from the Anomalous Scattering of Sulfur. *Nature*, 290, pp.107–113.
- Hillisch, A., Pineda, L.F. & Hilgenfeld, R., 2004. Utility of homology models in the drug discovery process. *Drug Discovery Today*, 9(15), pp.659–669.
- Holder, A.A. et al., 1992. A malaria merozoite surface protein (MSP1)-structure, processing and function. *Memorias do Instituto Oswaldo Cruz*, 87 Suppl 3, pp.37–42.
- Huang, L. et al., 2005. Binding of the Respiratory Chain Inhibitor Antimycin to the Mitochondrial bc1 Complex: A New Crystal Structure Reveals an Altered Intramolecular Hydrogen-bonding Pattern. *Journal of Molecular Biology*, 351(3), pp.573–597.
- Hülsen, G. et al., 2006. Protein crystallography with a novel large-area pixel detector. *Journal of Applied Crystallography*, 39(4), pp.550–557.
- Ingledeu, W.J. & Cobley, J.G., 1980. A potentiometric and kinetic study on the respiratory chain of ferrous-iron-grown *Thiobacillus ferrooxidans*. *Biochimica et Biophysica Acta - Bioenergetics*, 590, pp.141–158.
- Ishchenko, A. et al., 2012. Structure-based design technology contour and its application to the design of renin inhibitors. *Journal of Chemical Information and Modeling*, 52(8), pp.2089–2097.
- von Itzstein, M. et al., 1993. Rational design of potent sialidase-based inhibitors of influenza virus replication. *Nature*, 363(6428), pp.418–423.
- Iwata, S. et al., 1998. Complete structure of the 11-subunit bovine mitochondrial cytochrome bc1 complex. *Science*, 281(5373), pp.64–71.
- James, S. et al., 2006. Synthesis, solution structure and immune recognition of an epidermal growth factor-like domain from *Plasmodium falciparum* merozoite surface protein-1. *ChemBioChem*, 7, pp.1943–1950.
- Jhoti, H. et al., 2013. The ‘rule of three’ for fragment-based drug discovery: where are we now? *Nature Reviews Drug Discovery*, (July).
- Jiménez-Díaz, M.B. et al., 2009. Improved murine model of malaria using *Plasmodium falciparum* competent strains and non-myelodepleted NOD-scid IL2R γ null mice engrafted with human erythrocytes. *Antimicrobial Agents and Chemotherapy*, 53(10), pp.4533–6.
- Jones, J.L., Sehgal, M. & Maguire, J.H., 2002. Toxoplasmosis-Associated Deaths Human Immunodeficiency Virus-Infected Persons in the United States, 1992-1998. *Clinical Infectious Diseases*, 34(8), p.1161.
- Kadekoppala, M. & Holder, A. a., 2010. Merozoite surface proteins of the malaria parasite: The MSP1 complex and the MSP7 family. *International Journal for Parasitology*, 40(10), pp.1155–1161.
- Kanbi, L.D. et al., 2002. Crystal Structures of the Met148Leu and Ser86Asp Mutants of Rusticyanin from *Thiobacillus ferrooxidans*: Insights into the Structural Relationship with the Cupredoxins and the Multi Copper

- Proteins. *Journal of Molecular Biology*, 320(2), pp.263–275.
- Kao, W.-C. & Hunte, C., 2014. The molecular evolution of the qo motif. *Genome biology and evolution*, 6(7), pp.1894–910.
- Keiser, J. et al., 2005. Effect of irrigation and large dams on the burden of malaria on a global and regional scale. *American Journal of Tropical Medicine and Hygiene*, 72(4), pp.392–406.
- Kelly, J.X. et al., 2009. Discovery of dual function acridones as a new antimalarial chemotype. *Nature*, 459(7244), pp.270–273.
- Kendrew, J.C. et al., 1958. A three-dimensional model of the myoglobin molecule obtained by x-ray analysis. *Nature*, 181(4610), pp.662–666.
- Kessl, J.J. et al., 2006. Molecular basis of *Toxoplasma gondii* atovaquone resistance modeled in *Saccharomyces cerevisiae*. *Molecular and Biochemical Parasitology*, 146(2), pp.255–258.
- Kessl, J.J., Moskalev, N. V., et al., 2007. Parameters determining the relative efficacy of hydroxy-naphthoquinone inhibitors of the cytochrome bc1 complex. *Biochimica et Biophysica Acta - Bioenergetics*, 1767(4), pp.319–326.
- Kessl, J.J., Meshnick, S.R. & Trumppower, B.L., 2007. Modeling the molecular basis of atovaquone resistance in parasites and pathogenic fungi. *Trends in Parasitology*, 23(10), pp.494–501.
- Kim, C.H. & King, T.E., 1983. A mitochondrial protein essential for the formation of the cytochrome-c1-c complex - isolation, purification and properties. *Journal of Biological Chemistry*, 258(22), pp.13543–13551.
- Kim, C.U. et al., 1998. Structure-activity relationship studies of novel carbocyclic influenza neuraminidase inhibitors. *Journal of medicinal chemistry*, 41(14), pp.2451–2460.
- Klayman, D.L., 1985. Qinghaosu (artemisinin): an antimalarial drug from China. *Science*, 228(4703), pp.1049–1055.
- Knols, B.G.J., Bukhari, T. & Farenhorst, M., 2010. Entomopathogenic fungi as the next-generation control agents against malaria mosquitoes. *Future microbiology*, 5(3), pp.339–341.
- Korsinczky, M. et al., 2000. Mutations in *Plasmodium falciparum* cytochrome b that are associated with atovaquone resistance are located at a putative drug-binding site. *Antimicrobial Agents and Chemotherapy*, 44(8), pp.2100–2108.
- Köster, H. et al., 2011. A small nonrule of 3 compatible fragment library provides high hit rate of endothiapepsin crystal structures with various fragment chemotypes. *Journal of Medicinal Chemistry*, 54(22), pp.7784–7796.
- Kotecka, B., 2015. Call for Army to stop using malaria drug mefloquine. *BBC News*. Available at: <http://www.bbc.co.uk/news/uk-33943282> [Accessed September 7, 2015].

- Koussis, K. et al., 2009. A multifunctional serine protease primes the malaria parasite for red blood cell invasion. *The EMBO journal*, 28(6), pp.725–735.
- Kovacs, J.A. & NIAID-Clinical Center Intramural AIDS Program, 1992. Efficacy of atovaquone in treatment of toxoplasmosis in patients with AIDS. *The Lancet*, 340(8820), pp.637–638.
- Kremsner, P.G. & Krishna, S., 2004. Antimalarial combinations. *The Lancet*, 364(9430), pp.285–94.
- Krogh, A. et al., 2001. Predicting transmembrane protein topology with a hidden Markov model: application to complete genomes. *Journal of Molecular Biology*, 305(3), pp.567–580.
- Krotoski, W.A. et al., 1982. Observations on Early and Late Post-Sporozoite Tissue Stages in Primate Malaria. *The American Journal of Tropical Medicine and Hygiene*, 31(1), pp.24–35.
- Laing, A.B.G., 1964. Antimalarial Effect of Sulphorthodimethoxine (Fanasil). *British Medical Journal*, 2(5422), pp.1439–1440.
- Landau, E.M. & Rosenbursch, J.P., 1996. Lipidic cubic phases : A novel concept for the crystallization. *Proceedings of the National Academy of Sciences of the United States of America*, 93, pp.14532–14535.
- Langermans, J.A.M. et al., 2006. Preclinical evaluation of a chimeric malaria vaccine candidate in Montanide ISA 720: immunogenicity and safety in rhesus macaques. *Human vaccines*, 2(5), pp.222–226.
- Laskowski, R.A. et al., 1993. PROCHECK: a program to check the stereochemical quality of protein structures. *Journal of Applied Crystallography*, 26(2), pp.283–291.
- Von Laue, M., 1913. Interferenzerscheinungen bei Röntgenstrahlen. *Annalen der Physik*, 346(10), pp.971–988.
- Laufer, M.K. et al., 2006. Return of Chloroquine Antimalarial Efficacy in Malawi. *The New England Journal of Medicine*, 355(19), pp.1959–1966.
- Laveran, A., 1881. *De la nature parasitaire de l'impaludisme*, Paris: J. -B. Balliere.
- Lebedev, A.A. et al., 2012. JLigand: a graphical tool for the CCP4 template-restraint library. *Acta Crystallographica Section D: Biological Crystallography*, 68(Pt 4), pp.431–40.
- Lemonnier, M. et al., 1978. X-ray Curved-Crystal Monochromator System at the Storage Ring DC1. *Nuclear Instruments and Methods*, 152, pp.173–177.
- Leport, C. et al., 1988. Treatment of Central Nervous System Toxoplasmosis with Pyrimethamine/Sulfadiazine Combination in 35 Patients with the Acquired Immunodeficiency Syndrome. *The American Journal of Medicine*, 84, pp.94–100.
- Leslie, A.G.W. & Powell, H.R., 2007. Processing diffraction data with MOSFLM.

Evolving methods for macromolecular Crystallography, pp.41–51.

- Leung, S.C. et al., 2012. Identification, Design and Biological Evaluation of Heterocyclic Quinolones Targeting Plasmodium falciparum Type II NADH:Quinone Oxidoreductase (PfNDH2). *Journal of Medicinal Chemistry*, 55, pp.1844–1857.
- Li, D. et al., 2012. Use of a Robot for High-throughput Crystallization of Membrane Proteins in Lipidic Mesophases. *Journal of Visualized Experiments*, (67), pp.1–8.
- Lines, J., Whitty, C.J.M. & Hanson, K., 2007. *Prospects for Eradication and Elimination of Malaria: a technical briefing for DFID*,
- Lipinski, C. a et al., 2001. Experimental and computational approaches to estimate solubility and permeability in drug discovery and development settings1PII of original article: S0169-409X(96)00423-1. The article was originally published in *Advanced Drug Delivery Reviews* 23 (1997) 3. *Advanced Drug Delivery Reviews*, 46(1-3), pp.3–26.
- Liu, K.Y. et al., 2006. Biological role of surface Toxoplasma gondii antigen in development of vaccine. *World Journal of Gastroenterology*, 12(15), pp.2363–2368.
- Looasreesuwon, S. et al., 1999. Malarone® (Atovaquone and Proguanil Hydrochloride): A Review of its Clinical Development for Treatment of Malaria. *The American Journal of Tropical Medicine and Hygiene*, 60(4), pp.533–541.
- Luft, B.J. & Remington, J.S., 1992. Toxoplasmic encephalitis in AIDS. *Clinical Infectious Diseases*, 24(3), pp.211–222.
- Lukens, a. K. et al., 2014. Diversity-Oriented Synthesis Probe Targets Plasmodium falciparum Cytochrome b Ubiquinone Reduction Site and Synergizes With Oxidation Site Inhibitors. *Journal of Infectious Diseases*, 211(7), pp.1097–1103.
- Manley, P.W., Cowan-Jacob, S.W. & Mestan, J., 2005. Advances in the structural biology, design and clinical development of Bcr-Abl kinase inhibitors for the treatment of chronic myeloid leukaemia. *Biochimica et biophysica acta*, 1754(1-2), pp.3–13.
- Marinotti, O. et al., 2013. Development of a population suppression strain of the human malaria vector mosquito, Anopheles stephensi. *Malaria journal*, 12(1), p.142.
- Markley, L.D., Heertum, J.C. Van & Doorenbos, H.E., 1972. Antimalarial Activity of Clopidol 3,5-Dichloro-2,6-dimethyl-4-pyridinol, and its Esters, Carbonates and Sulfonates. *Journal of Medicinal Chemistry*, 15(11), pp.1188–1189.
- Marroquin, L.D. et al., 2007. Circumventing the Crabtree effect: replacing media glucose with galactose increases susceptibility of HepG2 cells to mitochondrial toxicants. *Toxicological sciences*, 97(2), pp.539–547.
- Maude, R.J., Woodrow, C.J. & White, L.J., 2010. Artemisinin Antimalarials:

- Preserving the 'Magic Bullet'. *Drug Development Research*, 71(1), pp.12–19.
- Mayo, C.W. & Brady, F.J., 1955. The Eighth World Health Assembly. *Public health reports*, 70(11), pp.1057–1060.
- McFadden, D.C. et al., 2000. Characterization of cytochrome b from *Toxoplasma gondii* and Qo domain mutations as a mechanism of atovaquone-resistance. *Molecular and Biochemical Parasitology*, 108(1), pp.1–12.
- McNeil, B.W.J. & Thompson, N.R., 2010. X-ray free-electron lasers. *Nature Photonics*, 4(12), pp.814–821.
- McPherson, A., 1991. A brief history of protein crystal growth. *Journal of Crystal Growth*, 110(1-2), pp.1–10.
- McPherson, A., 1985. Crystallization of Macromolecules: General Principles. *Methods in Enzymology*, 114, pp.112–120.
- Mendis, K. et al., 2009. From malaria control to eradication: The WHO perspective. *Tropical Medicine and International Health*, 14(7), pp.802–9.
- Meneceur, P. et al., 2008. In vitro susceptibility of various genotypic strains of *Toxoplasma gondii* to pyrimethamine, sulfadiazine, and atovaquone. *Antimicrobial Agents and Chemotherapy*, 52(4), pp.1269–1277.
- Michel, H., 1983. Crystallization of membrane proteins. *Trends in Biochemical Sciences*, 7(5), pp.56–59.
- Mills, A., Lubell, Y. & Hanson, K., 2008. Malaria eradication: the economic, financial and institutional challenge. *Malaria journal*, 7 Suppl 1, p.S11.
- Mineo, J.R. & Kasper, L.H., 1994. Attachment of *Toxoplasma gondii* to Host Cells Involves Major Surface Protein, SAG1 (P30). *Experimental Parasitology*, 79, pp.11–20.
- Mitchell, P., 1976. Possible molecular mechanisms of the protonmotive function of cytochrome systems. *Journal of Theoretical Biology*, 62(2), pp.327–67.
- Montoya, J.G. & Liesenfeld, O., 2004. Toxoplasmosis. *The Lancet*, 363(9425), pp.1965–1976.
- Montoya, J.G. & Remington, J.S., 2008. Management of *Toxoplasma gondii* infection during pregnancy. *Clinical infectious diseases: an official publication of the Infectious Diseases Society of America*, 47(4), pp.554–566.
- Morgan, W.D. et al., 1999. Solution structure of an EGF module pair from the *Plasmodium falciparum* merozoite surface protein 1. *Journal of Molecular Biology*, 289(1), pp.113–22.
- Mueller, M., Wang, M. & Schulze-Briese, C., 2012. Optimal fine phi-slicing for single-photon-counting pixel detectors. *Acta Crystallographica Section D: Biological Crystallography*, D68, pp.42–56.

- Mullard, A., 2014. New drugs cost US\$2.6 billion to develop. *Nature Reviews Drug Discovery*, 13(12), p.877.
- Muller, H.J., 1946. The Production of Mutations.
- Murray, C.J.L. et al., 2012. Global malaria mortality between 1980 and 2010: a systematic analysis. *The Lancet*, 379(9814), pp.413–31.
- Murshudov, G.N. et al., 2011. REFMAC5 for the refinement of macromolecular crystal structures. *Acta Crystallographica Section D: Biological Crystallography*, 67(4), pp.355–367.
- Naguleswaran, A. et al., 2008. Azurin-like protein blocks invasion of *Toxoplasma gondii* through potential interactions with parasite surface antigen SAG1. *Antimicrobial Agents and Chemotherapy*, 52(2), pp.402–408.
- Nahlen, B.L. & Low-Beer, D., 2007. Building to collective impact: The global fund support for measuring reduction in the burden of malaria. *American Journal of Tropical Medicine and Hygiene*, 77(SUPPL. 6), pp.321–327.
- Nájera, J. a., González-Silva, M. & Alonso, P.L., 2011. Some lessons for the future from the global malaria eradication programme (1955-1969). *PLoS Medicine*, 8(1).
- Neghina, R. et al., 2010. Malaria, a Journey in Time: In Search of the Lost Myths and Forgotten Stories. *The American Journal of the Medical Sciences*, 340(6), pp.492–498.
- Neutze, R. et al., 2004. Potential impact of an X-ray free electron laser on structural biology. *Radiation Physics and Chemistry*, 71(3-4), pp.905–916.
- Nicholls, R.A., Long, F. & Murshudov, G.N., 2012. Low-resolution refinement tools in REFMAC5. *Acta Crystallographica Section D: Biological Crystallography*, 68(Pt 4), pp.404–17.
- Nilsen, A. et al., 2014. Discovery, synthesis, and optimization of antimalarial 4(1H)-quinolone-3-diarylethers. *Journal of Medicinal Chemistry*, 57(9), pp.3818–34.
- Nilsen, A. et al., 2013. Quinolone-3-diarylethers: a new class of antimalarial drug. *Science Translational Medicine*, 5(177), p.177ra37.
- Nixon, G.L., Moss, D.M., et al., 2013. Antimalarial pharmacology and therapeutics of atovaquone. *Journal of Antimicrobial Chemotherapy*, 68(5), pp.977–985.
- Nixon, G.L., Pidathala, C., et al., 2013. Targeting the mitochondrial electron transport chain of *Plasmodium falciparum*: new strategies towards the development of improved antimalarials for the elimination era. *Future medicinal chemistry*, 5(13), pp.1573–91.
- Njau, R.J. a et al., 2009. Implementation of an insecticide-treated net subsidy scheme under a public-private partnership for malaria control in

- Tanzania--challenges in implementation. *Malaria journal*, 8(c), p.201.
- Nyarango, P.M. et al., 2006. A steep decline of malaria morbidity and mortality trends in Eritrea between 2000 and 2004: the effect of combination of control methods. *Malaria journal*, 5, p.33.
- Nzila, A., 2006. The past, present and future of antifolates in the treatment of Plasmodium falciparum infection. *Journal of Antimicrobial Chemotherapy*, 57(6), pp.1043–1054.
- Nzila, A.M. et al., 2000. Molecular evidence of greater selective pressure for drug resistance exerted by the long-acting antifolate Pyrimethamine/Sulfadoxine compared with the shorter-acting chlorproguanil/dapsone on Kenyan Plasmodium falciparum. *The Journal of infectious diseases*, 181(6), pp.2023–2028.
- O'Donnell, R. a et al., 2000. Functional conservation of the malaria vaccine antigen MSP-119 across distantly related Plasmodium species. *Nature Medicine*, 6(1), pp.91–95.
- O'Reilly, M. et al., 2006. High throughput protein crystallography: Developments in crystallisation, data collection and data processing. *Drug Discovery Today: Technologies*, 3(4), pp.451–456.
- Otendal, M. et al., 2008. A 9 keV electron-impact liquid-gallium-jet X-ray Source. *Review of Scientific Instruments*, 79(1).
- Otwinowski, Z. & Minor, W., 1997. Processing of X-ray diffraction data collected in oscillation mode. *Macromolecular Crystallography Part A*, 276, pp.307–326.
- Overington, J.P. et al., 2006. How many drug targets are there? *Nature Reviews Drug discovery*, 5(12), pp.993–6.
- Owens, R.C. & Ambrose, P.G., 2005. Antimicrobial safety: focus on fluoroquinolones. *Clinical infectious diseases: an official publication of the Infectious Diseases Society of America*, 41 Suppl 2(Suppl 2), pp.S144–S157.
- Painter, H.J. et al., 2007. Specific role of mitochondrial electron transport in blood-stage Plasmodium falciparum. *Nature*, 446(7131), pp.88–91.
- Painter, H.J., Morrissey, J.M. & Vaidya, A.B., 2010. Mitochondrial electron transport inhibition and viability of intraerythrocytic Plasmodium falciparum. *Antimicrobial Agents and Chemotherapy*, 54(12), pp.5281–7.
- Peterson, D.S., Milhous, W.K. & Wellems, T.E., 1990. Molecular basis of differential resistance to cycloguanil and pyrimethamine in Plasmodium falciparum malaria. *Proceedings of the National Academy of Sciences of the United States of America*, 87(8), pp.3018–3022.
- Peterson, D.S., Walliker, D. & Wellems, T.E., 1988. Evidence that a point mutation in dihydrofolate reductase-thymidylate synthase confers resistance to pyrimethamine in falciparum malaria. *Proceedings of the National Academy of Sciences of the United States of America*, 85(23), pp.9114–9118.

- Pfefferkorn, E.R., Borotz, S.E. & Nothnagel, R.F., 1993. Mutants of *Toxoplasma gondii* resistant to atovaquone (566C80) or decoquinate. *The Journal of parasitology*, 79(4), pp.559–564.
- Phillips-Howard, P. a et al., 2003. The efficacy of permethrin-treated bed nets on child mortality and morbidity in western Kenya II. Study design and methods. *The American Journal of Tropical Medicine and Hygiene*, 68(4 Suppl), pp.10–15.
- Phyo, A.P. et al., 2012. Emergence of artemisinin-resistant malaria on the western border of Thailand: A longitudinal study. *The Lancet*, 379(9830), pp.1960–1966.
- Pidathala, C. et al., 2012. Identification, Design and Biological Evaluation of Bisaryl Quinolones Targeting Plasmodium falciparum type II NADH:Quinone Oxidoreductase (PfNDH2). *Journal of Medicinal Chemistry*, 55(5), pp.1831–43.
- Pizarro, J.C. et al., 2002. Crystallization and preliminary structural analysis of an antibody complex formed with PfMSP1-19, a malaria vaccine candidate. *Acta Crystallographica Section D: Biological Crystallography*, D58(7), pp.1246–1248.
- Postila, P. a. et al., 2013. Key role of water in proton transfer at the Qo-site of the cytochrome bc1 complex predicted by atomistic molecular dynamics simulations. *Biochimica et Biophysica Acta - Bioenergetics*, 1827(6), pp.761–768.
- Pradines, B. et al., 2006. Prevalence of in vitro resistance to eleven standard or new antimalarial drugs among Plasmodium falciparum isolates from Pointe-Noire, Republic of the Congo. *Journal of Clinical Microbiology*, 44(7), pp.2404–2408.
- Privé, G.G., 2007. Detergents for the stabilization and crystallization of membrane proteins. *Methods*, 41(4), pp.388–397.
- Qinghaosu Antimalarial Co-ordinating Research Group, 1979. Antimalarial studies on qinghaosu. *Chinese Medical Journal*, 82, pp.811–16.
- Radioff, P.D. et al., 1996. Atovaquone and proguanil for Plasmodium falciparum malaria. *The Lancet*, 347(9014), pp.1511–1514.
- Rafael, M.E. et al., 2006. Reducing the burden of childhood malaria in Africa: the role of improved. *Nature*, 444 Suppl, pp.39–48.
- Rasmussen, S.G.F. et al., 2007. Crystal structure of the human beta2 adrenergic G-protein-coupled receptor. *Nature*, 450(7168), pp.383–387.
- Rhodes, G., 2010. *Crystallography Made Crystal Clear* third edit., Elsevier.
- Riccio, P. et al., 1977. bc1-complex from beef heart One-step purification by hydroxyapatite chromatography in Triton-X100, polypeptide pattern and respiratory chain characteristics. *Biochimica et Biophysica Acta*, 459, pp.250–262.
- Richards, J.S. & Beeson, J.G., 2009. The future for blood-stage vaccines against

- malaria. *Immunology and cell biology*, 87(5), pp.377–390.
- Robert-Gangneux, F. & Dardé, M.L., 2012. Epidemiology of and diagnostic strategies for toxoplasmosis. *Clinical Microbiology Reviews*, 25(2), pp.264–296.
- Roberts, D.R., 2007. Preventing malaria in endemic areas. *British Medical Journal*, 335(7628), pp.1001–1002.
- Roberts, D.R., Manguin, S. & Mouchet, J., 2000. DDT house spraying and re-emerging malaria. *The Lancet*, 356(9226), pp.330–332.
- Rodrigues, T. et al., 2009. Design, synthesis and structure-activity relationships of (1H-pyridin-4-ylidene)amines as potential antimalarials. *Bioorganic and Medicinal Chemistry Letters*, 19(13), pp.3476–3480.
- Rodriguez, D. et al., 2012. Practical structure solution with ARCIMBOLDO. *Acta Crystallographica Section D: Biological Crystallography*, D68, pp.336–343.
- Ronk, M. et al., 1991. Amino acid sequence of the blue copper protein rusticyanin from *Thiobacillus ferrooxidans*. *Biochemistry*, 30(39), pp.9435–9442.
- Rontgen, W.C., 1896. On a New Kind of Rays. *Science*, 3(59), pp.227–231.
- Ross, R., 1902. Researches on malaria. , pp.26–116.
- Rossmann, M.G., 2001. Molecular replacement - historical background. *Acta Crystallographica Section D: Biological Crystallography*, D57, pp.1360–1366.
- Rossmann, M.G. & Blow, D.M., 1962. The Detection of Sub-Units Within the Crystallographic Asymmetric Unit. *Acta Crystallographica*, 15, pp.24–31.
- RTS, S.C.T.P., 2015. Efficacy and safety of RTS,S/AS01 malaria vaccine with or without a booster dose in infants and children in Africa: final results of a phase 3, individually randomised, controlled trial. *The Lancet*, 386(15), pp.31–45.
- Rupp, B., 2009. *Biomolecular Crystallography: Principles, Practice and Application to Structural Biology* First Edit., New York: Garland Science.
- Russel, P.B. & Hitchings, G.H., 1951. Antimalarials. 1 1 1 . 5-Aryl Derivatives. *Journal of the American Chemical Society*, 73(6), pp.2–9.
- Sanchez-Weatherby, J. et al., 2009. Improving diffraction by humidity control: A novel device compatible with X-ray beamlines. *Acta Crystallographica Section D: Biological Crystallography*, 65(12), pp.1237–1246.
- Sanishvili, R. et al., 2011. Radiation damage in protein crystals is reduced with a micron-sized X-ray beam. *Proceedings of the National Academy of Sciences of the United States of America*, 108(15), pp.6127–6132.
- Scherf, A., Lopez-Rubio, J.-J. & Riviere, L., 2008. Antigenic Variation in *Plasmodium falciparum*. *Annual Review of Microbiology*, 62, pp.445–470.

- Schuck, D.C. et al., 2013. Biological evaluation of hydroxynaphthoquinones as anti-malarials. *Malaria journal*, 12(1), p.234.
- Shanks, G.D., Edstein, M.D. & Jacobus, D., 2014. Evolution from double to triple-antimalarial drug combinations. *Transactions of the Royal Society of Tropical Medicine and Hygiene*, 109(3), pp.182–188.
- Shuker, S.B. et al., 1996. Discovering High-Affinity Ligands: SAR by NMR. *Science*, 274(5292), pp.1531–1534.
- Sievers, F. et al., 2011. Fast, scalable generation of high-quality protein multiple sequence alignments using Clustal Omega. *Molecular systems biology*, 7(539), p.539.
- Silman, H.I. et al., 1967. A New Protein Component of Complex III of the Mitochondrial Electron Transfer Chain. *Journal of Biological Chemistry*, 242(21), pp.4867–4875.
- Siraj, A.S. et al., 2014. Altitudinal Changes in Malaria Incidence in Highlands of Ethiopia and Colombia. *Science*, 343, pp.1154–1158.
- Siregar, J.E. et al., 2015. Direct evidence for the atovaquone action on the Plasmodium cytochrome bc1 complex. *Parasitology International*, 64(3), pp.295–300.
- Slater, A.F.G. & Cerami, A., 1992. Inhibition by chloroquine of a novel haem polymerase activity in malaria trophozoites. *Nature*, 355, pp.167–169.
- Smith, J.L., Fischetti, R.F. & Yamamoto, M., 2012. Micro-crystallography comes of age. *Current Opinion in Structural Biology*, 22(5), pp.602–612.
- Smith, P.M., Fox, J.L. & Winge, D.R., 2012. Reprint of: Biogenesis of the cytochrome bc1 complex and role of assembly factors. *Biochimica et Biophysica Acta - Bioenergetics*, 1817(6), pp.872–882.
- Snider, W.D. et al., 1983. Neurological complications of acquired immune deficiency syndrome: analysis of 50 patients. *Annals of Neurology*, 14(4), pp.403–418.
- Snow, R.W. et al., 2005. The global distribution of clinical episodes of Plasmodium falciparum malaria. *Nature*, 434(3), pp.214–217.
- Snow, R.W., Trape, J.-F. & Marsh, K., 2001. The past, present and future of childhood malaria mortality in Africa. *Trends in Parasitology*, 17(12), pp.593–7.
- Srivastava, I.K. et al., 1999. Resistance mutations reveal the atovaquone-binding domain of cytochrome b in malaria parasites. *Molecular Microbiology*, 33(4), pp.704–11.
- Srivastava, I.K., Rottenberg, H. & Vaidya, a B., 1997. Atovaquone, a broad spectrum antoparasitic drug, collapses mitochondrial membrane potential in a malarial parasite. *Journal of Biological Chemistry*, 272(7), pp.3961–3966.
- Srivastava, I.K. & Vaidya, A.B., 1999. A Mechanism for the Synergistic Antimalarial Action of Atovaquone and Proguanil A Mechanism for the

- Synergistic Antimalarial Action of Atovaquone and Proguanil. *Antimicrobial Agents and Chemotherapy*, 43(6).
- Stevens, F.J., 2008. Homology versus analogy: Possible evolutionary relationship of immunoglobulins, cupredoxins, and Cu,Zn-superoxide dismutase. *Journal of Molecular Recognition*, 21(1), pp.20–29.
- Stickles, A.M., Ting, L.-M., et al., 2015. Inhibition of Cytochrome bc1 as a Strategy for Single-Dose, Multi-Stage Antimalarial Therapy. *American Journal of Tropical Medicine and Hygiene*, 92(6), pp.1195–1201.
- Stickles, A.M., Justino de Almeida, M., et al., 2015. Subtle Changes in Endochin-Like Quinolone Structure Alter the Site of Inhibition within the Cytochrome bc1 Complex of *Plasmodium falciparum*. *Antimicrobial Agents and Chemotherapy*, 59(4), pp.1977–1982.
- Stock, D., Perisic, O. & Löwe, J., 2005. Robotic nanolitre protein crystallisation at the MRC Laboratory of Molecular Biology. *Progress in Biophysics and Molecular Biology*, 88(3), pp.311–327.
- Stocks, P.A. et al., 2014. Novel inhibitors of the *Plasmodium falciparum* electron transport chain. *Parasitology*, 141(1), pp.50–65.
- Sullivan, D.J. et al., 1998. A common mechanism for blockade of heme polymerization by antimalarial quinolines. *Journal of Biological Chemistry*, 273(47), pp.31103–31107.
- Suswam, E., Kyle, D. & Lang-Unnasch, N., 2001. *Plasmodium falciparum*: the effects of atovaquone resistance on respiration. *Experimental Parasitology*, 98(4), pp.180–187.
- Syafruddin, D., Siregar, J.E. & Marzuki, S., 1999. Mutations in the cytochrome b gene of *Plasmodium berghei* conferring resistance to atovaquone. *Molecular and Biochemical Parasitology*, 104(2), pp.185–194.
- Taylor, G., 2003. The phase problem. *Acta Crystallographica Section D: Biological Crystallography*, 59(11), pp.1881–1890.
- Taylor, G.L., 2010. Introduction to phasing. *Acta Crystallographica Section D: Biological Crystallography*, D66, pp.325–338.
- Thomas, M.B. & Read, A.F., 2007. Can fungal biopesticides control malaria? *Nature Reviews Microbiology*, 5(5), pp.377–383.
- Torgerson, P.R. & Mastroiacovo, P., 2013. The global burden of congenital toxoplasmosis: a systematic review. *Bulletin of the World Health Organization*, 91(7), pp.501–8.
- Torrey, E.F. et al., 2007. Antibodies to *Toxoplasma gondii* in Patients With Schizophrenia: A Meta-Analysis. *Schizophrenia Bulletin*, 33(3), pp.729–736.
- Trape, J.F. et al., 1998. Impact of chloroquine resistance on malaria mortality. *Comptes Rendus de l'Academie des Sciences - Serie III*, 321(8), pp.689–697.
- Trumpower, B., 1990. The protonmotive Q cycle. *Journal of Biological*

- Chemistry*, 265(20), pp.11409–11412.
- Urquiza, M. et al., 1996. Identification of Plasmodium falciparum MSP-1 peptides able to bind to human red blood cells. *Parasite immunology*, 18(10), pp.515–526.
- Vagin, A. & Teplyakov, A., 2010. Molecular replacement with MOLREP. *Acta Crystallographica Section D: Biological Crystallography*, 66(1), pp.22–25.
- Vagin, A.A. & Teplyakov, A., 1997. MOLREP: an Automated Program for Molecular Replacement. *Journal of Applied Crystallography*, 30(6), pp.1022–1025.
- Vaidya, A.B. & Mather, M.W., 2009. Mitochondrial evolution and functions in malaria parasites. *Annual Review of Microbiology*, 63, pp.249–267.
- Vallièrès, C., Fisher, N.E. & Meunier, B., 2013. Reconstructing the Qo Site of Plasmodium falciparum bc1 Complex in the Yeast Enzyme. *PLoS ONE*, 8(8), p.e71726.
- Waisberg, M. et al., 2012. Plasmodium falciparum merozoite surface protein 1 blocks the proinflammatory protein S100P. *Proceedings of the National Academy of Sciences of the United States of America*, 109(14), pp.5429–5434.
- Walter, R.L. et al., 1996. Multiple Wavelength Anomalous Diffraction (MAD) Crystal Structure of Rusticyanin: a Highly Oxidizing Cupredoxin with Extreme Acid Stability. *Journal of Molecular Biology*, 263(5), pp.730–751.
- Walters, J., 2015. Martin Shkreli: entrepreneur defends decision to raise price of life-saving drug 50-fold. *The Guardian*.
- Wang, J. et al., 2010. Artemisinin directly targets malarial mitochondria through its specific mitochondrial activation. *PLoS ONE*, 5(3), p.e9582.
- Warhurst, D.C. & Hockley, D.J., 1967. Mode of action of chloroquine on Plasmodium berghei and P. cynomolgi. *Nature*, 214(5091), pp.935–936.
- Wasserman, S.R. et al., 2012. Rapid-access, high-throughput synchrotron crystallography for drug discovery. *Trends in Pharmacological Sciences*, 33(5), pp.261–267.
- van de Waterbeemd, H. & Gifford, E., 2003. ADMET in silico modelling: towards prediction paradise? *Nature Reviews Drug Discovery*, 2(3), pp.192–204.
- Waxdal, M.J. et al., 1968. The Covalent Structure of a Human G-Immunoglobulin. *Biochemistry*, 7(5), pp.1959–1966.
- Wellems, T.E. & Plowe, C. V., 2001. Chloroquine-Resistant Malaria. *Journal of Infectious Diseases*, pp.770–776.
- Wells, T.N. & van Huijsduijnen, R.H., 2015. Ferroquine: welcome to the next generation of antimalarials. *The Lancet Infectious Diseases*, 3099(15), pp.1–2.
- Wells, T.N.C., van Huijsduijnen, R.H. & Van Voorhis, W.C., 2015. Malaria

- medicines: a glass half full? *Nature Reviews Drug Discovery*, 14(6), pp.424–442.
- Williams, G., 2011. The Pyramid™ Approach to Fragment-Based Biophysical Screening. In *Label-Free Technologies for Drug Discovery*. John Wiley & Sons, Ltd, pp. 241–253.
- Winge, D.R., 2012. Sealing the Mitochondrial Respirasome. *Molecular and Cellular Biology*, 32(14), pp.2647–2652.
- Winn, M.D. et al., 2011. Overview of the CCP4 suite and current developments. *Acta Crystallographica Section D: Biological Crystallography*, 67(4), pp.235–242.
- Winter, R.W. et al., 2009. Antimalarial Quinolones: Synthesis, potency and mechanistic studies. *Experimental Parasitology*, 118(4), pp.487–497.
- Winter, R.W. et al., 2006. Evaluation and lead optimization of anti-malarial acridones. *Experimental Parasitology*, 114, pp.47–56.
- Winter, R.W. et al., 2011. Optimization of endochin-like quinolones for antimalarial activity. *Experimental Parasitology*, 127(2), pp.545–551.
- Wongsrichanalai, C. et al., 2002. Epidemiology of drug-resistant malaria. *The Lancet. Infectious diseases*, 2(4), pp.209–218.
- World Health Organization, 2013. *Global Status Report on Road Safety: Supporting a Decade of Action*, Luxembourg.
- World Health Organization, 1969. Re-examination of the Global Strategy of Malaria Eradication. *A report by the Director-General to the 22nd World ...*
- World Health Organization, 2011. *WHO | World Malaria Report 2011*, World Health Organization.
- World Health Organization, 2006. WHO briefing on Malaria Treatment Guidelines and artemisinin monotherapies. *Geneva: WHO*, (April).
- World Health Organization, 2014. *World malaria report 2014*.
- Xiang, H. et al., 2006. Preclinical Drug Metabolism and Pharmacokinetic Evaluation of GW844520 , A Novel Anti-Malarial Mitochondrial Electron Transport Inhibitor. *Journal of Pharmaceutical Sciences*, 95(12), pp.2657–2672.
- Yeates, C.L. et al., 2008. Synthesis and structure-activity relationships of 4-pyridones as potential antimalarials. *Journal of Medicinal Chemistry*, 51(9), pp.2845–52.
- Yildirim, M. a et al., 2007. Drug-target network. *Nature biotechnology*, 25(10), pp.1119–1126.
- Yu, C.A., Yu, L. & King, T.E., 1974. Soluble Cytochrome bc1 Complex and the Reconstitution of Succinate-Cytochrome c Reductase. *The Journal of biological chemistry*, 249(15), pp.4905–4910.
- Zara, V., Conte, L. & Trumpower, B.L., 2009. Biogenesis of the yeast

- cytochrome bc1 complex. *Biochimica et biophysica acta*, 1793(1), pp.89–96.
- Zhang, Z. et al., 1998. Electron transfer by domain movement in cytochrome bc1. *Nature*, 392, pp.677–684.
- Zhu, J. et al., 2007. Simultaneous reduction of iron-sulfur protein and cytochrome bL during ubiquinol oxidation in cytochrome bc1 complex. *Proceedings of the National Academy of Sciences of the United States of America*, 104(12), pp.4864–4869.
- Zhu, Y. et al., 2014. Nanoliter-scale protein crystallization and screening with a microfluidic droplet robot. *Scientific reports*, 4, p.5046.
- Zimmermann, J. et al., 1997. Potent and selective inhibitors of the Abl-kinase: Phenylaminopyrimidine (PAP) derivatives. *Bioorganic and Medicinal Chemistry Letters*, 7(2), pp.187–192.

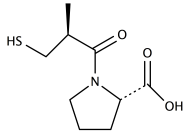
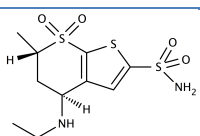
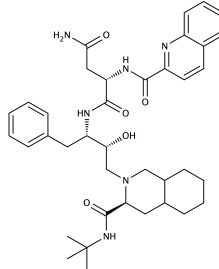
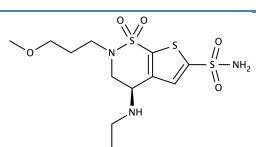
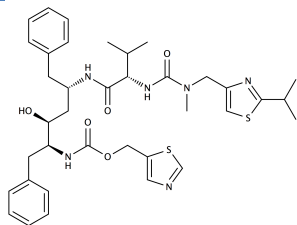
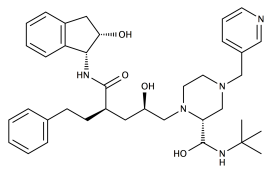
Supporting publications

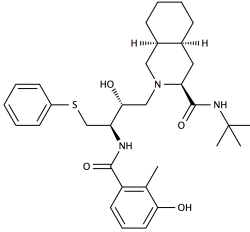
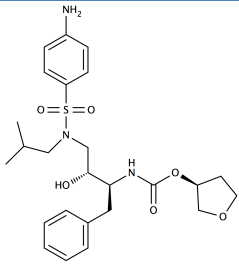
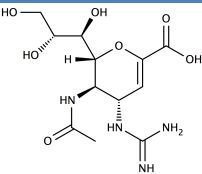
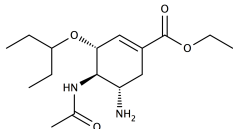
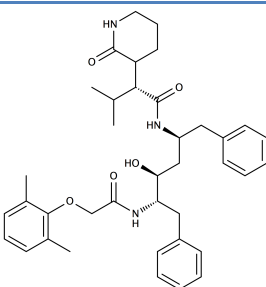
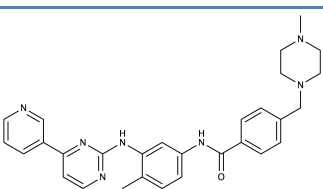
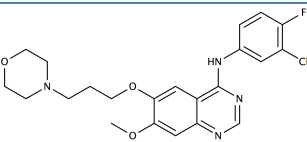
Capper, M. J., O'Neill, P. M., Fisher, N., Strange, R. W., Moss, D., Ward, S. A., Berry, N. G., Lawrenson, A. S., Hasnain, S. S., Biagini, G. A. & Antonyuk, S. V. *Antimalarial 4(1H)-pyridones bind to the Q_i site of cytochrome bc₁* Proc. Nat. Acad. Sci. USA **113**, 755-760 (2015)

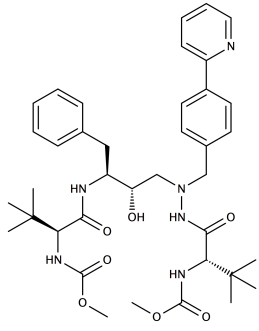
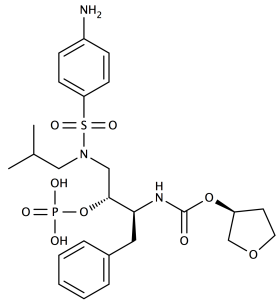
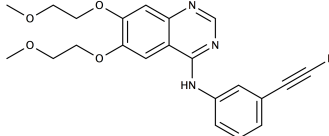
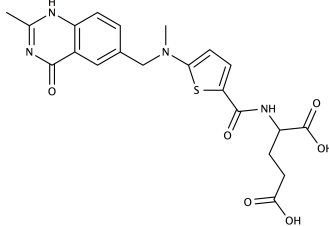
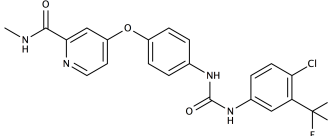
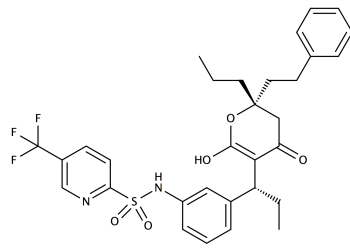
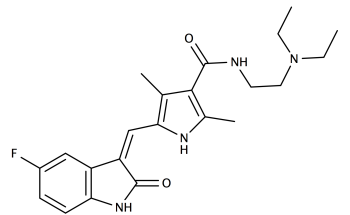
McPhillie, M., Zhou, Y., El Bissati, K., Dubey, J., Lorenzi, H., Capper, M. J., Lukens, A. K., Hickman, M., Muench, S., Kumar, S., Verma, S., Weber, C., Wheeler, K., Gordon, J., Sanders, J., Moulton, H., Wang, K., Taek-Kyun Kim, Santos, T., Woods, S., Lee, P., Donkin, D., Kim, E., Fraczek, L., Lykins, J., Esaa, F., Alibana-Clouser, F., Dovgin, S., Weiss, L., Brasseur, G., Wirth, D., Kent, M., Hood, L., Meunieur, B., Hasnain, S. S., Roberts, C., Antonyuk, S. V., Fishwick, C. & McLeod, R. (Under review) *Towards curing T. gondii infections, Toxoplasmosis and Malaria* Nature Medicine

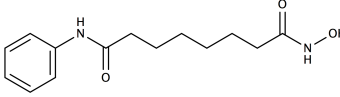
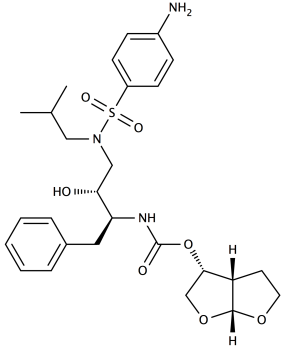
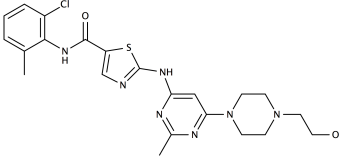
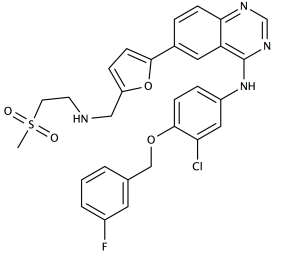
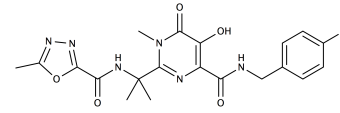
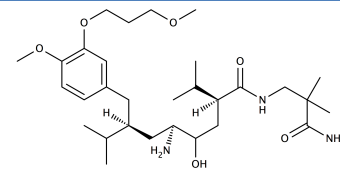
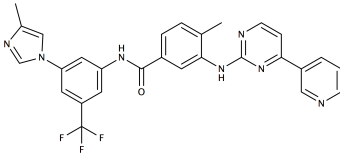
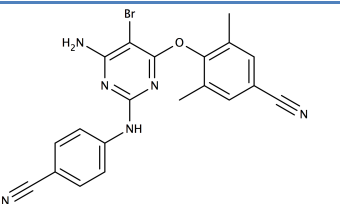
Appendix A

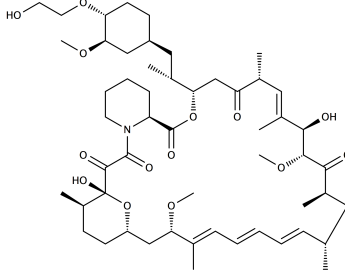
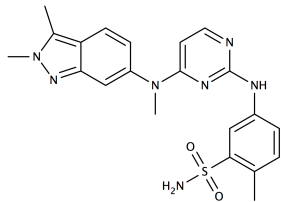
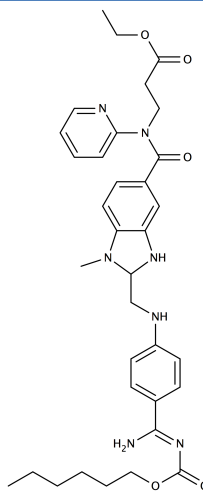
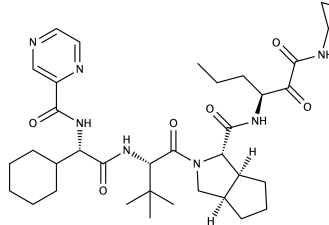
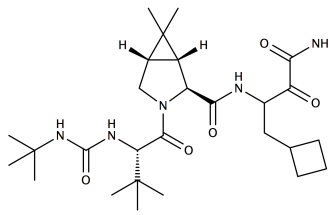
A table summarising all currently FDA approved drugs that have made it to market with input from structure-based drug design. This table was updated from similar tables previously published (Congreve et al. 2005; Alex & Millan 2012).

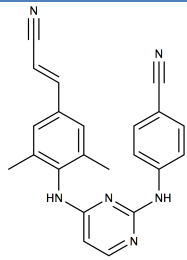
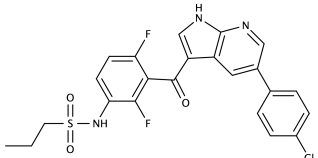
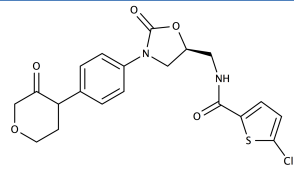
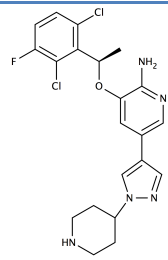
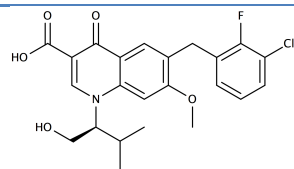
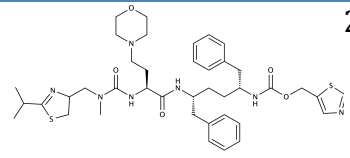
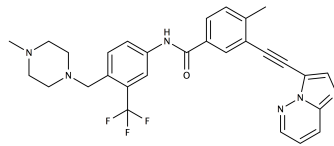
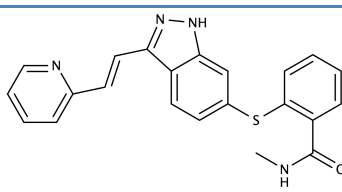
Target	Disease	Drug	Structure	Year of FDA approval
ACE protein	Hypertension	Captopril		1981
Carbonic Anhydrase	Glaucoma	Dorzolamide		1995
HIV protease	HIV/AIDS	Saquinavir		1995
Carbonic Anhydrase	Glaucoma	Brinzolamide		1996
HIV protease	HIV/AIDS	Ritonavir		1996
HIV protease	HIV/AIDS	Indinavir		1996

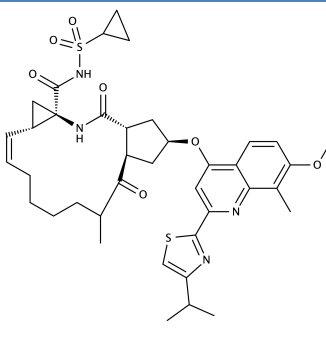
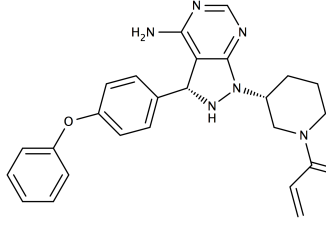
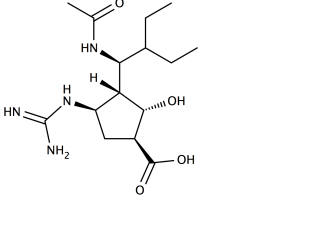
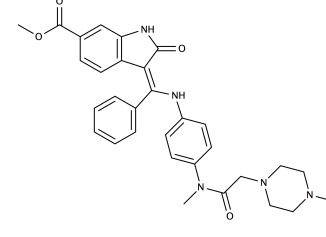
HIV protease	HIV/AIDS	Nelfnavir		1997
HIV protease	HIV/AIDS	Amprenavir		1999
Neuraminidase	Influenza	Zanamivir		1999
Neuraminidase	Influenza	Oseltamivir		1999
HIV protease	HIV/AIDS	Lopinavir		2000
Tyrosine kinases	Leukaemia	Imatinib		2001
EGFR tyrosine kinase	Certain cancers	Gefitinib		2003

HIV protease	HIV/AIDS	Atazanavir		2003
HIV protease	HIV/AIDS	Fosamprenavir (Amprenavir prodrug)		2003
EGFR tyrosine kinase	Certain cancers	Erlotinib		2004
Thymidilate synthase inhibitor	Various cancers	Raltixered (Tomudex)		2004
Tyrosine kinase inhibitor	Certain cancers	Sorafenib		2005
Protease inhibitor	HIV/AIDS	Tipranavir		2005
VEGFR tyrosine kinase inhibitor	Certain cancers	Sunitinib		2006

Histone deacetylase inhibitor	Cutaneous T cell lymphoma	Vorinostat		2006
Protease inhibitor	HIV/AIDS	Darunavir		2006
Tyrosine kinase inhibitor	Leukaemia	Dasatinib		2006
Tyrosine kinase inhibitor	Breast cancer	Lapatinib		2007
Integrase inhibitor	HIV/AIDS	Raltegravir		2007
Direct renin inhibitor	Hypertension	Aliskiren		2007
Tyrosine kinase inhibitor	Leukaemia	Nilotinib		2007
Reverse transcriptase inhibitor	HIV/AIDS	Etravirine		2008

mTOR inhibitor	Immuno-suppressant	Everolimus		2009
Tyrosine kinase inhibitor	Various cancers	Pazopanib		2009
Thrombin inhibitor	Thrombosis prophylaxis	Dabigatram		2010
Hepatitis C protease inhibitor	Hepatitis C	Telaprevir		2011 (Discontinued)
Hepatitis C protease inhibitor	Hepatitis C	Boriceprevir		2011

Reverse transcriptase inhibitor	HIV/AIDS	Rilpivirine		2011
B-raf enzyme inhibitor	Melanoma	Vemurafenib		2011
Factor Xa inhibitor	Thrombosis prophylaxis	Rivaroxaban		2011
Kinase inhibitor	Various cancers	Crizotinib		2011
Integrase inhibitor	HIV/AIDS	Elvitegravir		2012
Integrase inhibitor	HIV/AIDS	Cobicistat		2012
Tyrosine kinase inhibitor	Leukaemia	Ponatinib		2012
Tyrosine kinase inhibitor	Various cancers	Axitinib		2012

Hepatitis C protease inhibitor	Hepatitis C	Simeprevir		2013
Tyrosine kinase inhibitor	Mantle cell lymphoma	Ibrutinib		2013
Neuraminidase inhibitor	Influenza	Peramavir		2014
Tyrosine kinase inhibitor	Various cancers	Nintedanib		2014

Appendix B

Strains of microbes used in this work

Trade Name	Organism	Genotype	Supplier
Stellar™ cells	<i>E. coli</i>	F ⁻ , ara, Δ(lac-proAB) [Φ80d lacZΔM15], rpsL(str), thi, Δ(mrr-hsdRMS-mcrBC), ΔmcrA	Clontech
BL21 (DE3)	<i>E. coli</i>	fhuA2 [lon] ompT gal (λ DE3) [dcm] ΔhsdS λ DE3 = λ sBamHIo ΔEcoRI-B int::(lacI::PlacUV5::T7 gene1) i21 Δnin5	Merck
SMD1168	<i>P. pastoris</i>	his4, pep4	Invitrogen

Appendix C

Vector maps of plasmids used in this study for protein expression with relevant features annotated using Snapgene.

